# Ce/W MODIFIED MESOPOROUS CARBON SUPPORTED Pt-Pd ELECTRO CATALYSTS FOR FORMIC ACID OXIDATION

BY

ATEEQ UR REHMAN

A Thesis Presented to the
DEANSHIP OF GRADUATE STUDIES

**KING FAHD UNIVERSITY OF PETROLEUM & MINERALS**

DHAHRAN, SAUDI ARABIA

In Partial Fulfillment of the
Requirements for the Degree of

**MASTER OF SCIENCE**

In

CHEMICAL ENGINEERING

DECEMBER, 2013

KING FAHD UNIVERSITY OF PETROLEUM & MINERALS

DHAHRAN- 31261, SAUDI ARABIA

**DEANSHIP OF GRADUATE STUDIES**

This thesis, written by **Ateeq Ur Rehman** under the direction his thesis advisor and approved by his thesis committee, has been presented and accepted by the Dean of Graduate Studies, in partial fulfillment of the requirements for the degree of **MASTER OF SCIENCE IN CHEMICAL ENGINEERING.**

Dr. Mohammad M. Hossain
(Advisor)

Dr. Shakeel Ahmed
(Co-Advisor)

Dr. Usamah A. Al-Mubaiyedh
(Department Chairman)

Dr. Saleem Ur Rahman
(Member)

Dr. Mohammad Ba-Shammakh
(Member)

Dr. Salam A. Zummo
(Dean of Graduate Studies)

Date: 20/1/14

Dr. Abdallah Al-Shammari
(Member)

I dedicate my work to my family, friends and teachers and to all who loves me

# ACKNOWLEDGMENTS

*"In the name of Allah, The Most Merciful and The Most Gracious"*

All praise and thanks to Almighty, the Creator of all worlds for giving me the courage to accomplish this work sincerely and successfully. May there be every peace and blessings upon the holy prophet Muhammed (PBUH), his family and his companions.

I wish to express my appreciation to Chemical Engineering Department of King Fahad University of Petroleum & Minerals, for providing me an opportunity to continue my study. Also, I am grateful toall the faculty members, staff members and technicians of department for their support.

I would like to express my sincere gratitude to my thesis advisor Dr. M. Mozahar Hossain for his unlimited guidance, assistance and encouragement. I acknowledge the sincere efforts of my ex-advisor Dr. S U Rahman, for teaching me the philosophy of research and providing me the financial assistance for accomplishment ofsample characterization. Dr. Shakeel Ahmed and Dr. Safdar Hossain technical support, anytime accessibility for discussionduring catalysis synthesis, analysis and evaluation is highly appreciated. I must also extend deep sense of gratitude to my other thesis committee members Dr. Abdullah Al-Shammari and Dr Mohammad Ba-Shammakh for their immense contribution and suggestions through out the period of this work.

I thank all the collegues, students and friends of Chemical Engineering department for giving me remarkable company, specially appreciated to Waqas Aslam, M Ilyas, M Umer and my room mate Asim Ghaffar for making my state memorable. Also, I am grateful and very happy for supportive and good relationship of Pakistani Community in KFUPM.

Finally, but very important, special thanks to my parents, brothers, sister (Ghurya) and family for their encouragement, moral support and continuous prayers and enduring missing me among them.

# TABLE OF CONTENTS

# LIST OF TABLES

# LIST OF FIGURES

# LIST OF ABBREVIATIONS

| | | | |
|---|---|---|---|
| Ag/AgCl | Silver/ Silver Chloride | MCFC | Molten Carbonate Fuel Cell |
| AFC | Alkaline Fuel cell | MWCNT | Multi walled Carbon Nanotubes |
| BET | Brunauer–Emmett–Teller | OMC | Ordered Mesoporous Carbon |
| BJH | Barrett-Joyner-Halenda | ORR | Oxygen Reduction Reaction |
| CA | Chronoamperometry | PAFC | Phosphoric Acid Fuel Cells |
| CNT | Carbon Nanotubes | Pd | Palladium |
| CNF | Carbon Nanofibers | PEM | Proton Exchange Membrane |
| CV | Cyclicvoltametry | Pt | Palatinum |
| DFAFC | Direct Farmic Acid Fuel Cell | SEM | Scanning Electron Microscopy |
| DMFC | Direct Methanol Fuel Cell | SOFC | Solid Oxide Fuel Cells |
| EDX | Energy Dispersive X-ray Spectroscopy | TEM | Transmission Electron Microscopy |
| FAO | Formic Acid Oxidation | TGA | Thermo Gravimetric Analysis |
| FAOR | Formic Acid Oxidation Reaction | XRD | X-ray Diffraction |

# ABSTRACT

Full Name : Ateeq Ur Rehman

Thesis Title : Electrocatalytic Activity of Ce/W modified mesoporous carbon supported Pt-Pd catalysts for formic acid oxidation

Major Field : Chemical Engineering

Date of Degree : December 2013

In this thesis report, I investigate the Ce/W oxidesordered mesoporous carbon (OMC) support modification effect on PtPd based electrocatalyststowards formic acid oxidation reaction (FAOR). Oxides modified ordered mesoporous carbon (Oxide-OMC) support was prepared by hard template method. While PtPd bimetallic catalysts were synthesized using borohydride reduction method with different ratio of Pt and Pd metals.

Physical properties of $CeO_2$/$WO_3$-OMC supports and catalyst samples were characterized by TEM, XRD, SEM, EDX, $N_2$ adsorption/desorption isotherm and TGA. Both SEM& XRD analysis shows that modified support based PtPd catalysts exhibit uniform metal dispersion and increasing Pt to Pd ratio enhances crystal size reduction of metals. Whereas, Pt and Pd particle size reduction also verifies by TEM analysis.Surface properties of prepared catalyst samples were analyzed by BET and BJH pore size analysis. BET explains the higher surface area and smaller pore diameter for support modified samples. TGA analysis showed the support stability and oxidation temperature around 420-470°C.

Electrochemical analysis such as CV, CA, CO-stripping voltammograms and $H_2$ adsorption/desorption analysis were employed to evaluate the electro oxidation activity of electrocatalysts. CV results confirmed that modified support $CeO_2$-OMC and $WO_3$-OMCbased Pd catalyst exhibited much higher anodic oxidation current activity and stability than that of unmodified supported electrocatalysts.

# ملخص الرسالة

**الاسم الكامل**: عتيق الرحمن

**عنوان الرسالة:النشاط الإلكتروحفزي لحفازات الكربون المسامي المعدل Ce/W المدعمة بعنصري Pt و Pd في تفاعل أكسدة حمض الفورميك**

**التخصص:الهندسة الكيميائية**

**تاريخ الدرجة العلمية**:ديسمبر 2013

في هذا التقرير ، بحثتُ تأثير التعديل في دعامة أوكسيدات الكربون المسامي المرتب لـ Ce/W على الحفازات الكهربية المكونة من PtPd باتجاه تفاعل أكسدة حمض الفورميك. تمّ تحضير دعامة أوكيسدات الكربون المسامي المعدل المرتب بطريقة القالب الصعب بينما تمّ تحضير و تركيب الحفازات المحتوية على المعدنين PtPd باستخدام طريقة اختزال البوروهيدريد باستخدام نسب مختلفة من معدني Pt و Pd .

تمّ تحديد الخصائص الفيزيائية لعينات الدعامات و الحفازات $CeO_2/WO_3$-OMC باستخدام عدة تقنيات مثل : TEM و XRD و SEM و EDX و امتصاص و إفراز النيتروجين $N_2$ و TGA . كلا التقنيتين SEM و XRD تظهر أن الدعامة المعدلة للحفازات المحتوية على PtPd توزع منتظم للمعدن كما أن زيادة نسبة Pt إلى نسبة Pd تحسّن النقص في حجم البلورة للمعادن بينما النقص في حجم Pt و Pd قد تمّ تأكيده باستخدام تقنية TEM . تمّ تحليل خصائص السطح لعينات الحفاز المحضرة باستخدام BET و BJH التي تقيس حجم المسامات . تشرح تقنية BETمساحة السطح المرتفعة و قطر المسام المنخفض لعينات الدعامة المعدلة. أظهر تحليل TGA استقرار الدعامة و درجة الأكسدة التي تتراوح ما بين 420 – 470 مئوية .

تمّ توظيف التحليل الإلكتروكيميائي مثل CV و CA و CO-stripping voltammograms و امتصاص و إفزاز الهيدروجين $H_2$ لتقييم نشاط التأكسد الإلكتروني للحفازات الكهربية . أكّدت نتائج تحليل CV أنّ الدعامة المعدلة ($CeO_2$-OMC & $WO_3$-OMC)) المعتمدة على حفاز Pd تبدي نشاطا أنوديًّا تأكسديًّا أكثر من تلك باستخدامالحفاز الكهربي Pd/OMC . أثبت تحليل CV أيضا النسبة الأفضل من معدني Pd و Pt لتفاعل أكسدة حمض الفورميك . تمّ اختبار استقرار الحفازات الكهربية باستخدام قياسات CV .

# CHAPTER1
# INTRODUCTION

## 1.1 Fuel Cell

Currently, most of our energy demand is met by combustion of fossil fuels like petroleum, coal, and natural gas. Combustion of fossil fuels emits huge amount of carbon dioxide, a major green house gas, which led to the drastic climatic change[1]. The consumption of the fossil fuel is increasing at a brisk pace in order to meet the energy demand of the growing world population. The ever increasing fossil fuel consumption ledto the uncertainty of the availability of fossil fuel in the near future. Due to the fact, the renewable sources are increasingly seen as a viable option contributing to the worldwide energy demand. In this regard, solar and wind have been considered to be the most attractive renewable energy sources. However, the intermittent nature of these energies requires development of efficient technologies for their storage and perpetual use. One of the many most elegant ways to store these energies is to produce hydrogen or other materials using solar or wind energy and harness their chemical energy to produce green electrical energy[2, 3].

Fuel cells are the devices which convert chemical energy stored in fuels as hydrogen and other small chain organic moleculesinto electrical energy[4]. Fig. 1.1 shows the schematics of a generic polymer electrolyte membrane (PEM) Fuel Cell[5].There are different types of fuel cells available, out of them PEM is the most promising especially for power generation for portable applications. Different types of

feed can be used in the anode side of the PEM fuel cell. Apart from hydrogen, methanol and ethanol, formic acid been successfully implemented as a fuel in PEM fuel cell.

In addition to become a potential fuel in PEM fuel cell, formic found numerous applications as a useful chemical in the industry. In fact, formic acid is one of the most widely producedandconsumed industrial chemicals throughout the world. Its use as a feed for polymer electrolyte membrane fuel cell (PEMFCs) is particularly interesting and has been the topic of intense research for last couple of years. PEMFCs using formic acid as anode feed are called direct formic acid fuel cell (DFAFCs)[8].

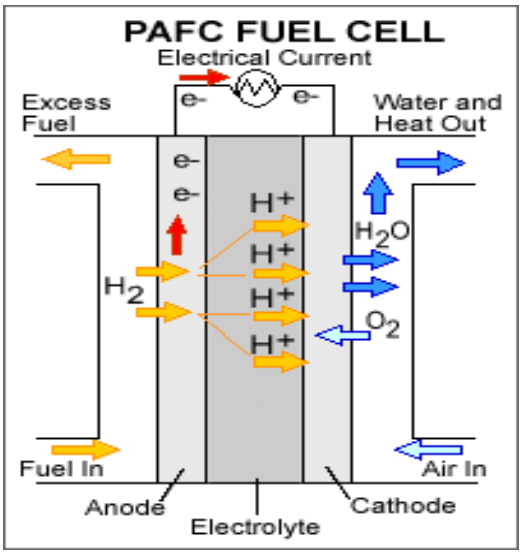


Figure 1.1: Working principle of a PEM fuel cell [5]

In recent years, DFAFC have received growing interest as a compact generator, for electronic devices and transportation means. In a DFAFC, formic acid oxidation (FAO) takes place at the anode side while reduction occurs at the cathode side

[9].Generally, the DFAFC has the following major advantages: (i) safe and easy to handle, given formic acid is non-toxic, (ii) can create high theoretical open circuit potential of 1.48 V which is larger than hydrogen (1.23 V) and methanol (1.21 V), and (iii) low cross over though membrane than methanol and ethanol. Although formic acid has lower energy density (2104 Wh/L) compared to methanol (4900 Wh/L), the low cross over though the membranes allows the DFACFs to operate at high formic acid concentrations (5-12 M) compared to methanol concentration (1-2 M), resulting an overall higher energy output [9- 12]. It also provides high practical power densities at low temperature. In addition to the above technical advantages, the mass scale applications of DFAFCs can also create opportunities of utilizing $CO_2$ (from fossil fuel combustion) as a source of formic acid production via electrochemical conversion of carbon dioxide. Electrochemical conversion of carbon dioxide to produce formic acid has been very recently commercialized. This integrated approach not only offers DFAFCs as way of efficient energy generator but also contribute to the global efforts on the $CO_2$ utilization/sequestration, addressing the green house gas effects [13-14]. With this system, the energy requirement for carbon dioxide conversion will come from formic acid fuel cell and in turn, the formic acid produced from carbon dioxide conversion can be used as feed for DFAFCs. Schematic of the process is shown in the Fig.1.2. This type of integrated process is not currently feasible for methanol and ethanol fuel cells with the

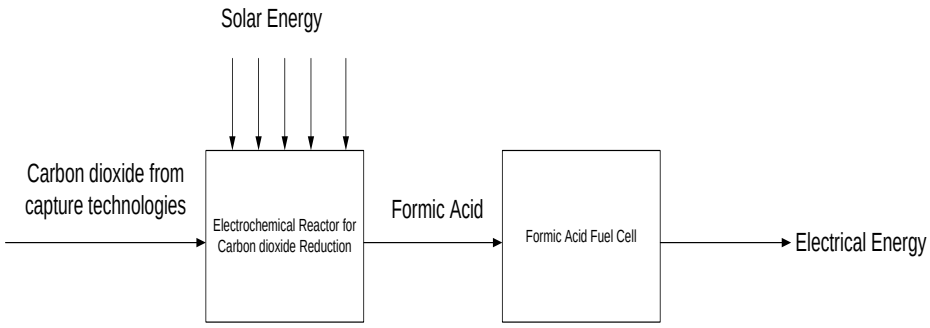


Figure 1.2:$CO_2$ capture system integrated with the formic acid fuel cell [13]

current technological status as, unfortunately, electrochemical conversion of carbon dioxide to methanol and ethanol is yet to be applied in any industrial scale [6- 8].Solar energy can be used as source of electricity required for the $CO_2$ conversion reactor[6]. Thus, formic acid, produced by electrochemical conversion of $CO_2$ by using solar energy, can act as convenient energy carrier.

In order to realize the after mentioned advantages of DFAFCs, there are significant research and development efforts being underway around the world. Despite some advancement, the present DFAFCs processes suffer from some practical issues which need to be addressed in order to exploit their full benefits. The foremost drawback of the present DFAFCs is the use of expensive and scarce noble metal based as electrocatalysts to accelerate the slow kinetics of the anodic electro oxidation of formic acid [15-17]. Electrocatalysts and polymeric membranes are the most expensive materials used in membrane electrode assembly, which is the heart of a fuel cell. In addition to their high costs, the noble metal based catalysts also suffer from severe poisoning due to the strong adsorption of the carbon monoxide [18], and chemical instability in acidic

environment. Among the noble metals, Pt and Pd are extensively investigated as anode electrocatalysts. Although, Pd based electrocatalysts showed much higher catalytic activity for FAO reactions compared to Pt, it still lacks stability for the long period of operations [19, 20].These difficulties warrant the development of highly durable and efficient Pd-based electrocatalysts for DFAFCs.In the open literature various metals have been investigated as promoter to enhance the catalytic activity and stability of Pd catalysts. The use of the non-noble metals also helps reducing the use of noble metals in the catalyst formulation while maintaining or even improving the catalytic activity. The most common bimetallic catalyst formulation includes PdCo, PdNi, PdAu, PdPt, PtBi, PdSn and PdFe [21-27].However, the activity and the stability of the catalysts need further improvement.

In order to achieve highest possible catalytic activity using a minimum amount of metal, the active metals/promoters are dispersed on a suitable support material. The support also provides the required strength of the electrocatalyst in acidic environment of the fuel cells [28]. Like the conventional supported catalysts, high surface area, large pore volume and high electrical conductivity of the support is highly desirable. The high surface area of the support allows better dispersion and minimal agglomeration of the nano sized active metal particles, resulting optimum catalytic performance. Among the studied support materials, the large surface area carbon such as Vulcan XC72 carbon black is possibly the most widely used support in electrocatalysts. With some advantages there are some drawbacks of Vulcan XC72 carbon black supported electrocatalysts. Among them the most important one is non contribution of some of the loaded expensive metals particles given they are trapped in the deep cracks of the phase boundaries and

micropores of the carbon black support [29]. Carbon black also suffers with serious corrosion problems in the fuel cell oxidation operation [30- 31]. In order to avoid these problems there are many other carbon materials that have been investigated as electrocatalyst support, including carbon nanotubes (CNTs) [10, 12, 27, 29- 30], nanofibers (CNFs) [17], ordered mesoporous carbon (OMCs) [33-38], graphene [32], metal carbides [56] among others.

Among the above support materials, ordered mesoporous carbon (OMCs) have found wide range potential applications due to their uniform pore structure, large pore volumes, high surface areas, superior electrical conductivity and good chemical stability [33- 38]. When a suitable noble metal was deposited on OMCs the resultant electrocatalysts showed excellent performances for methanol oxidations in a methanol fuel cell [33]. Lui et al. [38] also reported a better activity and stability of Pt/OMC in a formic acid fuel cell as compared to a Pt/C electrocatalyst.

The modification of the support material is also found beneficial to improve the activity of the supported catalysts. The commonly used modifiers includes $TiO_2$, $WO_3$, $CeO_2$, $ZrO_2$, NiO, and $Fe_2O_3$ metal oxides [11, 15, 33, 39- 41]. It is believed that partially filled d- or f- orbital of the transition metals allow them to switch between valences. Metal oxide-carbon composites as support material have been tested extensively for methanol electrocatalysts oxidation with improved catalytic activity and stability. There are reports on the effect of addition of metal oxides to Pd/C for FAO which includes NiO, $WO_3$ and $CeO_2$ [15, 33, 40]. In general, the addition of these metal oxides improved the overall performance of the Pd/C electrocatalysts.Among these metal oxides, $CeO_2$ and $WO_3$ are widely used as reducible oxides having high oxygen carrying

capacity. The $Ce^{4+}/Ce^{3+}$ couples (by redox cycles) release oxygen in different conditions, which enhance the electro oxidation abilities of Pt/C catalysts. Similarly, Z. Zhang et al. (2008) reported that Pd nanoparticles deposited on hybrid $WO_3$support has showed significant high electro oxidation activity for formic acid and $WO_3$ exhibited good catalytic assistant effect with noble metals. It is observed that $WO_3$ facilitate the formation of hydrogen bronze ($H_xWO_3$) which enhanced the rate of dehydrogenation during oxidation in acidic medium. Similarly like Ti and Nb (niobium) metals, the oxophilic nature of the $WO_3$also helped in removing the adsorbed CO intermediates from the Pt metal surface during the oxidation reaction. $WO_3$ prevented the catalyst long term degradation and ageing by physically separating the metal particles which decreased the rate of particle agglomeration. These reasons highlighted the tungsten oxide a considerable replacement of commercially available carbon black supports in order to get the efficient catalytic performance and CO tolerance for fuel cell anodic catalyst electrodes [33].

Thisresearch has been focused on investigating the Ce and W doped ordered mesoporous carbon as support material for the preparation of low cost Pd-Pt bimetallic catalyst for formic acid electrooxidation. The out come of this research would significantly contribute towards the development of new generation low cost fuel cells catalysts which will pave way for the possible integration with the carbon dioxide capture and utilization facilities.

# CHAPTER 2
# LITERATURE REVIEW

## 2.1 History

In 1839, William Robert Grove first time introduced the concept of fuel cell by demonstrating water electrolysis in reversible concentric hydrogen oxygen cell assembly. W Grove prepared first working prototype which consisted on platinum electrodes, surrounded by a glass cylinders. He named this prototype as “gas battery”. Inner cylinder was filled with hydrogen and outer with oxygen as shown in Fig. 2.1 [42].

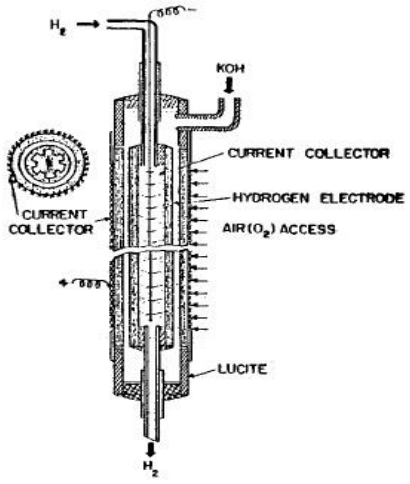


Figure2.1: Concentric Hydrogen oxygen fuel cell[42]

Later on in 1989, Mond and his associate Carl Langer performed their experiment on thin perforated platinum electrode cell using “Mond-gas” which they derived from

coal. At the same year, their theory on fuel cell coined by Charles R Alder Wright and C Thompson.Theoretical understanding about working was given by a Physical Chemistry Professor Friedrich W Ostwald in 1893. Experimentally he described the interconnected role of fuel cell components: electrode, oxidizing and reducing agents, anions, cations and electrolyte solutions [43]. In addition, he also provided the basic thermodynamic equations showing the definite advantages of "Low Temperature Electrochemical oxidation over High temperature combustions" of fuels.

After World War 1, serious efforts were started to build practical fuel cell but due to heat engine Carnot's Cycle theory evolution, all efforts remained unpractical. In 1930, G W Heise and E A Schumacher, practically formulated "Air Cells" using caustic electrolyte which proved more efficient as compared to ammonium chloride which was used in earlier cells operations [42]. Francis T Bacon constructed first successful fuel cell in 1932, using oxygen and hydrogen as fuel, nickel electrodes and alkaline as electrolyte solution [43]. Later in 1954, in London exhibition, Bacon demonstrated a six cell battery that produced 150W power, operated at 200°C and having electrodes of 5 inches diameter. In 1956, Bacon with his staff began development of large battery with 40 cells to show that a particular size of battery could be built. After three years in 1959, with the support of National Research development Corporation UK, they completed 6-kW fuel cell stack. This stack was used to power a fork- lift truck, welding equipment and a circular saw on trial base [44].

After World War-II, scientists started to think it might be the time to preserve fossil fuels reservoirs by obtaining high energy conversion efficiencies and fuel cell research was revived. Recent years have seen an upsurge interest in fuel cells for a range

of applications, especially for stationary power generation and portable automobiles. Depending on the load, type of fuel cell and operation conditions, a single cell has a potential of 0.5V to 1.0V. To yield a sufficient high voltage, a number of single cells are usually connected electrically in series in form of a stack.

## 2.2 Types of fuel cells

Fuel cell systems are classified according to the fuels or oxidants they used, working temperature and pressure conditions and by the electrolyte solution used for proton exchange carrier. On these basis fuel cells are distinguished to each other and their brief working is explained as follows in the following subsections.

### *2.2.1 Alkaline fuel cell (AFC)*

Alkaline fuel cells used compressed purified oxygen and hydrogen as fuel in potassium hydroxide electrolyte solution in water. Operating temperature for AFC is 90 to 120 °C and produced 10-100KW output power and water as shown in Fig. 2.2. Maximum efficiency of AFC is 60 to 90% and these cells are usually used in spacecraft to provide both drinking water and electricity. Main drawbacks for AFC are costly platinum electrode catalyst and handling of high purity $H_2$ fuel cylinders [7].

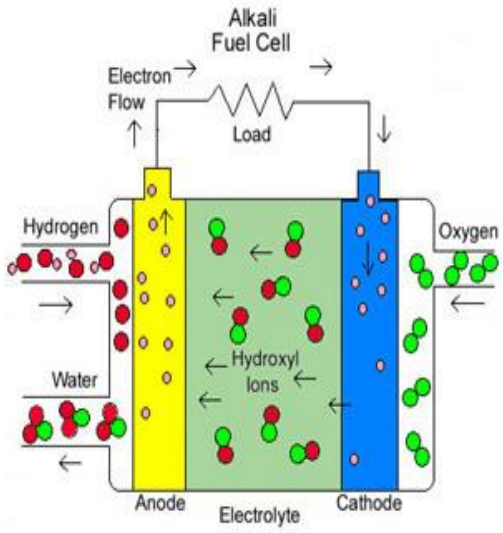


Figure 2.2: Working of alkaline fuel cell[7]

### *2.2.2 Molten carbonate fuel cell (MCFC)*

As shown in Fig.2.3, MCFC used sodium (Na) or magnesium (Mg) carbonate salts compound as electrolyte at high temperature i.e. 650°C and produced 300kW to 3MW power [43]. Efficiency of these cells is 50% and operating cost is also low as nickel electrolyte is used as catalysts. The high temperature limits damage from carbon monoxide "poisoning" of the cell and waste heat can be recycled to make additional electricity.Also, during the process, carbonate ions from the electrolyte are consumed, making it necessary to inject carbon dioxide to compensate.

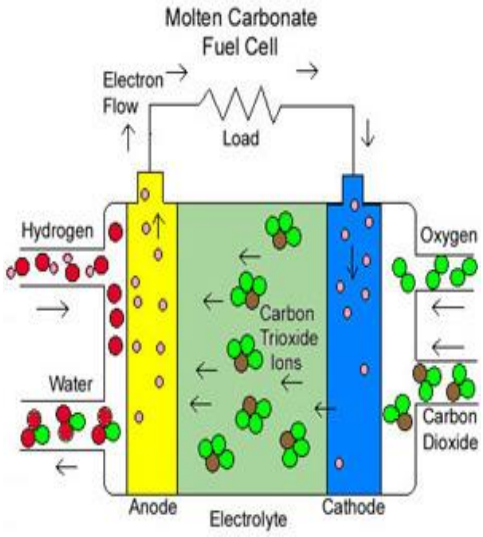


Figure 2.3: Working of molten carbonate fuel cell [43]

### *2.2.3 Phosphoric Acid Fuel Cells (PAFC)*

In PAFC, phosphoric acid is used as electrolyte solution (Fig.2.4). Operating temperature for these cells is 150-200 °C with 50 % mechanical efficiency. Platinum is used as electrode catalyst and they produced 200kW to 1 MW power. PAFCs tolerate a carbon monoxide concentration of about 1.5 percent, which broadens the choice of fuels they can use [7].

### *2.2.4 Proton Exchange Membrane Fuel Cells (PEM)*

PEM fuel cells work using a polymer electrolyte in thin and permeable sheet form. Efficiency of PEM cells is about 60% at operating temperature of 50-80°C.Platinum electrode catalysts at both side of thin membrane raised operating cast of PEM and it produced 1kW to 250kW. The easyhandling of solid flexible electrolyte and ability

tooperate at a low enough temperature makes them suitable for homes and cars.Combined working diagram of PAFC and PEM is shown in Fig.2.4.

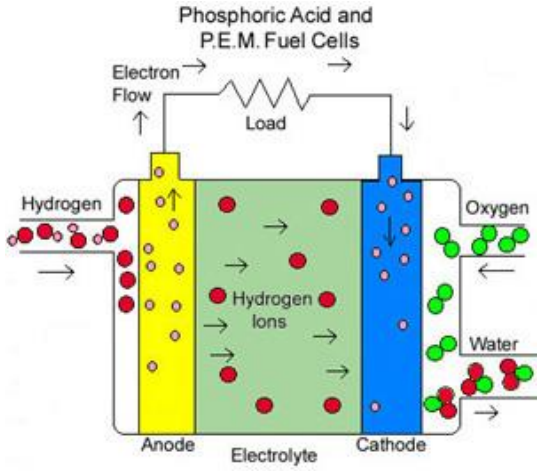


Figure 2.4: Working diagram of PAFC and PEM [43]

### *2.2.5 Solid oxide fuel cells (SOFC)*

SOFC used solid metals compounds of calcium or zirconium oxides as electrolyte at very high temperature about 700 to 1000°C. Cell efficiency is 60% and produces up to 2 MW power. High temperature operation of SOFC excludes the cost of extra fuel treatment equipments and additional humidifier and also no expensive catalysts are needed for these cells [45].

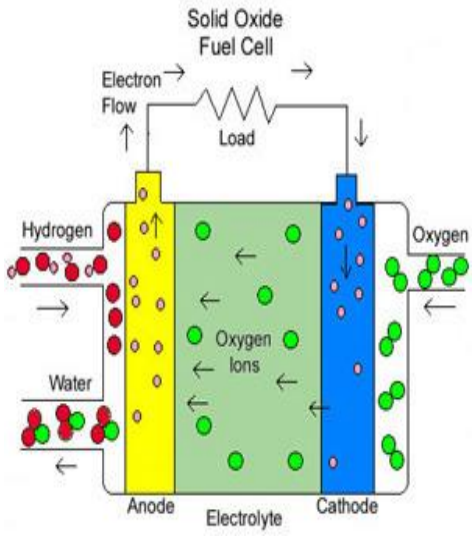


Figure 2.5: Working of solid oxide fuel cell [43]

### 2.3 Types of fuels

The primary fuels which aregenerally used in fuel cell stack are hydrogen, methanol, ethanol, carbon monoxide, ethylene glycol, formic acid and hydrazine depending upon fuel cell type. Hydrogen ($H_2$) is an optimal fuel which can be used for all type of cell and more than 90% composition of universe and more than 30% mass of sun consist of hydrogen [46]. The Classical hydrogen fuel cell suffers from several drawbacks. Each hydrogen molecule contains large amount of energy so safety is being the first and foremost issue in development of this technology at large scale [47]. Secure transportation method and storage ability of $H_2$ are also mentioned a serious problem. When demand and distribution hits on large scale then it is difficult to compress a sufficient amount of $H_2$ for direct use of consumer product like cars, because $H_2$ itself is of low density gas.

Another point for not using $H_2$ as fuel is that it is not naturally available on earth but it is extracted using technology with energy consumption. Hydrogen mostly comes from reforming of naphtha. This process again requires energy which comes from burning of fossil fuels. So this technology is viable only if the energy comes from renewable sources. This would require energy stations that would have to power the extraction process without using more energy resources than are being produced [48].

Therefore, instead of hydrogen being the feed to a fuel cell, liquid fuels have been proposed as a cathode feed for PEM fuel cells. Small chain organic molecules, methanol, ethanol, and formic acid are the potential liquid fuel substitute as feed for fuel cells pointed by recent research. Transportation and handling of liquid state fuels is relatively easy as compared to hydrogen, especially for low power applications [46].

If the fuel cell cars are commercialized, then the liquid fuel system can utilize the existing distribution and transportation system of gasoline. This is a remarkable economic advantage the liquid feed based fuel cells provide [48, 49]. Table 2-1 shows the list of the common liquid fuel with their energy density.

Every liquid fuels mentioned has its merits. In the following section, different fuels will be compared. One most important criterion for feed for cell is the volumetric energy density[50].From table, it is clear that the liquid fuel processed considerable high energy density value as compared to compressed hydrogen at ambient temperature, offer significant advantage of liquid organic fuels. Similarly, methanol has high energy density in comparison with formic acid. However, formic acid has higher thermodynamic

potential and the shows thermodynamic reversible energy efficiency 106%, very high compared to methanol 97%, as shown in Table 2-1.

Table 2-1: Organic liquid fuels and hydrogen fuel properties[49]

| **Fuel** | **Energy density(Wh/L)** | **E** | **Reversible energy efficiency (%)** |
|---|---|---|---|
| Ethanol | 6280 | 1.14 | 97 |
| Ethylene glycol | 5870 | 1.22 | 99 |
| Formic Acid | 1930 | 1.42 | 106 |
| Hydrazine | 5400 | 1.62 | 100 |
| Methanol | 4820 | 1.21 | 97 |
| 2-propanol | 7080 | 1.12 | 97 |
| Hydrogen | 180 @1000psig, 25 °C | 1.23 | 83 |

Anodic oxidation reaction (AOR) is the reason which exemplifies the lower energy density of formic acid as fuel. Per molecule of formic acid produced only two electrons, fewer than are produced by other organic molecules. On the other hand other organic fuels such as ethanol, methanol, methane and hydrazine produce 12 electrons, 6 electrons, 4 electrons and 4 electrons per molecule respectively. Although formic acid produces fewer electrons, it also follows the fewer electro-oxidation mechanism, which increases the reaction completion probability, and hence, results in optimal fuel use [50]. One considerable advantage of formic acid is that it does not require the extra water at anode for oxidation of formic acid to $CO_2$, as two oxygen atoms are already present in its

structure. But methanol requires water at the anode in one molar ratio for completion of oxidation reaction, according to following equation (2.1),

$$CH_3OH + H_2O \rightarrow CO_2 + 6H^+ + 6e^- \qquad (2.1)$$

The fundamental need for water in DMFC restricts the operational concentration of methanol less than 50% mol whereas formic acid can work without dilution. However, for safety reason due to flammability and membrane hydration, it is operated at concentration less than 85%.

Despite the advantage in thermodynamic efficiency, the volumetric energy density of formic acid is about only 40% of DMFCs.That is why DFAFCs are operated at high concentration which is practical. Fuel cell efficiency of DFAFC is much higher than that of DMFC; this result in higher output power as well as lower parasitic energy loses for the DFAFC.

Water management is a very critical issue in DMFC. Water is produced on the cathode side of the DMFC (3 moles of water per mole of methanol). This water management problem leads to more complex system and greater loss in energy. Hence in DFAFC, easy water balance due to simpler anode reaction, coupled with faster reaction kinetics make DFAFCs competitive in low power applications [51].

Moreover, formic acid has the advantage of nontoxicity, inflammability at room temperature, higher theoretical open circuit voltage, and low crossover through

membrane. Therefore, a compromise between the balance of plant and fuel concentration is made when considering the DFAFC advantages relative to DMFC. This limits the DFAFC advantage to low power applications, generally less than 20 W [52].

Formic acid is one of the most widely produced industrial chemical. It is used in various applications. Its use as a feed for polymer electrolyte fuel cell (PEMFCs) is particularly interesting and has been reported very recently. This type of fuel cell is called direct formic acid fuel cell (DFAFCs). Formic acid is particularly important because it is non toxic, has limited fuel cross over during the operation which is a serious concern in methanol and ethanol fuel cells. It also provides high practical power densities at low temperature [53-58].Formic acid is particularly important because it is non toxic, has limited fuel cross over during the operation which is a serious concern in methanol and ethanol fuel cells [59, 60].

**2.4 Mechanism of formic acid electro oxidation**

Major reactions occurring at the DFAFC are the oxidation reaction of formic acid at anode and reduction of oxygen which occurs at the cathode[61]. Cathodic reduction reaction mechanism is itself an important area of research and excellent reviews are available in open literature. Here, the anodic oxidation, that is, formic acid oxidation reaction will be considered. The anodic oxidation reaction is similar to that of combustion reaction of formic acid as shown in eq. (2.2).

$$HCOOH + \frac{1}{2}O_2 \rightarrow CO_2 + H_2O \qquad (2.2)$$

Electrons involvement is the only obvious difference in above formic acid oxidation and combustion reaction. Generally, two pathways for electro-oxidation of formic acid are accepted, differentiated by the intermediates involved. In first pathway named as 'direct oxidation pathway': formic acid undergoes through direct oxidation to $CO_2$ without producing the intermediate chemisorbed product. The other one is indirect pathway called '$CO_{ads}$ intermediate pathway': through this pathway CO intermediate produced by formic acid oxidation [51, 62- 63]. The two pathways are illustrated by the following two equations (2.3) & (2.4);

$$HCOOH \rightarrow X \rightarrow CO_2 + 2e^- + 2H^+ \qquad (2.3)$$

$$HCOOH \rightarrow X \rightarrow CO_{ads} + H_2O \qquad (2.4)$$

The in situ FTIR studies indicate that the reaction mechanism of Pt and Pd decorate Pt single crystals for formic acid oxidation reaction are different to each other. Pd has propensity to break the bond between O–H of HCOOH molecule in the potential region (0–0.9V vs. RHE) while Pt at lower potential, seems to have a tendency to break both the C–O and/or C–H bond as well as the O–H bond at high potentials. Consequently, on the surface of Pd metal formic acid oxidation takes place exclusively through the dehydrogenation reaction pathway, while on the surface of Pt the dehydration reaction step is predominant at low potentials [64].

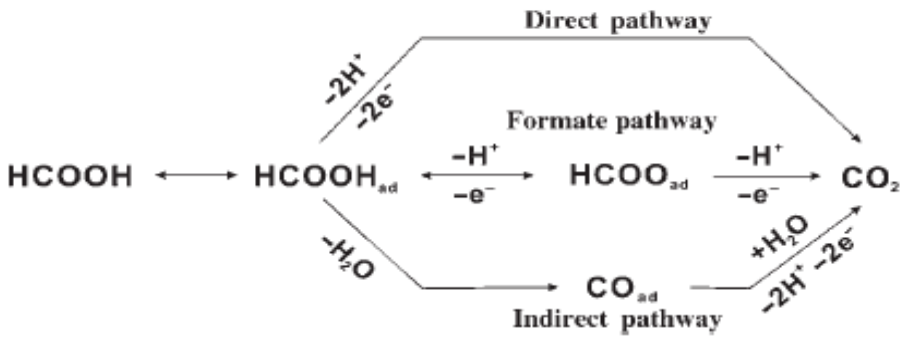


Figure2.6:Tentative reaction scheme for electro oxidation of formic acid[61]

**2.5 Electrocatalysts for formic acid oxidation**

An elctrocatalyst participates in an electron transfer reaction (at an electrode) and facilitates acceleration of a chemical reaction. Both the electron transfer and chemical kinetics proceed to be fast using an efficient electrocatalyst. Moreover, an efficient electrocatalyst also display a good thermodynamic match between the redox potential ($E_0$) for the electron transfer reaction and chemical reaction that is being catalyzed. These factors can be optimized by chemical tuning of the electrocatalyst for a particular reaction. Electrocatalyst are typically screened for their redox potential, current efficiencies, electron transfer rate and chemical kinetics in order to determine the best overall catalyst [65].

In the general sense, electrocatalyst are electron transfer agents that ideally operate near the thermodynamic potential of the reaction to be driven, $E_0$ (products/substrates). Thus, optimal electrocatalyst offers critical solutions to lower the over potentials, enhances selectivity, and increases the kinetics of formic acid electro oxidation reaction.

Regardless, DFAFC systems have achieved high power densities still these are facing several severe challenges which are not associated with $H_2$ fuel cells. The most significant challenges include poor electro oxidation kinetics cell compared with pure hydrogen especially for Pt-based electrocatalysts and fuel crossover. The reason for low anodic reaction kinetics is the tendency for methanol and formic acid oxidation to proceed though an indirect pathway with the formation of –CO type intermediate species which poisons Pt based catalysts materials. Among all other active metals, Pt and Pd are the most investigated for formic acid electro oxidation [66].We will discuss each of them separately in the following sections.

### *2.5.1 Platinum (Pt) based electrocatalysts*

Pt is considered one of the most attractive metals for methanol and ethanol electro oxidation because of its intrinsic high electro activity. With the evolution of DMFC, mono catalytic Pt catalysts have extensively used due to its single step oxidation mechanism described by most of researchers. Jianyu et al. (2012) studied the electro oxidation of Pt electrocatalyst in methanol electrolyte solution and found that for methane oxidation reaction, Platinum (II), the most active oxidation state of platinum, remain consistent during the oxidation of O-H bond of methane to generate power. According to Jianyu, methane oxidation yield of Pt electrocatalyst is greater than 70% on one pass operation which is 202mA$mg^{-1}$ and Pt catalyst also reported the low temperature, direct one step oxidation conversion of methane [67].

For formic acid oxidation Pt metal undergoes through dual pathway mechanism. Catalytic performance and stability for DFAFC as compared to methanol oxidation is still

not impressive because it is observed, that Pt is easily poisoned by CO during redox operation even at lower potential. Formic acid electro oxidation on the surface of Pt proceeds via indirect or dual mechanism stepsin which CO produced as intermediate which poisons the Pt catalysts [62-63].

Yang et al. in (2011) [17] predicted the dual pathway mechanism of Pt based electro catalyst for formic acid oxidation shown in the Fig 2.7. The first current density peak in CV curve at relatively low potential 0.4 - 0.5V verses Ag/AgCl, represents the direct pathway oxidation while second smaller current density peak occurring at 0.9V high potential represents the dual or indirect mechanism pathway. Yang also demonstrated that direct step oxidation is only viable on active and freshly reduced surface of Pt metal. But when Pt catalyst is subjected to formic acid oxidation for at least 5 minutes in open circuit, the intermediate poisoned CO product strongly adsorbed on Pt surface which cannot be detached until the dissociation of water occurs on surface at much higher potential.Therefore, Yang and his coworkers were agreed that for Pt catalyst, the electro oxidation of HCOOH proceed predominantly via the indirect oxidation mechanism.

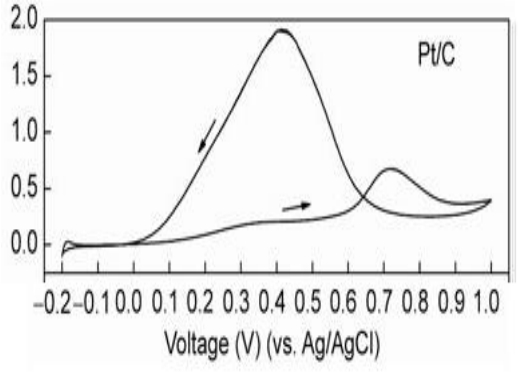


Figure 2.7: Cyclic voltammetry for Pt/C [17]

Fast deactivation of Pt electrodes due to CO adsorption led many investigations to improve its durability. Usually ad atoms are used. Pt is modified with another metal to improve its activity. Generally, there are two routes for modifications. In the first modification method, ad metals can be employed with Pt metal that allow low potential dissociation of water through a bi-functional mechanism and also assist the indirect pathway. The 2nd and preferred route, ad metals that facilitate the direct oxidation pathway to proceed unconstrained such as electronic modification can be employed. In any method, facilitation of the direct pathway is preferred as it occurs at low potential window (0- 0.5 V vs standard RHE), which is most appropriate for DFAFCs[61].

### *2.5.2 Pd based electrocatalysts*

Palladium is considered the most active metal for formic acid electro oxidation [61]. Electro oxidation dual pathway mechanism of Platinum is known for formic acid oxidation but for palladium metal mechanism there are still speculations. This could be partly due to the fact that there has not been any intermediate detected on Pd. However, it is generally agreed that the electro oxidation of formic takes place predominately by

direct pathway system having an active intermediate and in contrast to Pt, oxidation peak produced at very low potential usually between 0.1-0.4V. Mainly the reason is that no intermediate such as CO are produced and adsorbed on the surface. That is why no peak is observed at 0.8V which is supported by numerous studies [57-60, 63].

Bernard et al. (1984) first time investigated the catalytic activity of Pd catalyst for formic acid oxidation through theoretical modulation techniques. They resulted that with Pd metal oxidation reaction proceed 8 to 17 times faster than that using no catalyst and other active metals like Pt, Ru, Rd. Bernard suggested the reason that formic acid chemisorbed one site of Pd metal surface and oxygen is dissociatively chemisorbed on other type sites of the surface. While the surface reaction occurs between chemisorbed formic acid and chemisorbed oxygen atoms (Langmuir-Hinshelwood mechanism) [68].

H. Li et al. (2007) [69] analyzed the counterpart catalytic performance of Pd/C electrocatalyst and reported 22.32mAcm$^{-2}$ current density at 380mV peak potential which is 3 times greater than Pt/C (8.04 mAcm$^{-2}$) for formic acid oxidation reaction. Negative shift in potential is reasoned by author as small particle size of Pd nano particles which is around 3.3 nm, large specific available surface area of active Pd metal for oxidation process and less involvement of water molecules which generate during oxidation reaction. Experimental CV curves of Pd and Pt are shown in Fig. 2.8.

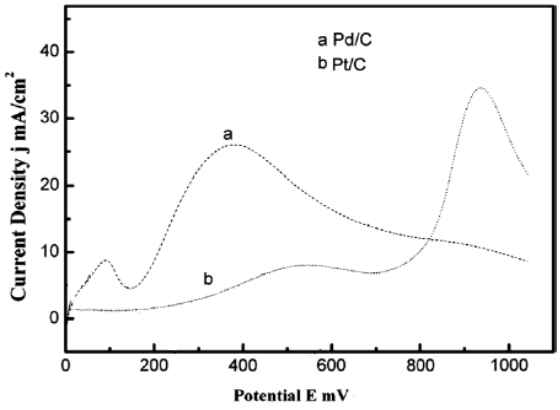


Figure 2.8: Cyclic voltammetry for Pd/C [69]

In above figure, Li explained that the 700mV higher onset potential of Pt/C electro catalyst is due to the oxidation of formic acid to $CO_2$ with the formation of CO reactive intermediate product. While lower onset potential of Pd/C (12 mV) catalyst revealed different parallel oxidation pathway than Pt/C in which HCOOH rapidly adsorbed on catalyst surface and directly oxidized to $CO_2$without intermediate adsorption. On the basis of lower onset, peak potentials and higher current density, author concluded that Pd based catalysts are best for formic acid electro oxidation reactions.

Similarly, Pd metal activity also investigated by Zhao et al. [70] in 2012 and Marjan et al. (2013) [71] in 0.5M HCOOH and 0.5M $H_2SO_4$solution by using different support materials and different reducing agent respectively. Both investigators reported that Pd catalyst showed current catalytic activity between 0.2-0.4V (vs. SHE) active potential. Zhao reported 400mA/mg current density using CNT support while Marjan reported maximum 1870mA/mg using SDS reducing agent.

### *2.5.3 Bimetallic Catalyst*

From above discussion, it is clear that poisoning of Pt metal surface by CO, intermediate product is the main reason for low kinetics during formic acid electro oxidation reaction. To solve this problem and to enhance the activity of Pt and Pd based electrocatalysts, advance electrocatalyst bi-functional design mechanism has been proposed. In this pathway, an ad metals such as Pd, Ru, Ni, Fe, Sn, Au, Co, Cu, $CeO_2$, $NiO_x$ and $TiO_2$ which have ability to assist the $CO_2$ oxidation by providing oxygen vacancy is used nearby the poisoned site of Pt catalyst surface [52, 58-66].

E. A. Baranova et al. (2010) [72] prepared Pd-Pt electrocatalysts by polyol method and tested their catalytic activity in 0.1M HCOOH and 0.1M $H_2SO_4$ solution in comparison of Pd and Pt catalysts alone. Baranova concluded that alloying of Pd metal has changed the surface electronic stateof Pt metal, resulting in an ensemble effect, which has reduced the bimetallic catalyst poisoning and increased the activity and stability of the PtPd electrocatalyst. As shown in Fig.2.9, CV scans of alloyed catalysts with varying ratios of Pt and Pd showed better current activity than non alloyed electrocatalysts. PtPd/C electrocatalyst exhibited 0.82A/mg current density, 5.1 and 4 times higher Pd/C and Pt/C respectively. Peak potential of PtPd bimetallic catalysts shifted positively.

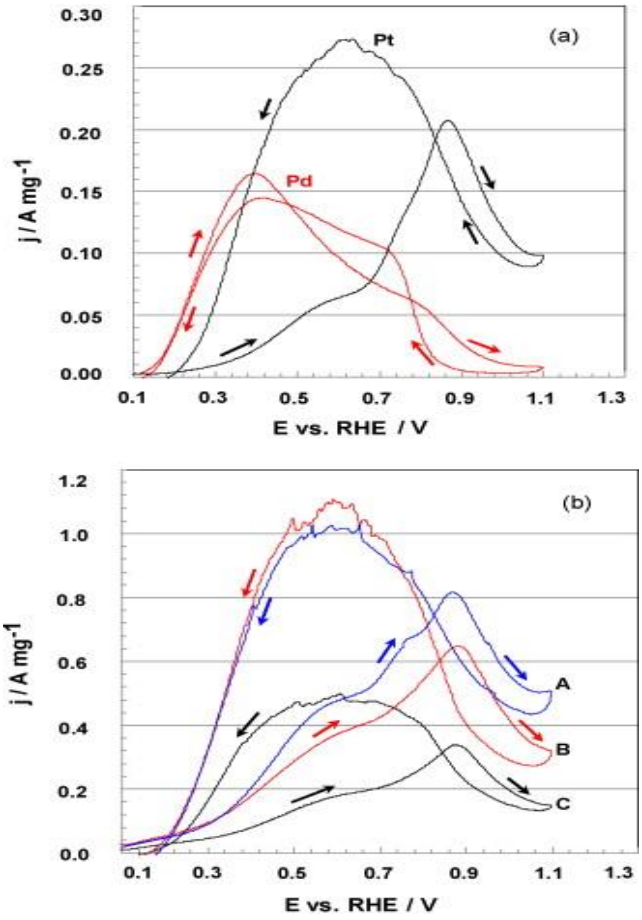


Figure 2.9: CVof carbon supported Pt and Pd (a); and PdPt nanoparticles (b): A, $Pd_{0.33}Pt_{0.67}$; B, $Pd_{0.5}Pt_{0.5}$; C, $Pd_{0.67}Pt_{0.33}$ in 0.1M HCOOH+0.1M $H_2SO_4$, 10mV$s^{-1}$[72].

Baranovaand his co worker also investigated the stability and lifespan effect by alloying Pt and Pd metal by using CA measurements as shown in Fig.2.10. They reported that catalytic activity of all catalysts initially decreased considerably, indicated the blockage of surface active sites by intermediate adsorption on surface.Then addition of Pd to Ptalloying, initially lowered the catalyst stability as compared to the pure single metal Pd and Pt catalysts.However, thePd stabilized of the overall performance of the bimetallic catalysts and showedhigher steady state current activity and stability of catalysts as shown in following figure.

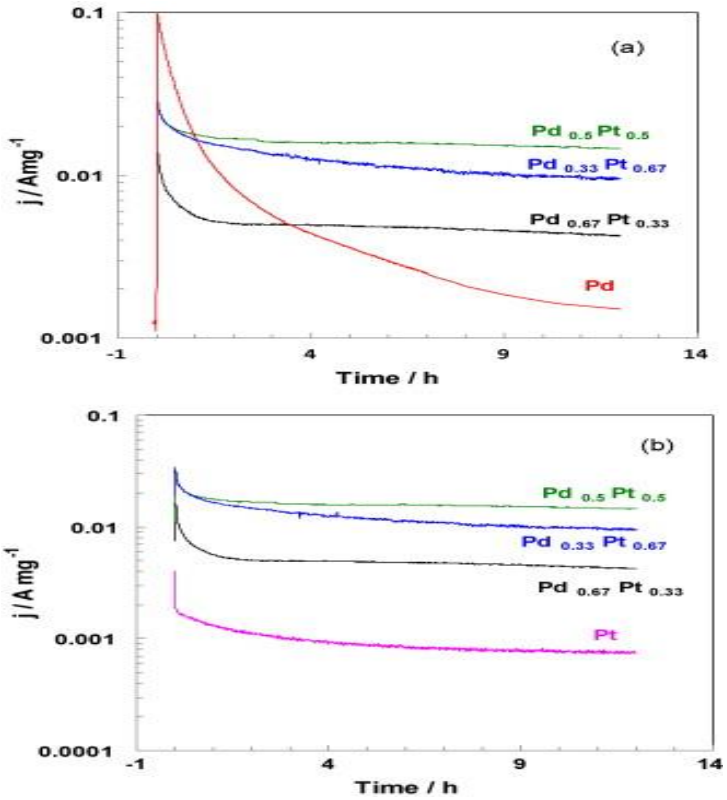


Figure 2.10: CA of the carbon supported PdPt nanoparticles in 0.1M HCOOH+0.1M $H_2SO_4$ at 0.3V.

R Wang et al. (2013) studied the NiPd catalyst performance towards formic acid oxidation in 0.5M HCOOH and 0.5M $H_2SO_4$ solution. He reported that among different ad metals catalysts, PdNi bimetallic electrocatalyst has attracted most attention due to its ability to enhance the active surface area of the Pd catalysts, offering more active sites necessary for the formic acid dissociation to $CO_2$, but also resulted electronic structure modification of palladium by Ni alloying atoms which provided the surface desorption facilities for the removal of poisoning intermediates adsorbed on Pd surface [73].

In 2013, A. S. Bauskar et al. [74] decorated the carbon supported platinum catalyst with Bi ad metal in order to enhance the formic acid activity of Pt electrocatalyst.

He analyzed that Bi addition has increased 54% of hydrogen adsorption and desorption ability as compared to Pt/C catalyst. $H_2$ surface adsorption was directly linked with the catalytic performance and onset potential also shifted more than 0.1V towards negative direction. The results reported by author, indicate that Bi decorated Pt nanoparticles have excellent electrochemical properties for the electro-oxidation of formic acid (high electro-catalytic activity and excellent stability) due to a combination of the electronic effect and third-body effect, thereby promoting the non-poisoning direct electro-oxidation reaction pathway. Based on position of CO stripping peak for 15% Bi coverage, $Pt–CO_{ads}$ bond strength decreased for 3.4 nm Pt/C whereas no shift was observed in the $Pt–CO_{ads}$ bond strength for 2.4 nm Pt/C. According to Bauskar, surface morphology, particle size and particle distribution also enhanced with the effect of Bi alloying.

Comparative combined catalytic performance of PtAu electrocatalyst was investigated by D Basu et al in 2011[75] in comparison of Pt/C and Au/C catalysts towards glucose electro oxidation reaction. Basu presented that current activity of PtAu/C catalyst ($5mA/cm^2$) was more than Pt and Au mono catalysts. Onset and peak potentials are the electrochemical properties which effected greatly by the addition of Au metal particles. 0.2V negative shifted in peak potential was observed in PtAu/C electrocatalyst after the alloying modification. Pseudo steady state stability of alloyed catalyst also enhanced which lied at $1.2mA/cm^2$ after 1 hr time.

In 2009, B Peng et al. found that electrocatalytic activity of PtSb/C exceed with doping modification of Pt with Sb particles. Bimetallic catalyst showed $14mA/cm^2$ current density at 0.27V peak potential which is 8 times greater than Pt/C electrocatalyst in 0.5M HCOOH solution with sulphuric acid. Negative shift in open circuit and onset

potential demonstrated that Sb addition changed the structure orientation of Pt catalyst which increased it's desorption ability and reduced the poisoning of active site of Pt metal. After analyzing surface and electrochemical properties of PtSb bimetallic catalyst, Peng concluded that Sb is one of best ad metal for Pt active metal which enhanced the anodic oxidation of formic acid [76].

G A. El-Nagar et al. (2013) [77]addressed the activity of binary nanoparticles Pt and $NiO_x$ electrocatalyst deposited on glassy carbon (GC) electrodes for formic acid electro oxidation. Results predicted that Pt catalyst showed two oxidation current peaks at ca. 0.25 and 0.65V vs. Ag/AgCl/KCl corresponding to the direct and indirect oxidation of HCOOH, respectively. Modified PtNiO catalyst showed superb current activity which is 7 times higher than nano Pt/GC catalyst at lower onset potential. A credible explanation for the observed catalytic activity is anticipated that nickel oxideacts as a catalytic mediator which facilitated the direct oxidation of formic acid and enhanced the retrieval of the Pt active sites via the oxidative removal of the adsorbed poison CO to $CO_2$.The proposed binary catalyst showed a satisfactory long-term stability and tolerance against the poisoning CO compared with nano-Pt/GC alone.

I. A. Rutkowska et al. (2013) examined the overall electrocatalytic activity of nano rods of tungsten oxide deposited on catalytic palladium nanoparticles (dispersed onto glassy carbon (GC) electrode) toward oxidation of formic acid in acid medium. The effect was particularly evident from the increase of chronoamperometric currents at a fairly low potential of 0.04V. Under such conditions, tungsten oxide nano rods seem to be partially and reversibly reduced not only to non stoichiometric hydrogen tungsten (VI,V) oxide bronzes ($H_xWO_3$, $0 < x < 1$) but also sub stoichiometric lower tungsten

(VI,IV) oxides ($WO_{3-y}$, $0 < y < 1$). Mutual interactions between tungsten oxides with Pd nanoparticles affect electrochemical characteristics of both components. The metal–oxide interactions, as well as high inhabitants of OH groups at the electrocatalytic interface (favoring oxidative removal of passivating CO adsorbates), are most likely responsible for the overall enhancement effect. In comparison to conventional electrodeposited microporous tungsten oxides, $WO_3$ nano rods, despite their small dimensions, are more robust and less hydrated [78].

In 2013, A. Ciftci et al [79] studied the decomposition reactions of ethanol and formic acid over a series of Au and Pt nano particle catalysts. $CeO_2$ nano rods and nano cubes served as model supports representing the {1 1 0} and {1 0 0} surfaces of $CeO_2$ nano crystals. Pt was more active than Au in low temperature (below 400°C) steam reforming, oxidation and decomposition (without an oxygen source) of ethanol. Similar trends were observed in the WGS reaction. Different from Au, for Pt the initial step of ethanol dehydrogenation to acetaldehyde is followed by the cleavage of the C-C bonds of acetaldehyde to $CH_4$ and CO due to the higher Pt-C bond strength when compared to that of Au-C. The catalysts supported on nano rod-shaped ceria were more active than those derived from nano cube-shaped ones in ethanol steam reforming and WGS reactions due to the abundance of OH species formed by activation of water on the oxygen vacancies in the $CeO_2$ {1 1 0} surfaces of ceria nano rod supported catalysts. Complete oxidation of ethanol to $CO_2$ and $H_2O$ was observed over the Pt and Au supported $CeO_2$ (rod) catalysts. For the former, complete oxidation took place starting from temperatures as low as 150°C. These catalysts were active for decomposition of formic acid starting from near-ambient temperatures ($T > 50$°C) up to 200°C, at which temperature HCOOH was

completely converted over all the catalysts. Au was more active and it selectively dehydrogenated formic acid into $CO_2$ and $H_2$. The intrinsic activity of the CN-leached $Au/CeO_2$ (rod) catalyst containing highly dispersed sub-nanometer Au clusters was higher than the parent catalyst. Pt, on the other hand, showed lower selectivity toward the dehydrogenation pathway due to its higher activity in WGS reaction and enhanced Pt-O bond strength resulting in decarbonylation of formic acid.

M. S. El-Deab et al. (2012) y proposed a novel binary catalyst system (composed of metal/metal oxide nanoparticles) as a promising electrocatalyst in formic acid oxidation. The electro-catalytic oxidation of formic acid is carried out with binary catalysts of Pt nanoparticles (nano-Pt) and manganese oxide nano rods (nano-$MnO_x$) electrodeposited onto glassy carbon (GC) electrodes. Cyclic voltammetry (CV) measurements showed that unmodified GC and nano-$MnO_x$/GC electrodes have no catalytic activity. While two oxidation peaks were observed at nano-Pt/GC electrode at ca. 0.2 and 0.55 V (corresponding to the direct oxidation of formic acid and the oxidation of the poisoning CO intermediate, respectively). The combined use of nano-$MnO_x$ and nano-Pt results in superb enhancement of the direct oxidation pathway. Nano-$MnO_x$ is shown to facilitate the oxidation of CO (to $CO_2$) by providing oxygen at low over-potential. This leads to retrieval of Pt active sites necessary for the direct oxidation of formic acid. The higher catalytic activity of nano-$MnO_x$/nano-Pt/GC electrode (with Pt firstly deposited) compared to its mirror image electrode (i.e. with $MnO_x$ firstly deposited, nano-Pt/nano-$MnO_x$/GC) reveals that the order of the electro deposition is an essential parameter [80].

## 2.6 Support materials

Most important criteria for selection of any porous support material for electrochemical application are surface area and electrical conductivity. Electrodes require an electrically conductive material to provide a conductive path for the electrons to travel from the reaction site to the current collector. Often, the electrocatalyst serves the dual purpose of facilitating the electrochemical reaction and transporting the electrons. However, when the electrocatalyst is a precious metal such as platinum, it is advantageous to support it on a conductive substrate such as carbon. This enables the expensive electrocatalyst to be highly dispersed, thus minimizing the amount of precious metal without sacrificing catalytic activity. Dispersion of precious metals onto inexpensive supports is the same approach used in heterogeneous catalysts for non-electrochemical reactions. In these cases though, the support is often an insulating metal-oxide material that has high surface area and promotes catalytic activity (i.e., enhanced catalyst-support interactions). In electrochemical applications (e.g., proton exchange membrane fuel cells), the typical support material is carbon due to its high surface area and high electron conductivity rather than any enhanced catalyst-support interactions. However, carbon-supported electrodes that operate at voltages above ~0.9 V in the presence of water are known to undergo carbon corrosion. Corrosion of the support can create a loss of electrical contact with the catalyst particle, thus decreasing the performance of the cell.

Maiyalagan et al. [81] reported that the nitrogen containing carbon nano tube-supported Pt shows a ten-fold increase in the catalytic activity compared to the commercial Vulcan supported Pt. The higher electrocatalytic activity of Pt/N-CNT was ascribed to the higher dispersion and a good interaction between the support and the Pt

particles. According to the authors, the nitrogen functional group on the carbon nanotubes surface intensifies the electron withdrawing effect against Pt and the decreased electron density of platinum facilitate oxidation of methanol. However there is an optimum amount of nitrogen content necessary for increased activity for methanol oxidation. This optimum amount is around 10% which shows that the isolated nitrogen sites favour the better dispersion of Pt and also controls the metal crystallite sizes.

Arbizzani et al. [82] prepared two carbon cryogels, named CC1 and CC2, with pore-sizedistribution centred at 6 and 20nm, respectively, by sol–gel R/F poly condensation. Electrodeposited PtRu on CC2-Nafion support with ca. 0.1 mg Pt $cm^{-2}$ displayed a good catalytic activity for methanol oxidation of 85mA$mg^{-1}$ Pt after 600 s at 492mV vs. NHE and 60°C in 0.5 M $H_2SO_4$and 0.1 M/$CH_3OH$ solution. The catalytic activity tests and XRD and SEM analyses demonstrated the stability of the prepared electrodes upon catalysis in the time scale of the measurements. The same authors prepared mesoporous cryo- and xero gel carbons, and investigated the catalytic activity of PtRu catalysts chemically and electrochemically deposited on such carbons. Cryo- and xero gel carbons presented higher specific total volume and surface area and, more importantly, higher mesoporosity than that of Vulcan. The carbon featuring the highest mesoporosity was the C5.7-500 cryo gel (prepared using a dilution factor, i.e. the water to gel precursors molar ratio, and a resorcinol to gelation catalyst molar ratio of 5.7 and 500, respectively), which exhibits 1.35 $cm^3g^{-1}$ and 285 $m^2g^{-1}$ meso-macropore specific volume and surface area, respectively, and such values increase by 20% after activation at 400°C.

The long-term performance of PtRu particles supported on MWCNTs and on carbon black towards the methanol oxidation reaction was compared by Prabhuram et al.

[83]. They carried out chronoamperometry tests in 0.5 M H2SO4 solution containing methanol for 3000 s. The close observation of the chronoamperometry curves revealed that potentiostatic current decreases very rapidly for MWCNT-supported PtRu. According to the authors, this might be due to the higher deactivation of the Pt (1 1 0) crystallite phase by the $CO_{ads}$ species during the methanol oxidation reaction. At long times, however, although the current gradually decays forall the catalysts, the MWCNT-supported PtRu catalysts maintained a slightly higher current than the carbon black supported PtRu.

CNF-supported catalysts were prepared for use in fuel cells and their metal dispersion and catalytic activity was compared with that of other carbon supports. . Park et al. [84] obtained three types of CNFs by chemical vapour deposition method, i.e. ribbon-like, spiral-like and platelet-like. The surface areas of these CNFs were 85, 45 and 120 $m^2g^{-1}$, respectively. The diameter andlength of the GNF were 100–150 nm and 5–50 mm, respectively.

Activated carbon fibers (ACF) represent a novel kind of porous material, with high surface area (>1000 $m^2g^{-1}$), and the presence of a lot of functional groups on the surface. Bulushev et al. [85] characterized activated carbon fibers in the form of a woven fabric by temperature-programmed decomposition. TPD method showed the presence of two main types of functional groups on the ACF surface: the first type was associated with carboxylic groups easily decomposing to $CO_2$, and the second one corresponded to more stable phenolic groups decomposing to CO.

### *2.6.1 Ordered mesoporous carbon (OMC)*

The ordered mesoporous carbons have recently received great attention because of their potential use as catalytic supports in fuel cell electrodes. They have controllable pore sizes, high surface areas and large pore volumes. Nanoporous carbons with 3D ordered pore structures have been shown to improve the mass transport of reactants and products during fuel cell operation. MCM-48, SBA-1 and SBA-15 silicas were successfully used to synthesize carbons with cubic or hexagonal frameworks, narrow mesopore-size distributions, high nitrogen BET specific surface areas (up to 1800 $m^2g^{-1}$), and large pore volumes. There are various types of ordered mesoporous carbons. The most tested as fuel cell catalyst support is the ordered CMK-3 carbon [30].

The first ordered mesoporous carbon that was a faithful replica of the template was synthesized by Jun et al. [86] using SBA-15 silica as a template. This material consists of uniformly sized carbon rods arranged in a hexagonal pattern. CMK-3 synthesized by Jun exhibited large adsorption capacity; with a nitrogen BET specific surface area of about 1500 $m^2g^{-1}$ and total pore volume of about 1.3$cm^3g^{-1}$.CMK-3 has a primary pore size of about 4.5 nm, accompanied by micropores and some secondary mesopores. As previously reported, the pores with 3–8 nm size are useful for the fuel diffusion, but the Pt in these pores is considered not to contribute to the reaction for the PEMFC, because the particles of ionomer are larger than the pore diameters and the Pt cannot contact the ionomer.

Joo and co-workers [87] described a general strategy for the synthesis of highly ordered, rigid arrays of nanoporous carbon having uniform but tunable diameters (typically 6 nm inside and 9 nm outside). The resulting material supports a high

dispersion of platinum nanoparticles, exceeding that of other common microporous carbon materials. The platinum cluster diameter can be controlled to below 3 nm, and the high dispersion of these metal clusters gives rise to promising electrocatalytic activity for oxygen reduction.

Calvillo et al. [88] prepared functionalized OMC with a specific area of $570 m^2 g^{-1}$.An OMC supported Pt electrocatalyst was prepared by the impregnation method followed by reduction of Pt precursor with sodium borohydride. Fig.2.11 shows TEM images of platinum supported on functionalized CMK-3. According to the authors, platinum was well dispersed over the functionalized mesoporous support and its catalytic performance towards methanol oxidation improved when compared with carbon Vulcan XC-72. By an accurate observation of Fig. 2.11, however, it results the presence of some particle agglomeration. The better performance of the OMC supported catalyst, notwithstanding the presence of some particle agglomeration, was due to higher amount of mesopores in the support, aiding the reactant flow.

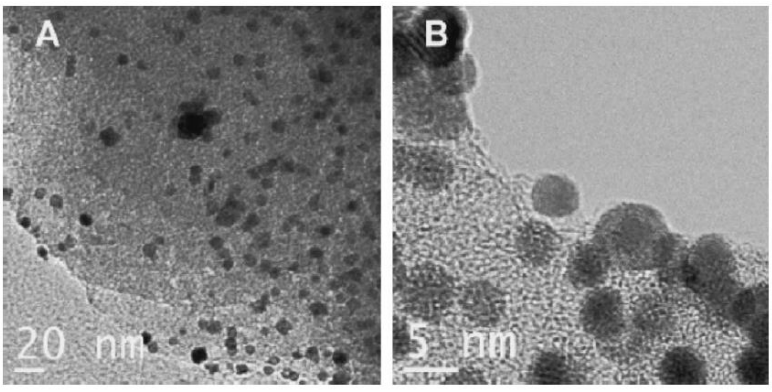


Figure 2.11: TEM images of platinum supported on functionalized CMK-3[18]

Jooet al. [89] prepared two OMC samples with hexagonal mesostructure from phenanthrene and sucrose by nano-replicationmethod using mesoporous silica as a template. Structuralcharacterizations revealed that both OMCs exhibited large BETsurface area and uniform mesopores, while the OMC synthesizedfromphenanthrene exhibited lower sheet resistance than the OMCderived fromsucrose. The Pt nanoparticleswere supported on bothOMCs with very high dispersion, as the particle size was estimatedunder 3 nm despite high metal loading of 60 wt%. In single DMFCtest, the OMC supported Pt catalysts exhibited much higherperformance than the commercial catalyst, which may beattributed to the high surface area and uniform mesopores networks of OMC.

## 2.7 Strategies and scope of works

The comprehensive literature review reveals that electro oxidation alcohol and acids can be carried out using variety of electrode catalysts. Mostly, methanol oxidation reactions are studied which proceeded via direct and indirect (dual) pathway mechanism depending on electrode metal using $H_2SO_4$ as electrolyte solution. Anodic current density and corresponding electrode potentials are the main parameters during electrochemical process which directly depend upon the type of electrode material (catalyst), nature of feed (oxidizing agent) and medium of electrolytic solution (acidic or basic). Attention is needed in order to oxidize feed mixture with high current efficiencies at lowest possible peak electrode potentials. So main challenges associated with the electrochemical oxidation includes: (1) to select such feed (formic acid, methanol, ethanol) which have lower oxidation temperature (2) to use electrode catalysts at anode and cathode which can oxidize the feed mixture at minimum electrode potential and can produce maximum current density.

As per the catalysts, most commonly bulk metals are mainly studied. On the other hand, oxides modified support materials has showed superior performance in most of electro catalytic oxidation processes. Therefore, there is wide scope of developing novel support catalysts using different metal oxides as support modifier.

The present research is focused on the development of the electrocatalysts for formic acid electro oxidation reactions (FAOR). In this regard, ordered mesoporous carbon modified with cerium oxide ($CeO_2$) and tungsten oxide ($WO_3$) are considered as potential support material, given its high surface area, superior long term stability, nano sized mesopores and pore volume favorable as support material for preparing bimetallic

electrocatalyst. After critical literal review, we found out that high performance OMC required more attention as support material for formic acid oxidation reactions. As per metals, Pt and Pd are considered because of their proven catalytic performance for fuel cell application.

# CHAPTER 3
# RESEARCH OBJECTIVES

The ultimate goal of this research was to develop low cost electrocatalyst(s) for direct formic acid fuel cell (DFAFC) applications. Towards the end, Ce/W modified mesoporous carbon supported Pt-Pd bimetallic catalysts have been investigated to achive high activity and stability using minimum amount of noble metals.

The following are the specific objectives of this research:

1. To synthesizeSBA-15 as the support material and modify it with Ce/W oxides and finally transform them to mesoporous carbon support by an in-situ method.

2. To synthesize bimetallic Pt-Pd electro catalysts using various (Pt-Pd)/support ratios.

3. To characterize the synthesized catalysts and support material using techniques such as X-ray diffraction spectroscopy (XRD), Scanning electron microscopy (SEM) and Energy dispersive X-ray spectroscopy (EDX), Transmission Electron Microscopy (TEM), Nitrogen adsorption isotherm analysis and Thermo gravimetric (TGA) analysis.

4. To evaluate the overall formic acid electro-oxidation performance of the prepared catalysts by cyclicvoltametry (CV) and chronoamperometry (CA) measurements.

# CHAPTER 4
# EXPERIMANTAL METHODS

## 4 Introduction

From the critical analysis of the literature, it has been found that the active metals, support materials and morphology determine the activity of the electrocatalyst. To achieve the stated objectives of this research work, experiments were designed and performed. In this chapter, experimental procedure for catalysts synthesis and their physical as well as electrochemical characterization are discussed in details.

## 4.1 Materials

Tetraethoxysilane (TEOS, $Si(OC_2H_5)_4$ 99 wt.%), sucrose ($C_{12}H_{22}O_{11}$, 98 wt.%) purchased from LOBA Chemical Pvt. Ltd. Cerium nitrate hexa hydrate ($Ce(NO_3)_3{\cdot}6H_2O$) extra pure,phosphotungstic acid ($H_3PW_{12}O_{40}$), Palladium nitrate dihydrate ($Pd(NO_3)_2 \,.\, 2H_2O$, 40 wt.%Pd), Hexachloro Platinic (IV) acid hexahydrate ($H_2(PtCl_6).6H_2O$, 40 wt. %), Sodium borohydrite ($NaBH_4$) were purchased from MERCK. Hydrofluoric acid (HF, 40 % wt.), sulphuric acid ($H_2SO_4$, 97–98 % wt.), ethanol ($C_2H_5OH$, 99.8 % wt.), hydrochloric acid (HCl, 37 % wt.), phosphotungstic acid hydrate (99.99 % metal) and 5 % Nafion ion Exchange resin were purchased from Sigma Aldrich. All chemicals were used as received, without any further treatment. Millipore Milli-Q system with resistivity >18 M_cm−1 was used to get ultrapure deionized (DI) water for the preparation of all aqueous solutions. Gases, $H_2$ in nitrogen (10 % vol.), 99.99 % pure $N_2$ and $H_2$ were supplied in cylinders by SiGas.

## 4.2 Electro catalysts preparation andtreatment

Oxides modified ordered mesoporous carbon (OMC) has been used as support materials for the catalysts synthesized in this work.Three steps involved in electrocatalysts preparation. In 1st step, SBA-15 were prepared by polymerization of TEOS using hard template method which impregnated with appropriate amount of Cerium salt by wetness impregnation method and then oxidized to produce $CeO_2$-SBA-15. In 2nd step, $CeO_2$-OMC support were synthesized by carbonization of sucrose which followed by the HF treatment for the complete removal of unconverted silica traces. In final step, bimetallic PtPd based electrocatalysts were prepared by loading Pt and Pd respective salts in cerium modified mesoporous carbon support material using borohydride reduction method. All three synthesis steps were discussed as follows,

### *4.2.1 Metal oxides-SBA-15 synthesis*

SBA-15 was prepared by polymerization of Tetraethylorthosilicate (TEOS) by using hard-template synthesis method [90]. In this method, 1g, structure directing agent Pluronic P-123 ($EO_{20}PO_{70}EO_{20}$- tri block copolymer) was dispersed in 30ml distilled water and stirred at room temperature for 4 hrs. Stirring was continued after addition of 120ml of 2M hydrochloric acid solution for further 2 hrs at 40°C. Then 1.5g TEOS was added in above suspension and kept the solution under 1 day continuous stirring at the same temperature conditions. The resulting gel was aged @ 130°C for 24 hrs which followed by filtration and several time washing with deionized water and dried at 100°C overnight. For the preparation of $CeO_2$-SBA-15 and $WO_3$-SBA-15, specific amount of metal salts (10 wt. %) was incorporated with SBA-15 by wet impregnation method. SBA-15 was impregnated with pore volume deionized water solution of metal oxide precursor.

The solutions were stirred for 24 hrs at room temperature and then evaporated to get dry powders. Finally, the grinded powder was oxidized under air supply at 450°C for 4 hrs to get stable $CeO_2$-SBA-15 and $WO_3$-SBA-15. Schematic procedures for synthesis of SBA-15 and Metal oxide-SBA-15 are shown in Fig 4.1 & 4.2 respectively.

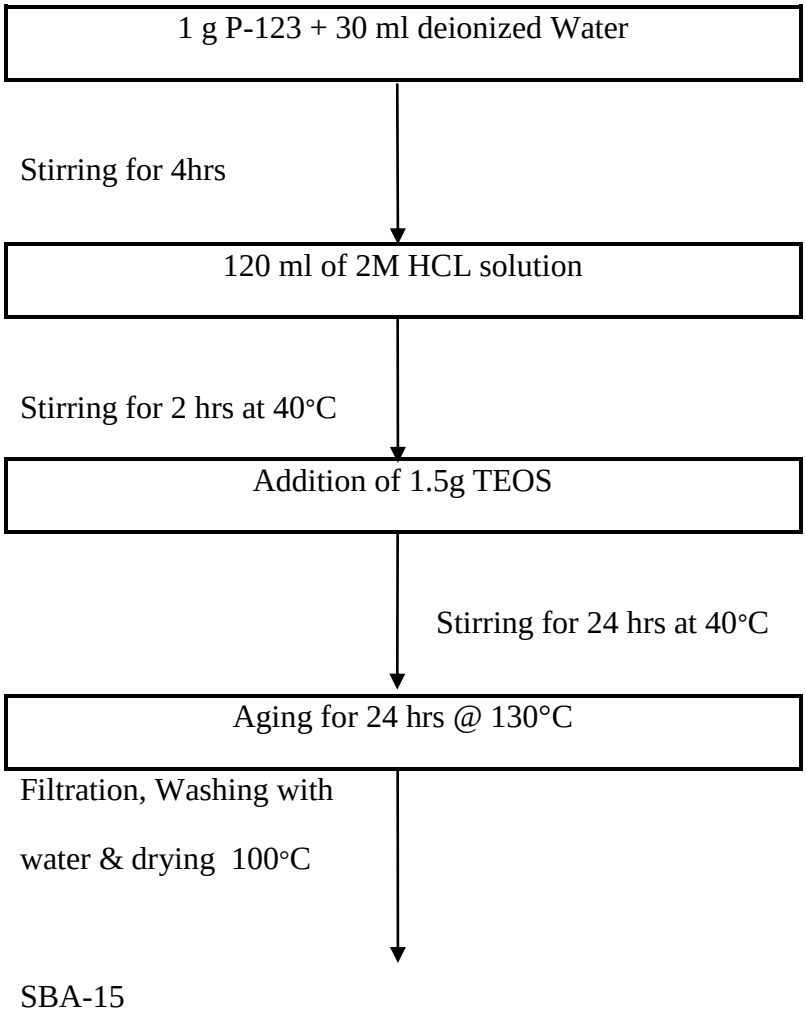


Figure 4.1: Synthesis Procedure for SBA-15

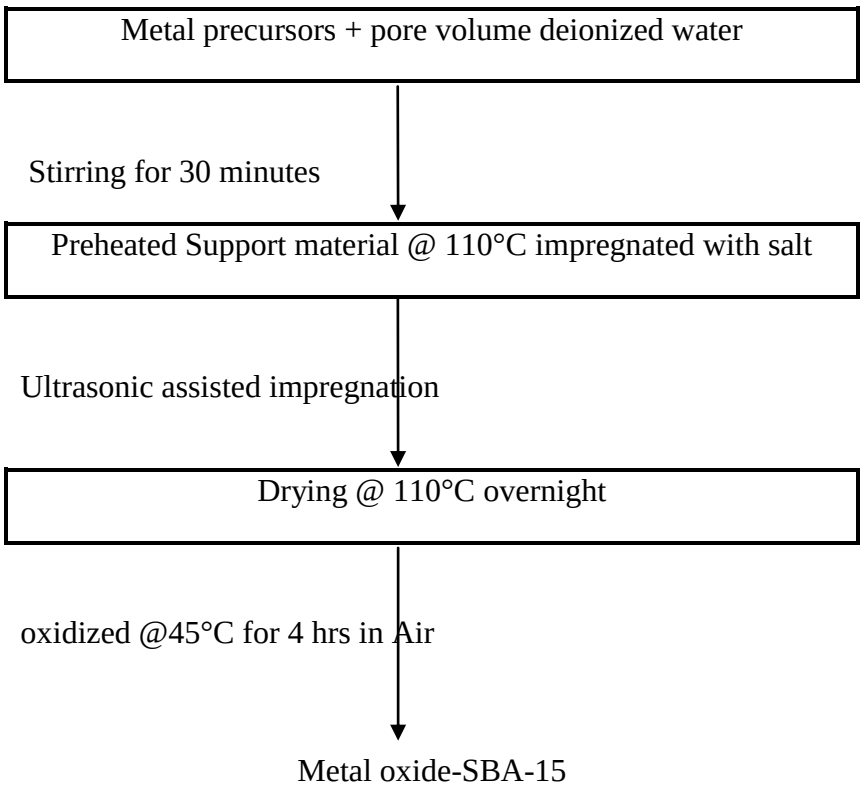


Figure 4.2: Synthesis Procedure for Metal oxide-SBA-15

### *4.2.2 $WO_3$/$CeO_2$-OMC support synthesis*

Metal oxide modified ordered mesoporous carbon support has prepared by hard template method. This method is unique due to its simplicity and the products obtained, are of uniform shape and required size. Oxides-OMC was produced by Carbonization of sucrose into mesopores of the SBA-15 as reported by Wang et al. (2005) [91].In this procedure, 1.0 g of SBA-15 silica incorporated with $CeO_2$ and $WO_3$separately, was added to a solution containing 1.25 g of sucrose, 0.14 g of sulphuric acid and 5.0 g of deionized water. The resulting suspensionwas kept in oven for 1 hr at 100 $^{\circ}$C, subsequently; the temperature was increased to 160 $^{\circ}$C @ 2°C/min heating rate and maintained at for another 6 hrs.In order to completely fill the internal pores of the SBA-15 silica with the carbon precursor, the heating procedure was repeated after the addition of 0.8 g of sucrose, 0.09 g of $H_2SO_4$ and 5.0 g of $H_2O$. In this process polymerization of the sucrose take place. Obtained black powder was heated in presence of $N_2$flow in a tubular furnace at 800°C at a very small heating rate of 1°C/min for 5 hrs and then cooled down @ 2°C/min. In this step carbonization of the polymerized sucrose was completed. The dark black powder then treated with 5% hydrofluoric acid (HF) solution to remove the silica template traces and subsequently washed with deionized water many times. The process was completed with drying at 100°C for 4 hrs and oxides incorporated ordered mesoporous carbon obtained which grinned and used as support material.

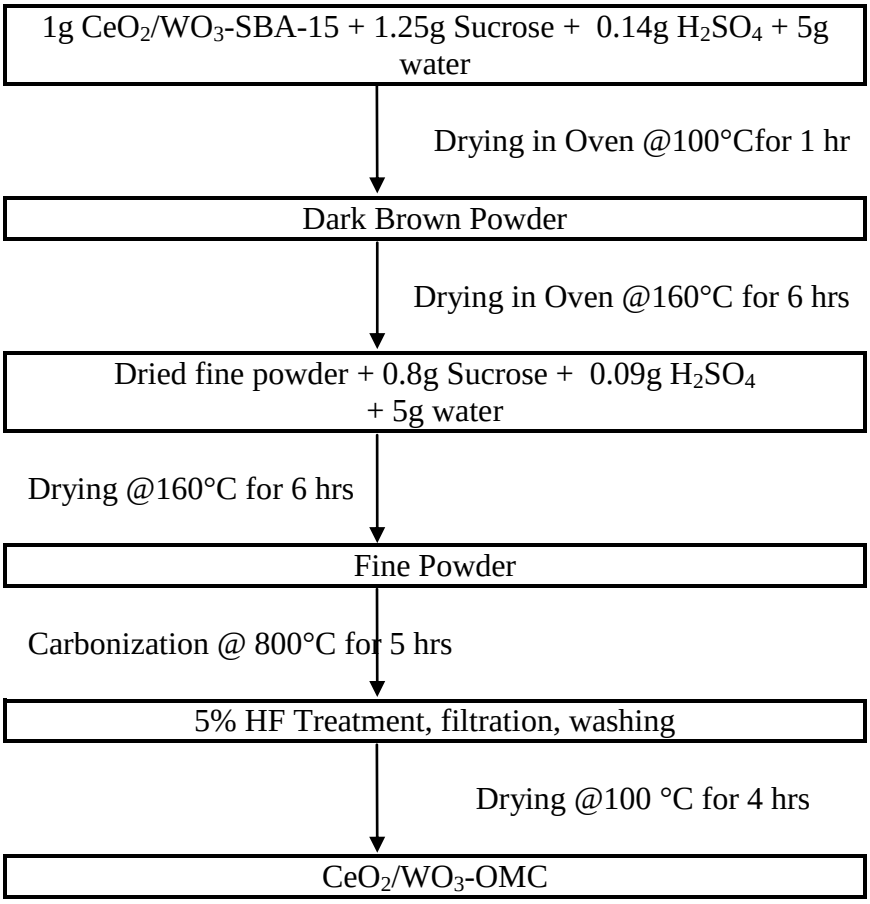


Figure 4.3: Synthesis Procedure for Metal oxide-OMC

### *4.2.3 PtPd/$CeO_2$/$WO_3$-OMC bimetallic electro catalysts synthesis*

Borohydride reduction method is standard method for synthesis of fuel cell electrocatalysts in which $NaBH_4$ is used as reducing agent. In this method,required amount of metal salts (Palladium nitrate and hexachloro Platinic acid), which used as precursor, were added drop wise in a constant stirring suspension made by suspending appropriate amount of preheated support $CeO_2$/$WO_3$-OMC, in 30 ml deionized water. The resulting suspension was first sonicated and then mechanically stirred for 3 hrs. Then slowly add 120 mg (3 times molar ratio of active metals) freshly prepared solution of $NaBH_4$ in suspension and set for another 4 hrs stirring to allow complete reduction of Pd and Pt salts at room temperature. Appropriate amount of sodium citratesolution, used as stabilizer, was added in suspension with vigorous stirring and allowed overnight stirring. Then the solid material was recovered by centrifuge, washed with water several time and dried at 110°C for 4 hrs. Synthesis procedure is shown in Fig4.4

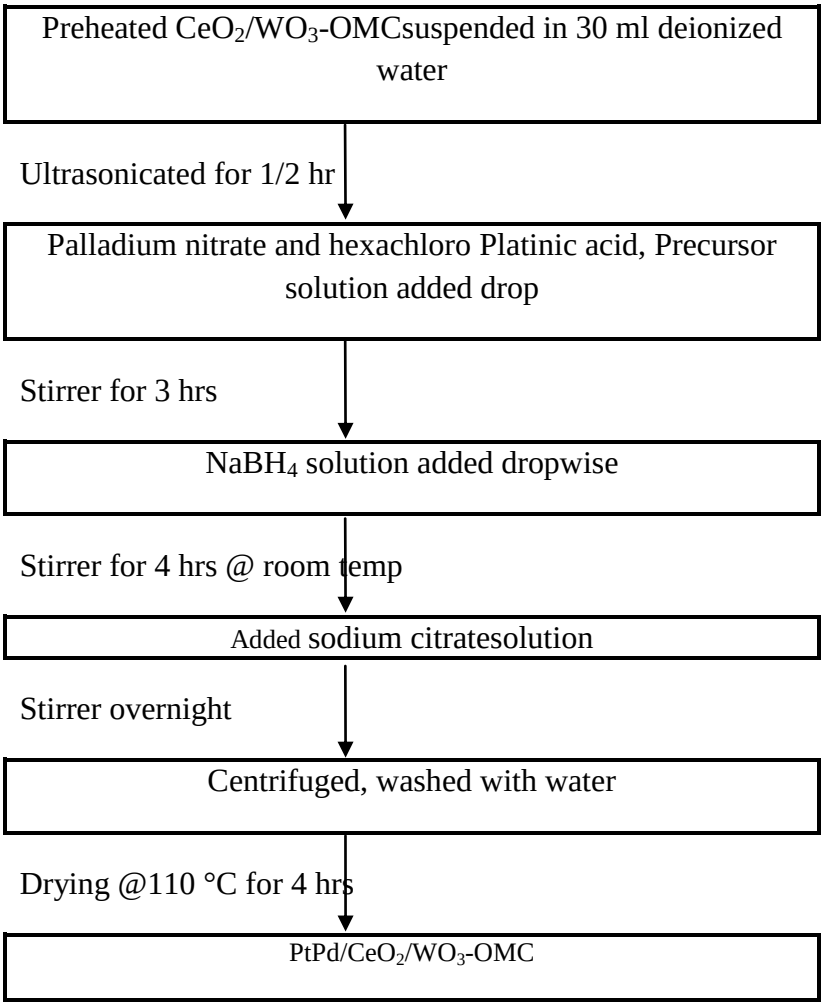


Figure 4.4: $NaBH_4$ reduction method for Metal oxide-OMC

### 4.3 Ordered mesoporous carbon based electrocatalysts

Oxides modified OMC was used as support material to synthesize platinum and palladium electro catalysts. Single metal as well as binary catalysts were synthesized. Details of the catalysts as well as their synthesis method are summarized in the Table 4-1.

Table 4-1: Catalyst synthesized in this work and their synthesis procedure

| **Support Material** | **Metals loaded 20 Wt. %** | **Electrocatalysts** | **Synthesis Method** |
|---|---|---|---|
| OMC | Pd | Pd/OMC | Borohydride reduction Method |
| $CeO_2$-OMC | Pd | Pd/ $CeO_2$-OMC | Borohydride reduction Method |
| $CeO_2$-OMC | Pd:Pt::3:1 | $Pd_3Pt_1$/ $CeO_2$-OMC | Borohydride reduction Method |
| $CeO_2$-OMC | Pd:Pt::1:3 | $Pd_1Pt_3$/ $CeO_2$-OMC | Borohydride reduction Method |
| $CeO_2$-OMC | Pt | Pt/ $CeO_2$-OMC | Borohydride reduction Method |
| $WO_3$-OMC | Pd | Pd / $WO_3$-OMC | Borohydride reduction Method |
| $WO_3$-OMC | Pd:Pt::1:1 | $Pd_1Pt_1$/ $WO_3$-OMC | Borohydride reduction Method |
| $WO_3$-OMC | Pd:Pt::2:1 | $Pd_2Pt_1$/ $WO_3$-OMC | Borohydride reduction Method |
| $WO_3$-OMC | Pd:Pt ::1:2 | $Pd_1Pt_2$ / $WO_3$-OMC | Borohydride reduction Method |

## 4.4 Physical characterization

The synthesized elctrocatalyst and support material were characterized for their morphology which includes particle size and its dispersion, composition, and surface area and pore volume. These properties reveal very important features of the catalysts and bear direct relationship with their activity. In this work following techniques have been used for characterization:

X-ray diffractogram (XRD)

Thermo Gravimetric Analysis (TGA)

Scanning Electron Microscopy (SEM)

Transmission Electron Microscopy (TEM)

Surface area and Pore Volume (BET & BJH)

### *4.4.1 X-ray diffractogram (XRD)*

X-ray diffraction is the most of the widely used technique to characterize materials. It is a non-destructive technique that reveals the detailed information about the chemical composition and the crystalline phase of synthesized materials. Higher amount of crystalline materials mean higher active surface are and thus the enhanced catalytic Activity. The XRD patterns were obtained from 2-theta scanning diffractometer. It scanned from 4 to 80°. The obtained XRD patterns were compared with the patterns of International Center Diffraction Data (ICDD) or formerly known as Joint Committee on Powder Diffraction Standards (JCPDS).

Fine powdered samples were spread onto a glass slide using double sided sticky tape and X-ray diffractograms were collected using a Smart Lab (9kW) Rigaku XRD X-ray diffraction X-ray diffractometer, with a diffraction angle range 2θ = 20–80° using Cu Kα radiation. From the resulting diffratogram the crystallite size (d, nm) was estimated using the Scherrer equation,

$$d = \frac{0.9\lambda}{\beta \cos\theta} \tag{4.1}$$

where**λ** is the X-ray wavelength (1.54°A), **θ** is the Bragg angle of the peak of interest and **β** is the line broadening measured from the increased peak width at half height through a Gaussian fit obtained from Origin plotting software. The analysis was done by PDXL software which uses database provided by ICDD.

### *4.4.2 Scanning Electron Microscopy (SEM)*

Scanning Electron microscopy is a powerful visualization tool for the investigation of catalyst morphology including particle size, pore size, structure, surface characteristics and dispersion of impregnated metals on the catalyst support. EDX was carried out to find out the composition of the catalyst.

The morphologies of the support and catalysts were investigated by using a scanning electron microscope (JEOL JSM-6460LV) operated at 20 kV equipped with energy dispersive X-ray (EDX).

### *4.4.3 Transmission Electron Microscopy (TEM)*

TEM is used to examine the structure, composition, or properties of a specimen in submicroscopic detail. One can see objects to the order of a few Angstrom ($10^{-10}$ m). Using TEM offers the advantage of increased magnification and resolution. The TEM passes an accelerated electron beam through a thin sample (50-300°A). Some of the electrons are scattered by the atoms in the sample. A phase distortion is created, resulting in a phase contrast that is used to create the image. The TEM enables the operator to see the "inside" of the sample rather than the surface.

In this work TEM was done at King Abdullah Institute of Nanotechnology (KIAN) at king Saud University. TEM images were obtained with ultra-high resolution FETEM (JEOL, JEM-2100F) at an accelerating voltage of 200 kV.

The sample for both TEM and SEM was prepared by one milligram of pre reduced catalyst was sonicated in 10 ml of ethanol for 30 minutes and then a drop of the suspension was placed on a an aluminum foil which was mounted on the sample holder by means of a double sided adhesive tape. In order to facilitate charge transfer for titania based catalysts, a thin gold film is deposited on the sample using plasma deposition. No such coating was used for mesoporous carbon.

### *4.4.4 Thermo gravimetric Analysis (TGA)*

Thermo gravimetric analysis or thermal gravimetric analysis (TGA) is a type of testing performed on samples that determines changes in weight in relation to change in temperature. Such analysis relies on a high degree of precision in three measurements: weight, temperature, and temperature change. Approximately 5 mg of sample was placed

into an aluminum sample pan for TGA using an empty aluminum pan as a reference. All TGA were recorded on a Shimadzu TGA-60 between 25°C and 800°C at the default ramp rate of 10°C/min in air atmosphere. TGA was used to find the optimum calcination temperature of the supported catalyst materials as well the metal loading on the OMC support.

### *4.4.5 Surface Area & Pore Volume*

Surface area and pore volume were evaluated by the Brunauer, Emmett and Teller (BET) analysis of the support and the synthesized catalysts was carried out using Micromeritics model ASAP 2010. Physical adsorption was done at liquid nitrogen temperature of 77K. In this method the amount of nitrogen at the equilibrium and at the normal boiling point (-195.8°C) is measured over a range of nitrogen pressure below one atmosphere. In essence, the Langmuir adsorption isotherm is extended to apply to multilayer adsorption, arriving at the following equation called Brunauer-Emmet-Teller.

$$\frac{p}{v(p_0 - p)} = \frac{1}{V_m C} + \frac{(c-1)p}{cV_m p_o} \qquad (4.2)$$

where $\mathbf{p_0}$ is the saturation or vapor pressure, $\mathbf{V_m}$ is the volume of monolayer of the adsorbed gas and **c** is a constant for the particular temperature and gas-solid system.

## 4.5 Electro- catalytic activity characterization

Electrochemical activities of as prepared catalysts were determined by cyclic voltammetry (CV) and Chronoamperometry (CA) measurements at ambient temperature in a conventional three electrode cell assembly. 5 mm diameter glassy carbon electrode (geometrical working area of the electrode 0.076 $cm^2$), covered with a thin layer of

Nafion impregnated catalyst metal was used as the working electrode. A Pt-wire and an Ag/AgCl electrode (3.5M KCl) were used as the counter and reference electrodes, respectively.CV electrochemical studies were carried out in 0.5 M $H_2SO_4$ solution with and without 0.5 M HCOOH. In cyclic voltammetry measurements, the electrode potential applied between working and reference electrodes is linearly ramped verses time similar as in linear sweep voltammetry (LSV) experiment. But unlike LSV after reaching peak set potential, working electrode potential in CV is ramped in reverse direction. This ramping is experimentally known as scan rate V/s. For applying this applied working potential current flows between working electrode and counter electrode and in cyclic voltammogram this produced current is plotted verses applied voltage to analyze the catalytic activities of tested catalysts in electrolyte solution.

CO stripping voltammetry was performed in 0.5 M $H_2SO_4$ solution at a scan rate of 20mV/s, to calculate the electrochemical active surface area (ECAS) of metals loaded on support materials. In stripping cyclic voltammetry measurements, during the reduction step of metal, protons (hydrogen ions) from the sulphuric acid solution are adsorbed at the active sites of the metals, but these hydrogen atoms are desorbed back to solution during the oxidation step according to the following electrochemical reaction[92].

$$H_{ad}\,(\text{Reduction}) \rightarrow H^{+}+e^{-}(\text{oxidation})$$

During oxidation, the number of electrons (current) liberated from catalyst surface at given set potentials, gives the corresponding equal number of hydrogen atoms

desorbed and thus the adsorption sites available on the catalyst surface. This defines the electrochemical active surface area of the catalyst or electrode.

Chronoamperometry (CA) is an electrochemical technique used to check the stability and sustainability of synthesized electrocatalysts and analyzed in $N_2$-saturated 0.5 M $H_2SO_4$ and CHOOH solution at 0.3 V applied potential for half an hour time span. In CA measurements, current variation or fall is monitored and plotted as a function of time keeping working potential fixed at 3V. Trend of current time graph showed the stability of the tested catalysts.All electrochemical activity measurements were performed with a Biologic Potentiostat (VMP-3 Biologic Science Instruments France.) at 25°C temperature.

## 4.6 Experimental setup

The electrochemical experiment uses working electrode, reference electrode, and counter electrode which in combination are referred as a three-electrode setup. To enhance the sufficient conductivity of test solution, usually an electrolyte is added. Thus, the combination of the solvent, electrolyte and specific working electrode material determines the range of the potential.

### *4.6.1 Electrolyte Solution Preparation*

0.5M solutions of $H_2SO_4$ with and without 0.5 M formic acid were prepared using deionized water as solvent. For preparing 0.5 M $H_2SO_4$ solutions alone, 27.8 ml concentrated sulphuric acid of 18M was added slowly in sufficient DI water such that the

final volume of 0.5M became 1000 ml. Then flask was shakes well to get the homogeneous solution. For preparing 0.5M HCOOH with $0.5MH_2SO_4$ solutions, 21.4 ml formic acid of 23.4M was added in $0.5MH_2SO_4$ solutions and then shakes. Millipore Milli-Q system was used to obtain deionized water. For electrochemical measurements, 300ml solutions were taken in electrochemical cell and deaerate the solution with $N_2$ gas before it used for oxidation reaction.

### *4.6.2 Electrode Preparation*

***Working electrode***

Glassy carbon (GC) was used as working electrode. 5mm dia, GC electrode is completely surrounded by glass sheet except $0.076cm^2$ graphite tip area, where catalyst ink was deposited. GC electrodes are widely used in electrochemistry due to its high temperature withstand ability, low density, least affinity towards chemical attack and for impermeability to liquids and gases. Electrocatalyst ink and its deposition on working electrode was done by ultra sonicating 5 mg of prepared catalyst along with 1mL ethanol and 30µL Nafion solution (5 % wt.) for 30 min. Then with the help of micro pipette, 10µL of ink was transferred to polished surface (Aluminum powder of 0.3 µ and 0.5µ) of the glassy carbon and dried in open atmosphere at room temperature. Before start up of electrocatalytic oxidation, GC electrode deposited with catalyst ink was purged in $N_2$ gas for complete removal of oxides traces at the surface of catalyst. GC electrode is shown in following Fig. 4.5.

Figure 4.5: Glassy Carbon Electrode (Working Electrode)

***Counter andreference electrode***

Anode is working as counter electrode. A platinum mesh wire with surface area much higher than working electrode was used as counter electrode while Standard Ag/AgCl electrode (3.5M KCl) was used as reference electrode, as shown;

Figure 4.6: Platinum Mesh Counter Electrode


Figure 4.7: Reference Electrode

### *4.6.3 Electrochemical Cell Setup*

300 ml 0.5M HCOOH solutions incorporated with 0.5M $H_2SO_4$ electrolyte solution was taken in electrochemical cell. Working electrode, counter electrode and reference electrode were inserted in electrolyte solution such that tip of all electrodes must be dipped in it. Before start the oxidation reaction, cell was purged with $N_2$ gas in order to remove the dissolved oxygen and to make the system inert. The potential was applied between working and reference electrodes with a scan rate of 20mV/s by using Biologic Potentiostat and the response of the current was measured between working and counter electrodes. Scheme for electrochemical cell setup is shown in Fig.4.8.

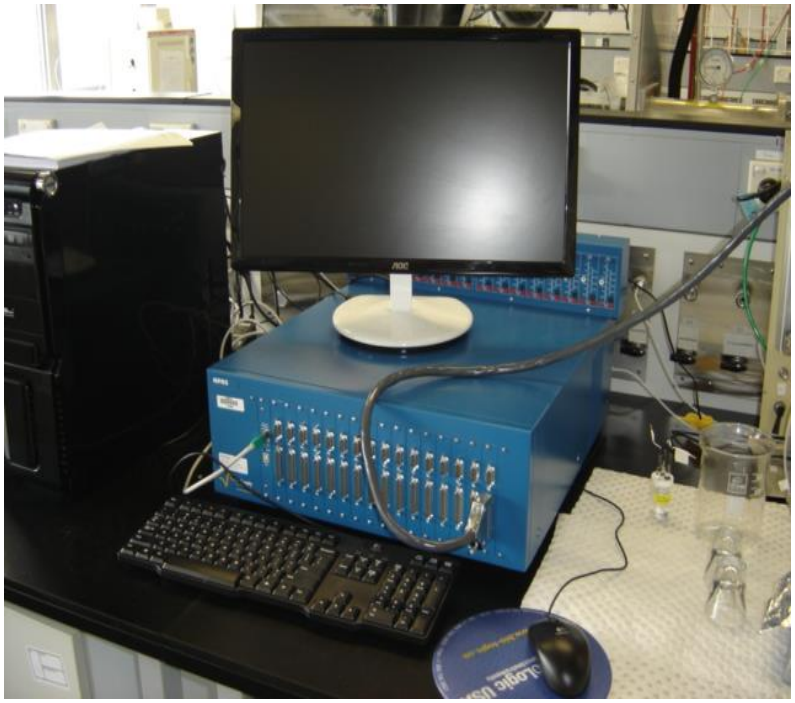

Figure 4.8: Electrochemical Cell

# CHAPTER 5
# RESULTS AND DISCUSSION

## 5 Introduction

All the electrocatalysts synthesized in this work were mentioned in the Table 4-1 along with their composition. Physical and electrochemical characterizations which employed to evaluate prepared catalysts are discussed in detail in the following sections.In this section, physical characterizations results of the single and binary PtPd based electrocatalysts supported on cerium/tungsten modified OMC are presented and discussed, and later, their catalytic activities for electrochemical oxidation for formic acidare discussed.

## 5.1 Physical Characterization

### *5.1.1 SEM and EDX analysis*

The morphology of as synthesized $CeO_2$-OMC support and PtPd based electrocatalysts are obtained by using scanning electron microscopy is presented in this section. One can see from the SEM images that the OMC support retained aggregated rope-like structure with smooth surfaces having broad interconnection between the ropes as seen in Fig. 5.1. The length of rope is estimated to be around 4-8 μm [91].SEM images of Pd/$CeO_2$-OMC in Fig. 5.2shows the uniform loading of metal particles on support. The Pd metal crystal sizes also appeared to be narrowly distributed, indicating the effectiveness of support modification.Similarly, as Pt to Pd ratio was increased, the metal particle reduced in size which evident from the comparison of SEM micrographs of $Pd_3Pt_1$/$CeO_2$-OMC,

$Pd_1Pt_3/CeO_2$-OMC and$Pt/CeO_2$-OMC (Fig 5.3 – 5.5), but the PtPd particles remains homogenously coated on the surface of the support. Within the resolution level of SEM, it is not possible to differentiate any significant changes in shape between support and catalyst material except length of rope reduced to 3-5 μm.

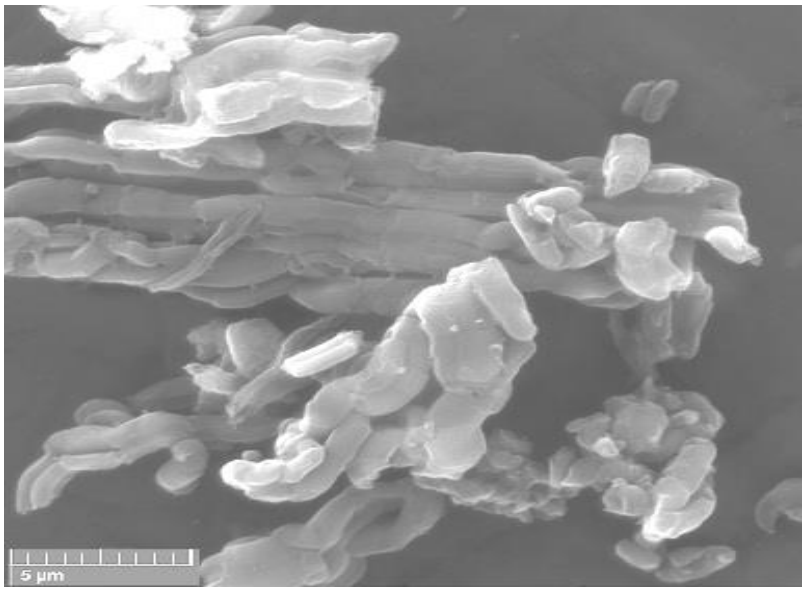


Figure 5.1: SEM image of $CeO_2$-OMC support

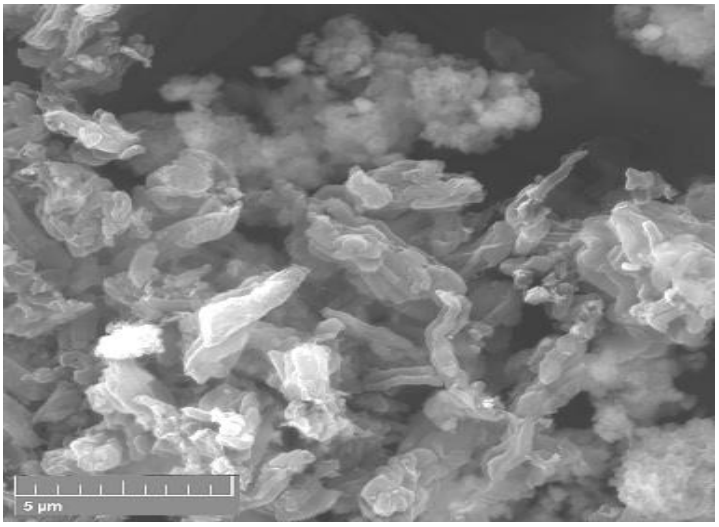


Figure 5.2: SEM image of $Pd/CeO_2$-OMC catalyst

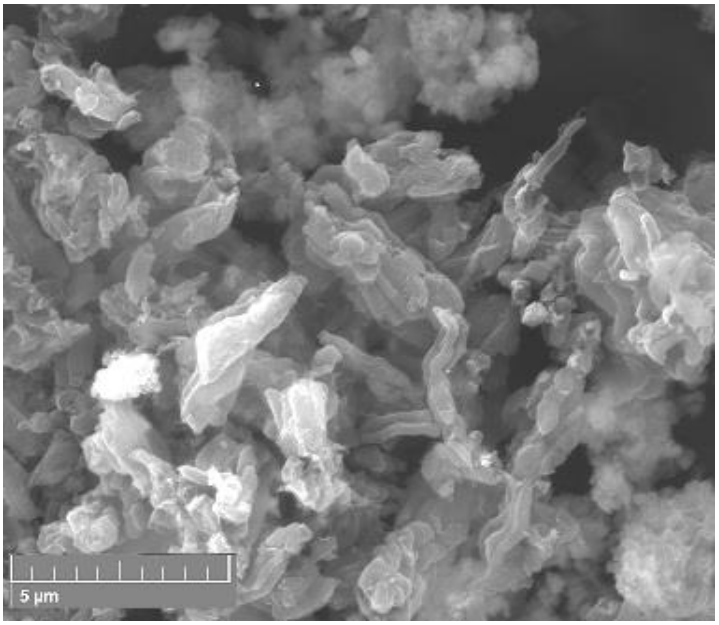


Figure 5.3: SEM image of $Pd_3Pt_1/CeO_2$-OMC catalyst

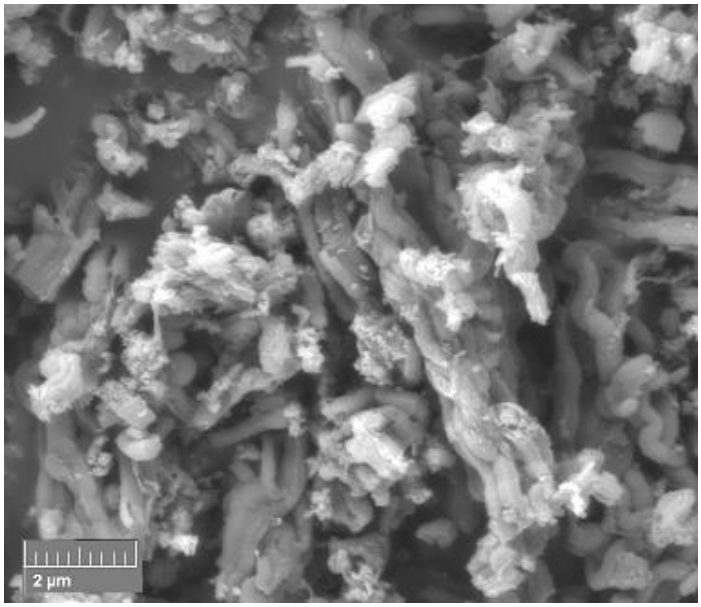


Figure 5.4: SEM image of $Pd_1Pt_3/CeO_2$-OMC catalyst

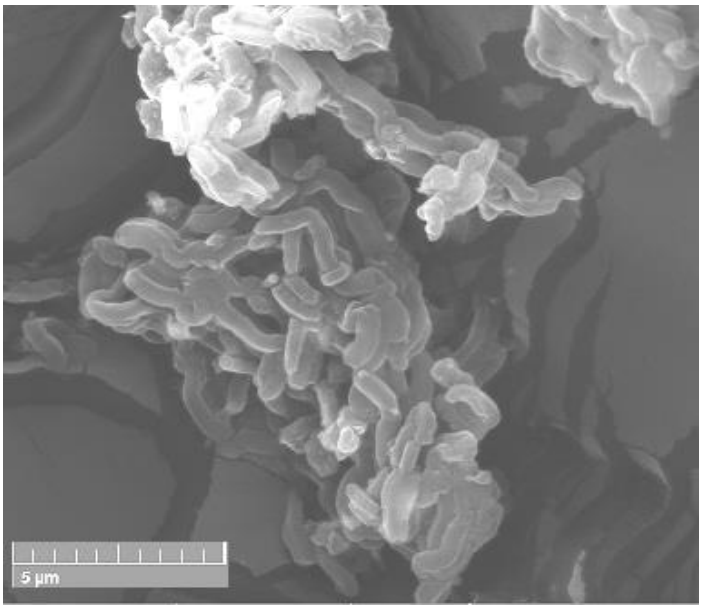


Figure 5.5: SEM image of $Pt/CeO_2$-OMC catalyst

The morphology of asPtPd/$WO_3$-OMC electrocatalysts with varying ratios of Pd to Pt has also been obtained by SEM analysis and shown in Fig 5.6. SEM images clearly elaborate the aggregated rope-like structure with smooth surfaces for $WO_3$-OMC support (A) which remained unchanged with increasing the Pt to Pd metal ratio.1-2 μm estimated length of rope with ropes interconnection can be seen in Fig.6 (B). Similarly uniform Pd and Pt metal loading on support material and crystal narrowly distribution are the result of $WO_3$modification as clearly demonstrated in Fig. 5.6(C) and 5.6(D) using $Pd_2Pt_1$/$WO_3$-OMC and $Pd_1Pt_2$/$WO_3$-OMC catalyst samples respectively. Clearly observed from high magnified SEM images that $WO_3$-OMC support and Pt and Pd coated catalysts are very consistent in morphology except slight reduction in rope length is prominent in $Pd_1Pt_1$/$WO_3$-OMCand $Pd_1Pt_2$/$WO_3$-OMC catalysts.

Above discussion evidently verified that cerium and tungsten oxide modification did not affect the base morphology of OMC support except enhanced the metals dispersion with least agglomerationon modified support material. Rope length reduction and interconnection is seemed a significant result of $CeO_2$ and $WO_3$modification.

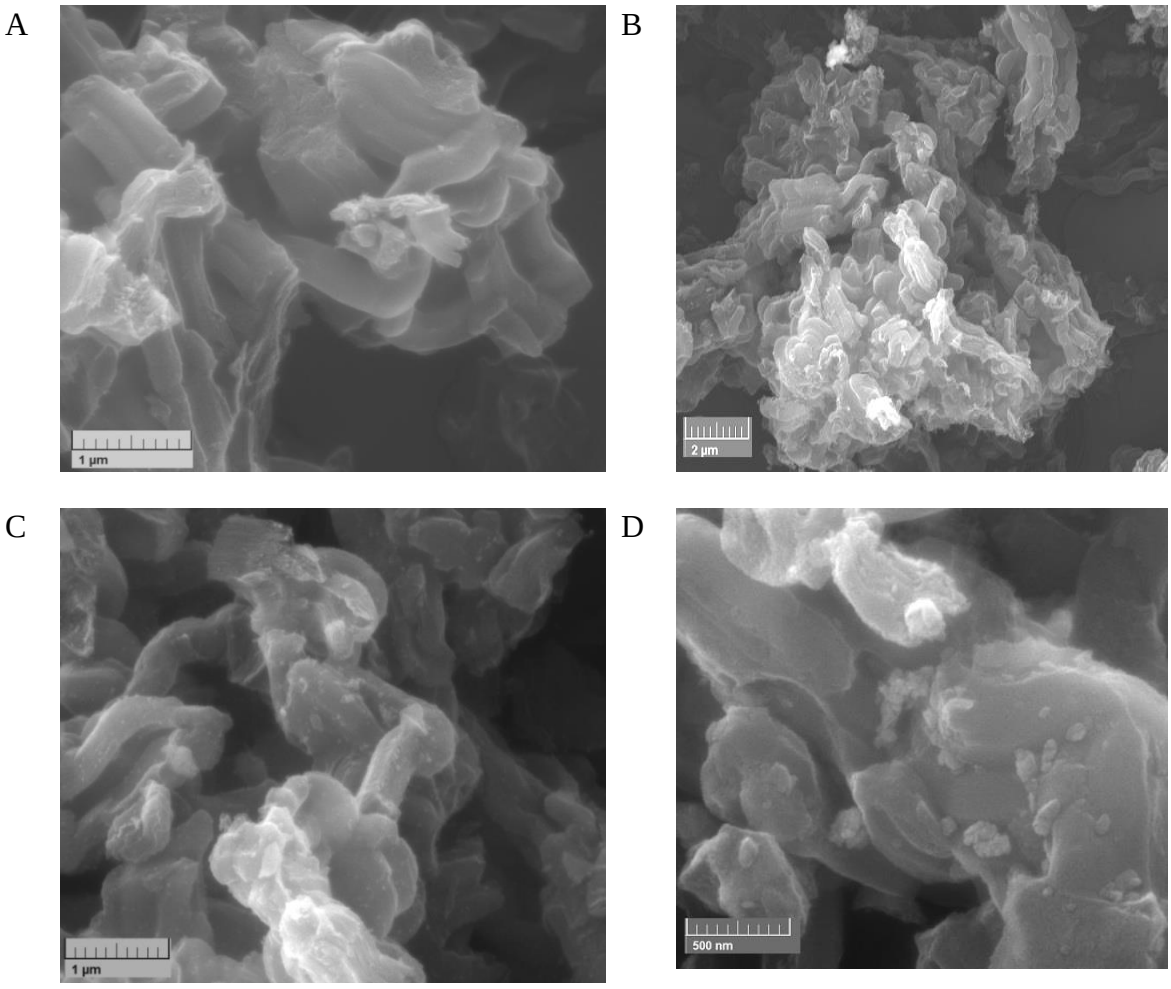


Figure 5.6:SEM images of $WO_3$-OMC support and PtPd/ $WO_3$-OMC catalyst samples

The EDX images of $CeO_2$-OMC and $WO_3$-OMC supported catalysts samples in respective Fig. 5.7 and Fig 5.8 reveal the presence of carbon, cerium, tungsten and other respective metals (Pt, Pd). The initial unknown peak represents the aluminum holder which is used in JEOL JSM-6460LV machine. Presence of metal elements such as Pd, Pt and Ce and W in both catalysts samples reveals the successful deposition of metals on

mesoporous carbon. Composition of Pd, Pt and Cein all catalyst samples are shown in Table 5-1.

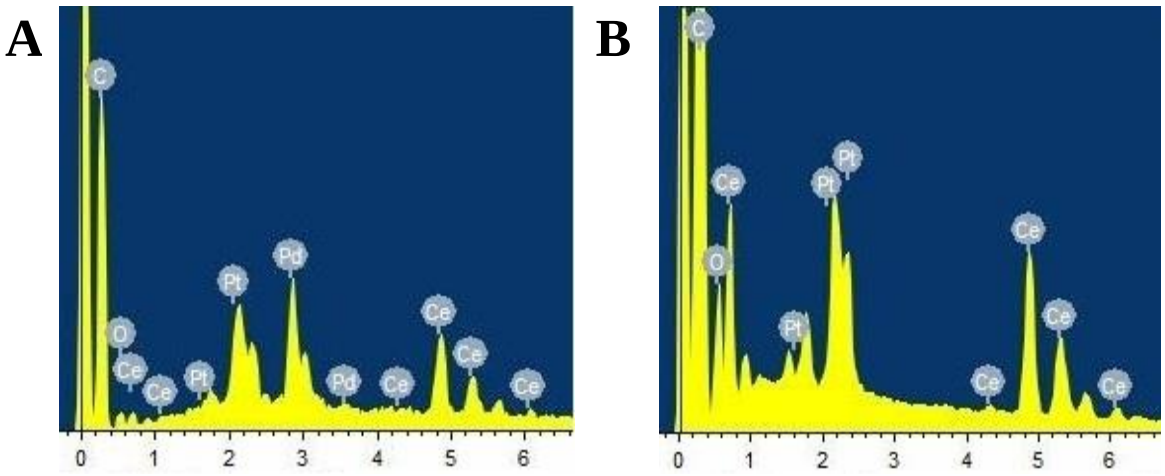


Figure 5.7: EDX images of (A) $Pt/CeO_2$ OMC and (B) $Pt/CeO_2$-OMC catalysts

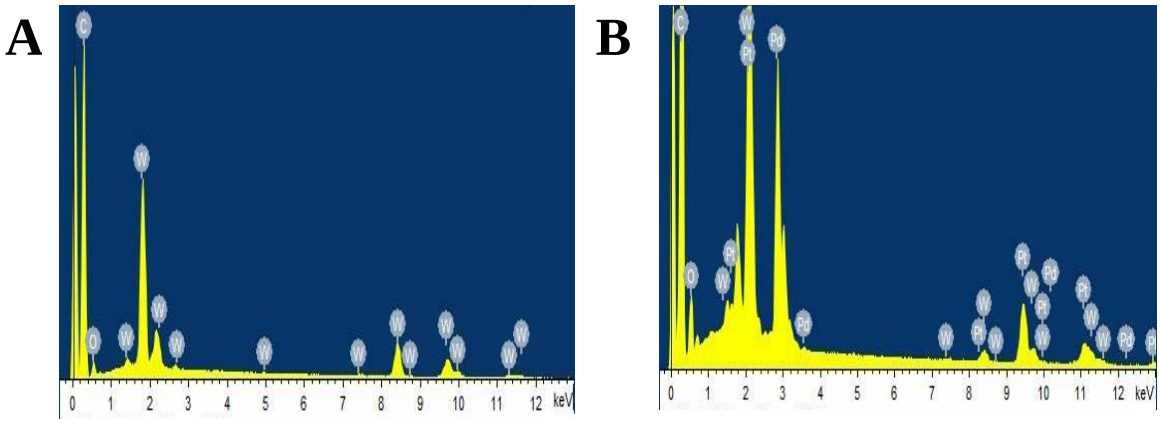


Figure 5.8: EDX images of (A) $WO_3$-OMC and (B) $Pd_2Pt_1/WO_3$-OMC

Table 5-1: EDX elemental analysis of $CeO_2$-OMC support & catalysts samples

| **Sample** | **Weight %** | | |
|---|---|---|---|
| | **Pd%** | **Pt%** | **Ce%** |
| $CeO_2$-OMC | -- | -- | 8.31 |
| Pd/$CeO_2$-OMC | 6.49 | -- | 8.07 |
| $Pd_3Pt_1$/$CeO_2$-OMC | 13.27 | 9.34 | 8.49 |
| $Pd_1Pt_3$/$CeO_2$-OMC | 7.81 | 7.93 | 7.26 |
| Pt/$CeO_2$-OMC | -- | 11.81 | 8.12 |

### *5.1.2 XRD Analysis*

The XRD analysis was conducted to detect the crystalline structure and size of the prepared sample composites. Fig. 5.9 shows the XRD patterns of Pd/OMC, Pd/$CeO_2$-OMC, Pt/ $CeO_2$-OMC, and PtPd/$CeO_2$-OMC catalysts with various Pd to Pt ratios. Catalysts with Pd to Pt ratios are denoted as $Pd_3Pt_1$/$CeO_2$-OMC and $Pd_1Pt_3$/$CeO_2$-OMC. In all samples, diffraction peak (19.18°) at 2θcorresponds to the (002) planes of the carbon support as reported by Yang LJ et al. (2012) [17]. From the figure, it is clear that

the XRD patterns of both Pd and Pt are quite similar. For Pd/OMC, Pd/$CeO_2$-OMC and PtPd/$CeO_2$-OMC catalysts, the peaks at 40.4°, 47°and 68° correspond to the (111), (200) and (220) planes of Pd, respectively, indicating the characteristics of face-centered cubic (fcc) crystalline structure of palladium nanoparticle's (JCPDS, Card No. 65-6174). The XRD patterns of both the $CeO_2$-OMC and OMC supported catalysts shows that the support modification and decreasing Pd content ratio has no prominent effects on diffraction peaks except making it broader and slightly moving the peaks to lower angle. In Pt/$CeO_2$-OMC catalyst, the XRD patterns showed similar Pt diffraction peaks at 40°, 46.7° and 68° angles corresponds to (111), (200) and (220), respectively. These observations are in line with what has been also reported by Z. P. Sun et al. (2009) [39].

Cerium oxide peaks appeared at 27.6°,44°,53° and 69.7° places, indexed to fcc-phase of ceria (JCPDS no. 34-0394) [93] and their diffraction peaks intensity are too weak to be useful for the calculation of cerium crystalline size.

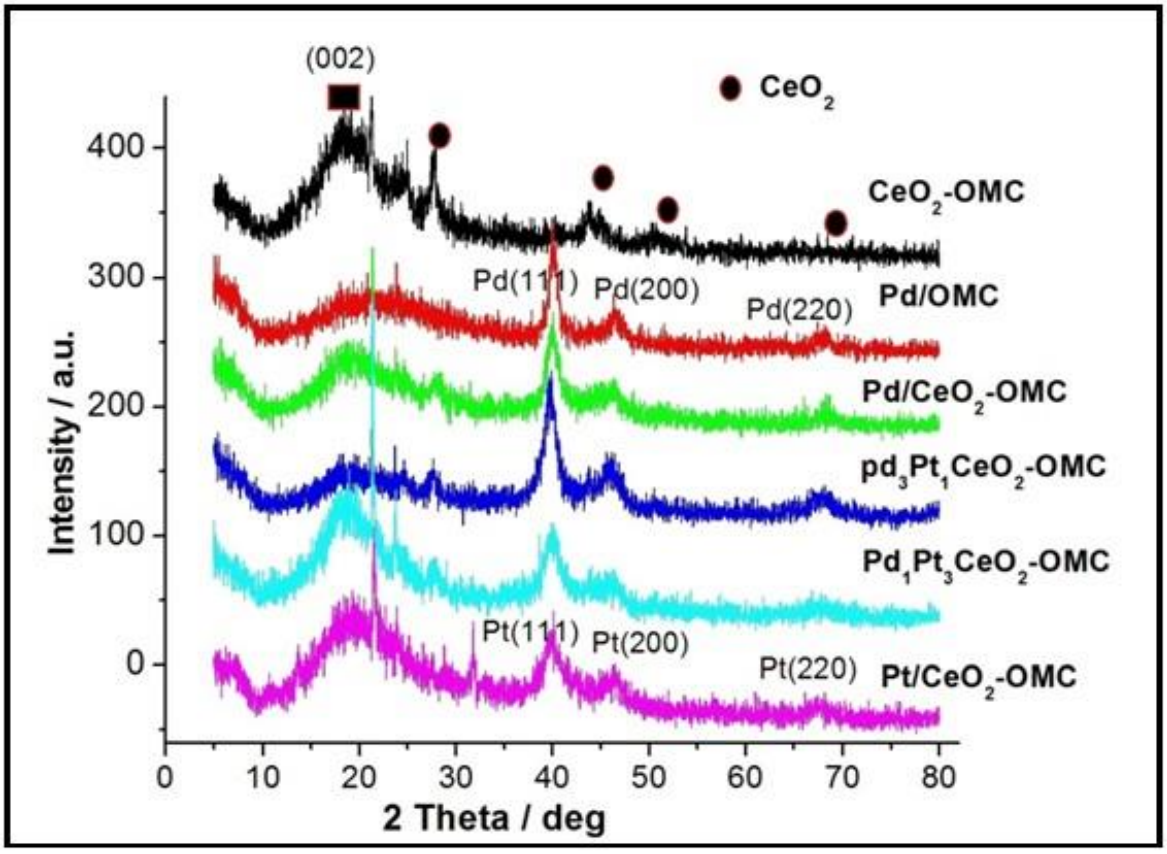


Figure 5.9: Wide angle XRD pattern of $CeO_2$-OMC support, Pd/OMC and PtPd/$CeO_2$-OMC catalysts with varying ratios of Pt and Pd.

The crystalline size of Pd and Pt crystals was calculated using Sherrer's Equation by for the Pt/Pd (111) peak [40].

$$d = \frac{0.9\lambda}{(\beta \, Cos\theta)}$$

Where d is the average particle size, λ is the X-ray wave length 0.154 nm, θ is the diffraction angle of the Pd (111) peak and β is the peak broadening (FWHM). The crystalline size obtained for PtPd based catalysts are found to be between 7-4nm and

shown in Table 5-2. It was noticed that the crystalline size of samples decreased with the increase of Pt to Pd ratio in the catalyst.

The crystalline structure of $WO_3$-OMC support, Pd/$WO_3$-OMC, $Pd_1Pt_1$/$WO_3$-OMC, $Pd_2Pt_1$/$WO_3$-OMC and $Pd_1Pt_2$/$WO_3$-OMCcatalysts were determined by using X-ray diffraction technique and results are shown in Fig.5.10. Diffraction peak at 20.12°corresponds to the (002) planes of the carbon support. For Pd/OMC, Pd/$WO_3$-OMC and PtPd/$WO_3$-OMC electrocatalysts, the peaks at 39.4°, 47.7°and 68° correspond to the (111), (200) and (220)planes of Pd, respectively, indicating the characteristics of face-centered cubic (fcc) crystalline structure of palladium nanoparticle's (JCPDS, Card No. 65-6174). The XRD patterns of both the $WO_3$-OMC and OMC supported catalysts shows that the support modification and decreasing Pdcontent ratio has no prominent effects on diffraction peaks except making it broader and slightly moving the peaks to higher angle. In $Pd_1Pt_2$/ $WO_3$-OMC catalyst, the XRD patterns showed similar Pt diffraction peaks at 40°, 47.9° and 69.3°angles corresponds to (111), (200) and (220), respectively. These observations are in line with what has been also reported by Z. P. Sun et al. (2009).

Tungsten oxide appeared at 21.7°, 32.4°, 40.1° and 46.7° places, indexed to fcc-phase of tungsten (JCPDS card no. 20-1324) andindicating significant crystallite $WO_3$ framework growth. The crystalline size of Pd and Pt was also calculated using Sherrer Equation.

The crystalline size obtained for Pd/ OMC, Pd/$WO_3$-OMC, $Pd_1Pt_1$/ $WO_3$-OMC, $Pd_1Pt_2$/ $WO_3$-OMC and $Pd_2Pt_1$/ $WO_3$-OMC was found to be 6.5 nm, 6.5 nm, 6.2 nm, 6.6

nm and 6.0respectively as shown in Table 5-2. It was noticed that the crystalline size of samples decreased with the increase of Pt to Pd ratio in the catalyst. Also face centered cubic structures of $WO_3$ and PtPd bimetallic catalysts coexist in all samples.

Table 5-2: XRD data analysis for CeO2-OMC and WO3-OMC supported catalysts

| **Sample Catalyst** | **2θ angle (degree)** | **FWHM (degree)** | **Crystal size (nm)** |
|---|---|---|---|
| Pd/OMC | 39.91 | 1.29 | 6.5 |
| $Pd/CeO_2$-OMC | 39.86 | 1.371 | 6.2 |
| $Pd_3Pt_1/CeO_2$-OMC | 39.77 | 1.442 | 5.8 |
| $Pd_1Pt_3/CeO_2$-OMC | 39.74 | 1.739 | 4.8 |
| $Pt/CeO_2$-OMC | 41.74 | 1.89 | 4.3 |
| $Pd/WO_3$-OMC | 39.86 | 1.30 | 6.5 |
| $Pd_1Pt_1/ WO_3$-OMC | 39.89 | 1.35 | 6.2 |
| $Pd_2Pt_1/ WO_3$-OMC | 39.78 | 1.28 | 6.6 |
| $Pd_1Pt_2/ WO_3$-OMC | 40.04 | 1.40 | 6.0 |

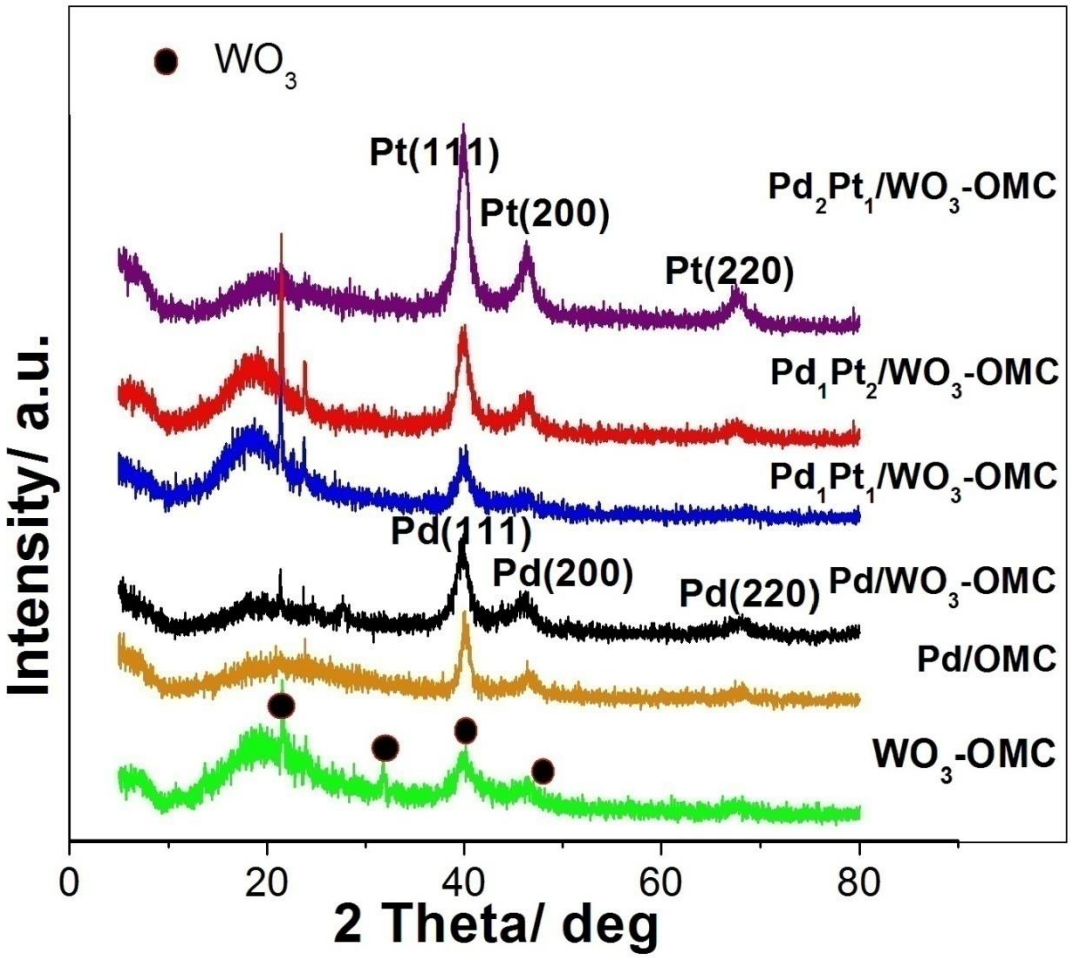


Figure 5.10: XRD pattern of $WO_3$-OMC support, Pd/OMC and PtPd/$WO_3$-OMC catalysts

### *5.1.3 TEM Analysis*

Particle size and uniform dispersion of metal particles on support surface strongly affect the catalytic properties of the catalysts. TEM image for Pd/$CeO_2$-OMC in Fig.5.11 shows that most of Pd nano particles are uniformly dispersed on the surface of $CeO_2$-OMC support and no agglomeration appear on the surface. Increase in mass ratio of Pt particles (Fig 5.12 and 5.13), enhances the size reduction of particles and their dispersion was seemed more ordered. Uniform particles dispersion and much smaller particle size were also due to the presence of $CeO_2$-modified support, as same result concluded by Yang LJ et al. [17]. Pure Pt nano particle distribution is shown inFig. 5.14.

Average particle size of Pd/$CeO_2$-OMC, $Pd_3Pt_1$/$CeO_2$-OMC, $Pd_1Pt_3$/$CeO_2$-OMC and Pt/$CeO_2$-OMC was found to be 4.82 nm, 3.3 nm, 3.1 nm and 2.3 nm respectively, which is good agreement with XRD data obtained.

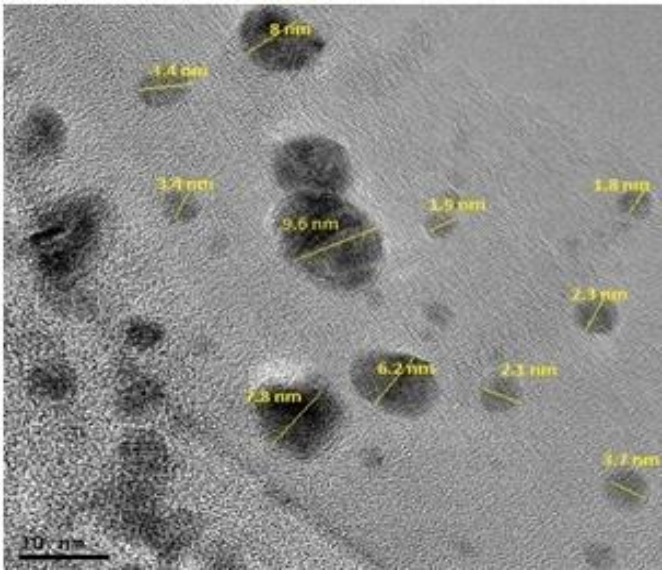


Figure 5.11: TEM image of Pd/$CeO_2$-OMC catalyst sample

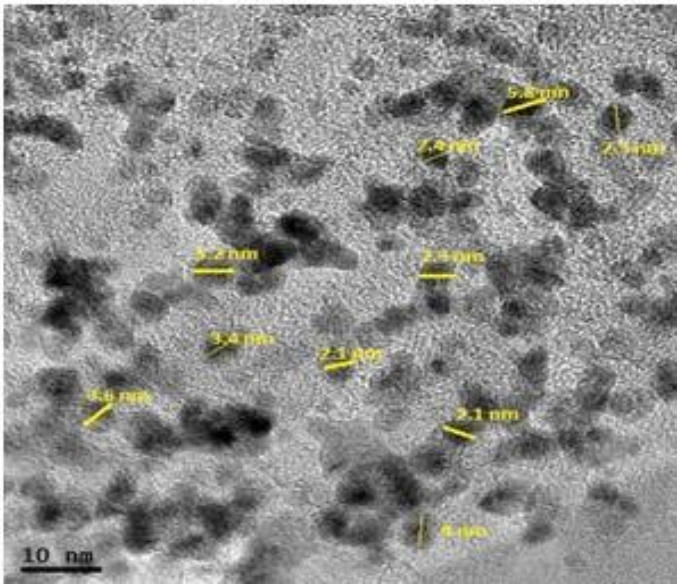


Figure 5.12: TEM image of $Pd_3Pt_1/CeO_2$-OMC catalyst sample

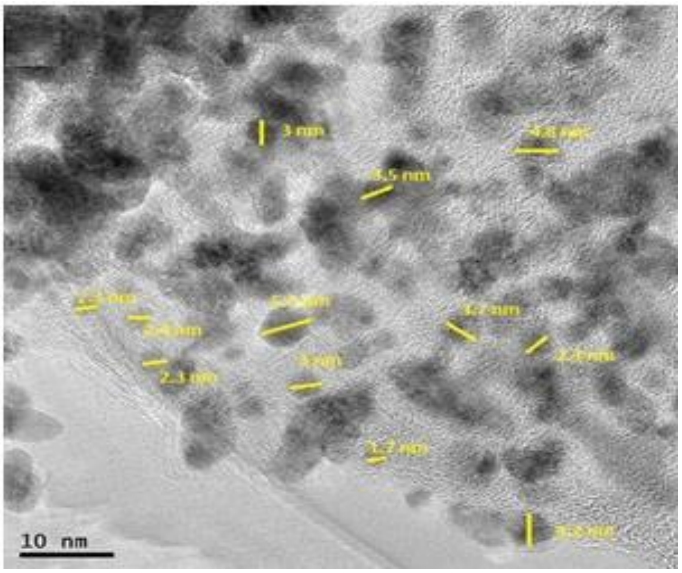


Figure 5.13: TEM image of $Pd_1Pt_3/CeO_2$-OMC catalyst sample

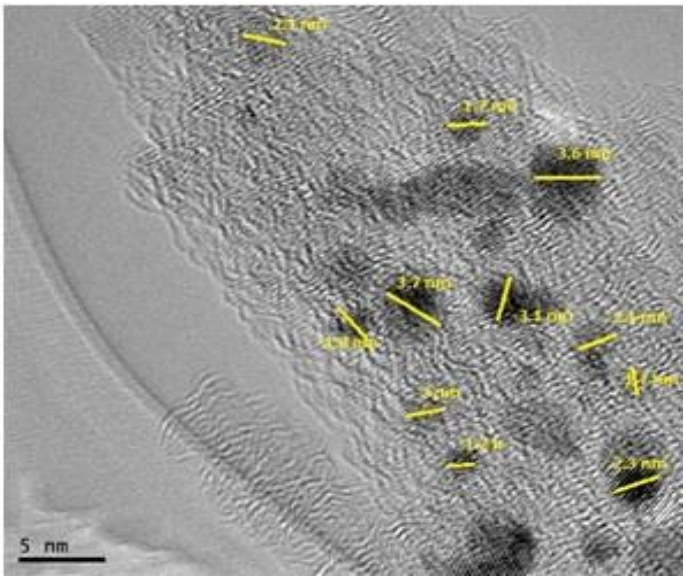


Figure 5.14: TEM image of $Pt/CeO_2$-OMC catalyst sample

In Fig.5.15, TEM images shows that Pt and Pd nano particles are uniformly dispersed on the surface of $WO_3$-OMC support.Agglomeration of Pd particles on the surface of OMC material in Fig 5.15 (A) confirmed that $WO_3$modification has enhanced the evenly dispersion of Pd and Pt nano particles(Fig 5.15 (B, C and D)) and increase of Pt to Pd ratios influenced the formation of smaller size crystals of metals on the support surface. The average crystal size of $Pd/WO_3$-OMC, $Pd_1Pt_1/WO_3$-OMC, $Pd_2Pt_1/WO_3$-OMC and $Pt/WO_3$-OMC catalysts are found to be 7.2 nm, 6.9 nm, 6.7 nm and 6.2 nm, respectively which reinforcedthe results as calculated from Sherrer Equation using XRD data.

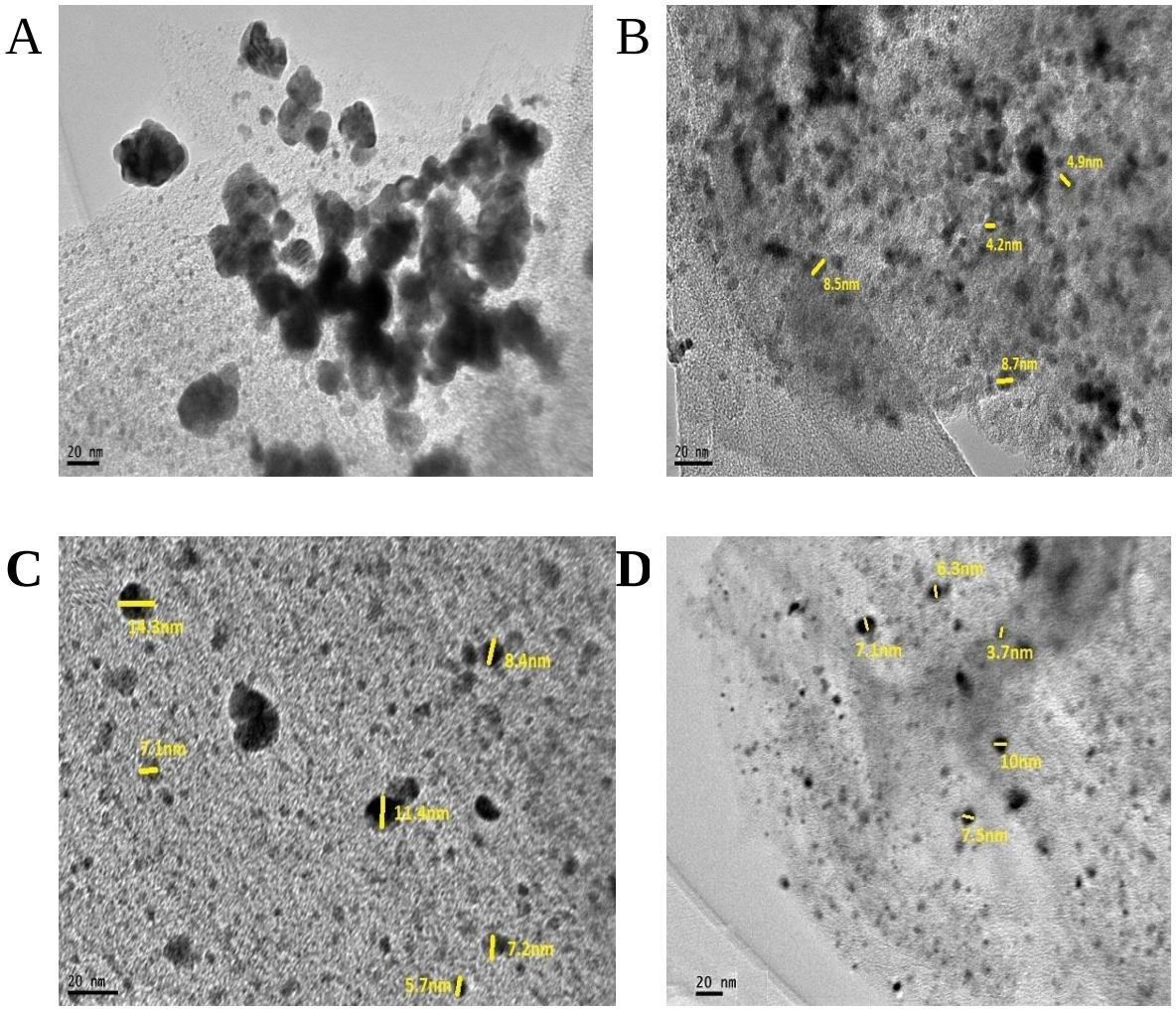


Figure 5.15: TEM images of (A) Pd/OMC, (B) Pd/$WO_3$-OMC, (C) $Pd_2Pt_1$/$WO_3$-OMC and (D) $Pd_1Pt_2$/$WO_3$-OMC

### *5.1.4 TGA Analysis*

TGA measurements of $CeO_2$-OMC and $Pd_3Pt_1/CeO_2$-OMC catalysts in dry air atmosphere are shown in Fig. 5.16. The temperature range was selected as 25°C to 800°C for complete combustion of mesoporous carbon support [94]. The TGA profiles show the thermal stability of OMC between 25°C to 420°C. Initial mass reduction was the result of moisture evaporation, present in the samples. Quick weight loss at temperature between 470°C to 560°C for $CeO_2$-OMC support and from 420°C to 565°C for $Pd_3Pt_1/CeO_2$-OMC catalyst were recorded. This loss was due to the fast oxidation of OMC. TGA analysis also indicates the steady weight loss of mesoporous carbon which was according to the carbon fraction added in samples. The amount greater than 20% in catalysts showed the oxides formation of PtPd catalyst which may cause at 800°C [17]. These observations confirm that actual and expected compositions are quite consistent.

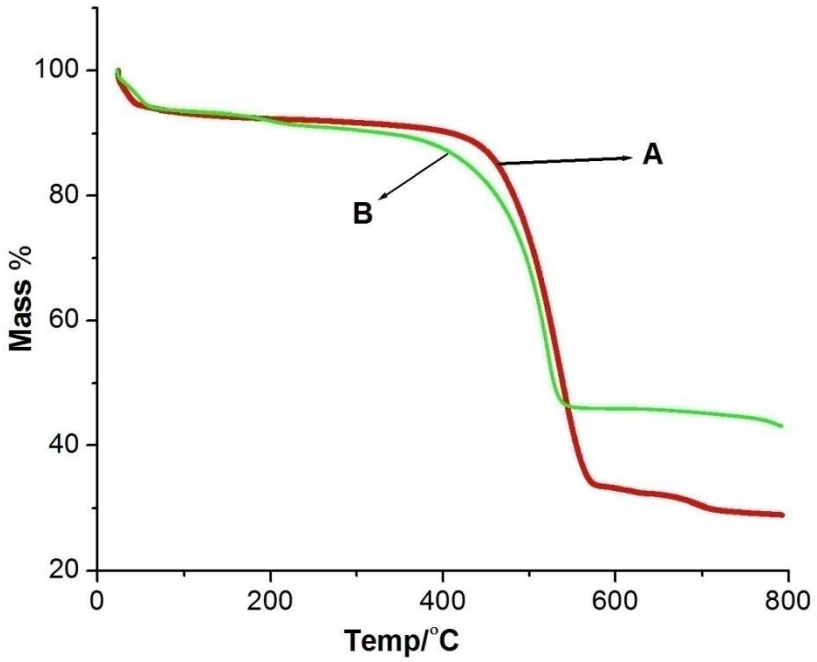


Figure 5.16: TGA curves of (A) $CeO_2$-OMC (B) $Pd_3Pt_1/CeO_2$-OMC @10°C/min

TGA measurement is shown in Fig. 5.17 as temperature vs. mass % plot for$WO_3$-OMC support, Pd/$WO_3$-OMCand $Pd_2Pt_1/WO_3$-OMC catalysts in dry air atmosphere. To ensure complete evaporation of mesoporous carbon through oxidation, the final temperature was keptat 800°C. Thermal stability of OMC support was recorded between 25°C to 460°C range. Initial rapid mass reduction was the result of moisture evaporation, present in the samples. Due to the oxidation of OMC, themajor weight loss is found from496°C to 610°C for $WO_3$-OMC support, from 465°C to 560°C for Pd/$WO_3$-OMCand from 440°C to 565°C for $Pd_2Pt_1/WO_3$-OMC catalysts. The amount greater than 20% in catalysts showed the oxides formation of PtPd catalyst which may cause at 800°C. These observations confirm that actual and expected compositions are quite consistent.

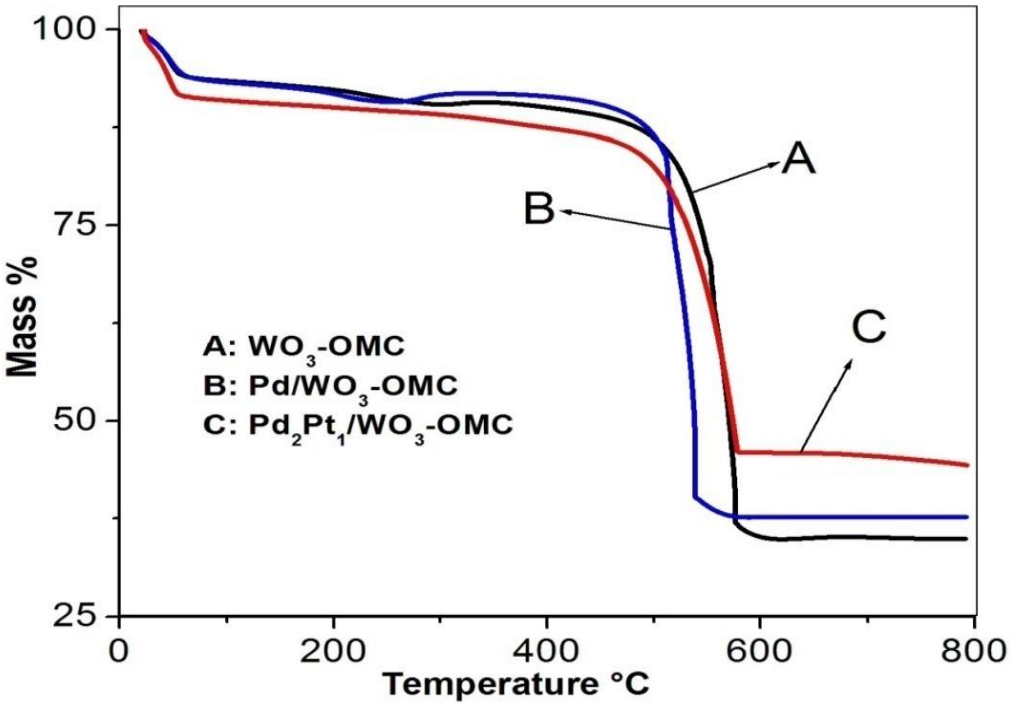


Figure 5.17: TGA curves of (A) $WO_3$-OMC (B) Pd/$WO_3$-OMC (C) $Pd_2Pt_1$/$WO_3$-OMC @10°C/min

### *5.1.5 $N_2$ adsorption/desorptiom isotherms Analysis*

Fig. 5.18 shows the $N_2$ adsorption–desorption isotherms and corresponding BJH (Barret-Joyner-Halenda) pore size distribution curves of the OMC, $CeO_2$ modified OMC and the prepared catalyst samples. Monolayer–multilayer adsorption, a capillary condensation, and a multilayer adsorption on the outer particles surface are the three phases which can be distinguished from the figure in all samples. OMC and the $CeO_2$-OMC samples exhibited a type IV isotherm with a slightly sharp capillary condensation step between $p/p_0$ = 0.42 and 0.95. This lower pressure capillary condensation indicates that OMC and

$CeO_2$-OMC support contains smaller average pore sizes. BET surface area, pore size and total volume of OMC and PtPd based catalysts were calculated from the nitrogen adsorption isotherm data and summarized in Table 5-3.The measured BET surface area of OMC 1005 $m^2/g$ is in agreement with material as reported by J. Zeng et al. [36]. It is interesting to observe (in Table 5-3) that the BET surface area of the $CeO_2$ modified $CeO_2$-OMC support is 1119 $m^2/g$ which is 1.12 times higher than that of the unmodified support material. The total pre volume of $CeO_2$-OMC support remains almost same as the total pore volume of OMC support. The BJH pore size for OMC and $CeO_2$-OMC is measured as 3.8 nm and 3.4 nm, respectively. These observations suggest that the characteristics surface area and other properties of OMC have significantly improved by the addition of cerium. From BJH, pore size distribution curve it is quite clear that pore size of all sample is very consistent and is between 3 and 4 nm.

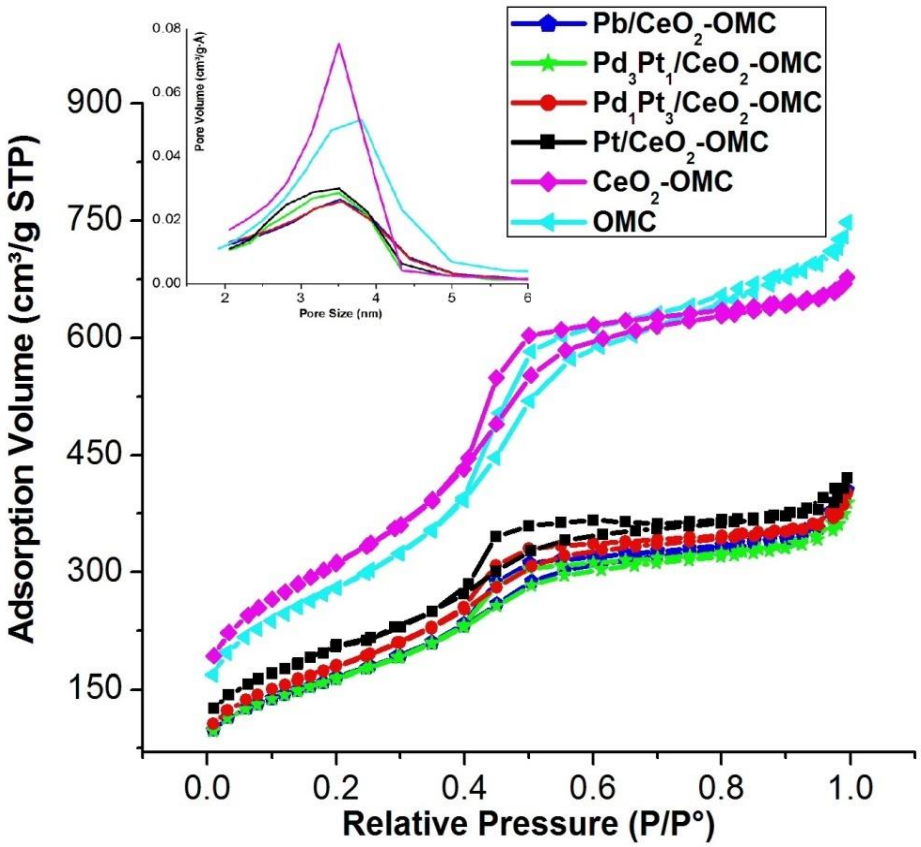


Figure 5.18: $N_2$ adsorption-desorption isotherm & BJH pore size Distribution of OMC, $CeO_2$-OMC, Pd/$CeO_2$-OMC, $Pd_3Pt_1/CeO_2$-OMC, $Pd_1Pt_3/CeO_2$-OMC and Pt/$CeO_2$-OMC

$N_2$ adsorption–desorption isotherms and corresponding BJH (Barret-Joyner-Halenda) pore size distribution curves of the OMC, $WO_3$ modified OMC support and the prepared catalyst samples are shown in Fig. 5.19. BET surface area, pore size and total volume of OMC and PtPd based catalysts were calculated from the nitrogen adsorption isotherm data and summarized in Table 5-3.The BJH pore size for OMC and $WO_3$-OMC is measured as 3.8 nm and3.4 nm, respectively. 1.16 times reduced BET surface area of the

$WO_3$ modified support (861m²/g) showed the blockage of surface due to deposition of tungsten oxide inside the mesopores of OMC. These observations suggest that the pore size and other characteristic properties of OMC have significantly improved after tungsten oxide modification. From BJH, pore size distribution curve it is quite clear that pore size of all sample is very consistent and is between 3 and 4 nm.

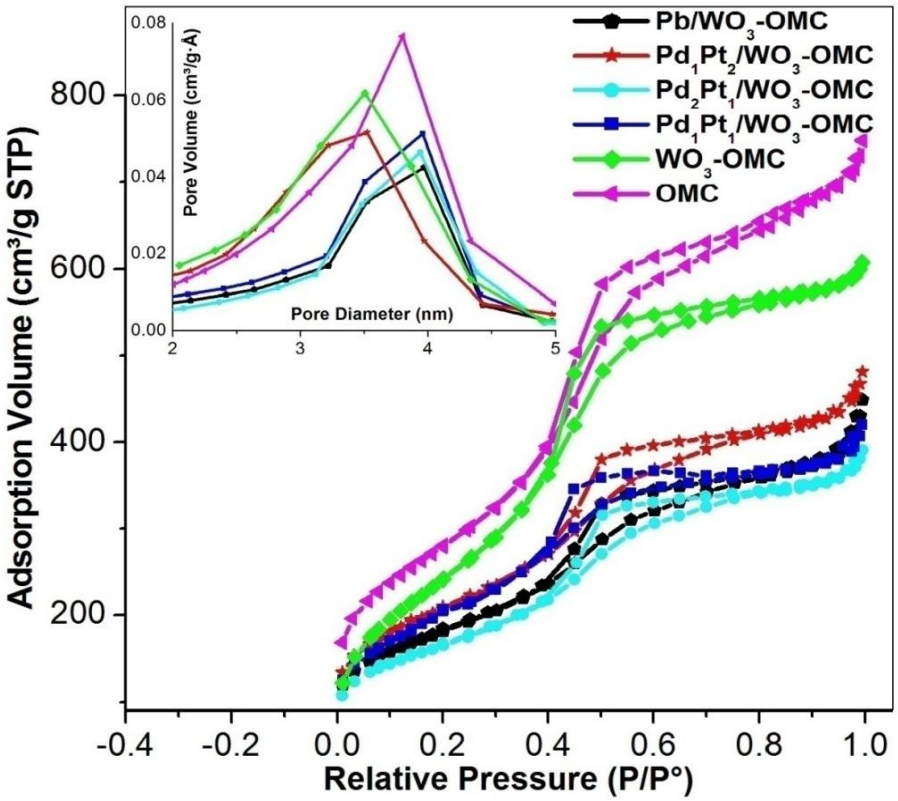


Figure 5.19: $N_2$ adsorption-desorption isotherm & BJH pore size Distribution of OMC, $WO_3$-OMC supported PtPd catalysts

Table 5.3: Surface properties of OMC, supports & catalysts samples

| **Sample** | **$S_{BET}$** ($m^2g^{-1}$) | **$d_{BJH}$** (nm) | **$V_{total}$** ($cm^3g^{-1}$) |
|---|---|---|---|
| OMC | 1005 | 3.82 | 1.23 |
| $CeO_2$-OMC | 1119 | 3.44 | 1.24 |
| Pd/$CeO_2$-OMC | 595 | 3.49 | 0.68 |
| $Pd_3Pt_1$/$CeO_2$-OMC | 592 | 3.54 | 0.66 |
| $Pd_1Pt_3$/$CeO_2$-OMC | 646 | 3.51 | 0.68 |
| Pt/$CeO_2$-OMC | 697 | 3.48 | 0.67 |
| $WO_3$-OMC | 861 | 3.4 | 0.79 |
| Pd/ $WO_3$-OMC | 577 | 4.1 | 0.68 |
| $Pd_1Pt_1$/ $WO_3$-OMC | 629 | 3.9 | 0.66 |
| $Pd_2Pt_1$/ $WO_3$-OMC | 646 | 3.8 | 0.67 |
| $Pd_1Pt_2$/ $WO_3$-OMC | 721 | 3.5 | 0.69 |

## 5.2 Electrochemical characterization

### *5.2.1 Hydrogen adsorption/desorption Analysis*

Fig. 5.20 shows a distinct hydrogen adsorption/desorption CV curves for $CeO_2$-OMC supported PtPd electrocatalysts in 0.5M $H_2SO_4$ saturated with $N_2$ at a scan rate of 20mV/s. From the CV curves, one can see that the catalysts with higher Pd-contents have sharp and narrow $H_2$ adsorption and desorption peaks at higher potential. Inside and outside movement of H atoms from the PtPd lattice alloy surface is the main reason for adsorption and desorption peaks of hydrogen. This in and out motion is accompanied by H electro-reduction and H electro-oxidation [95]. From Fig.5.20 it is obvious that the bimetallic $Pd_3Pt_1/CeO_2$-OMC shows broader adsorption/desorption peak which is negatively shifted as compared to monometallic $Pd/CeO_2$-OMC and Pd/OMC catalysts. Peak current density and corresponding area also varied according to Pt to Pd weight ratios.

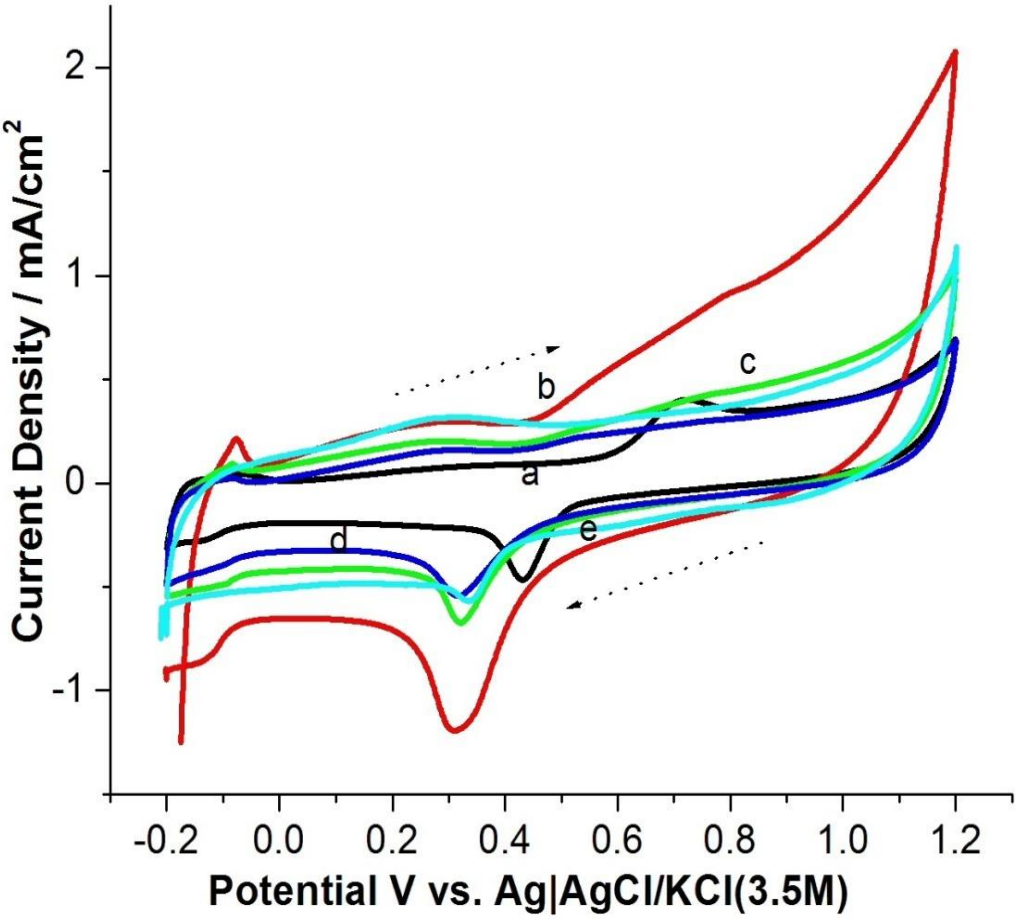


Figure 5.20: CV for (a) Pd/$CeO_2$-OMC, (b) $Pd_3Pt_1$/$CeO_2$-OMC, (c) $Pd_1Pt_3$/$CeO_2$-OMC, (d) Pt/$CeO_2$-OMC and (e) Pd/OMC in 0.5M $H_2SO_4$ at a scan rate of 20 mV/s

Hydrogen adsorption/desorption CV curves for $WO_3$-OMC supported PtPd electrocatalysts in 0.5M $H_2SO_4$ saturated with $N_2$ at a scan rate of 20 mV/s are shown in Fig. 5.21. From the CV curves, one can see that the catalysts with higher Pd-contents have broad and wider $H_2$ adsorption and desorption peaks at higher potential. From Fig.5.21, it is obvious that the bimetallic $Pd_2Pt_1$/$WO_3$-OMC shows broader

adsorption/desorption peak which is negatively shifted as compared to monometallic Pd/$WO_3$-OMC and Pd/OMC catalysts. Peak current density and corresponding area also varied according to Pt to Pd weight ratios.

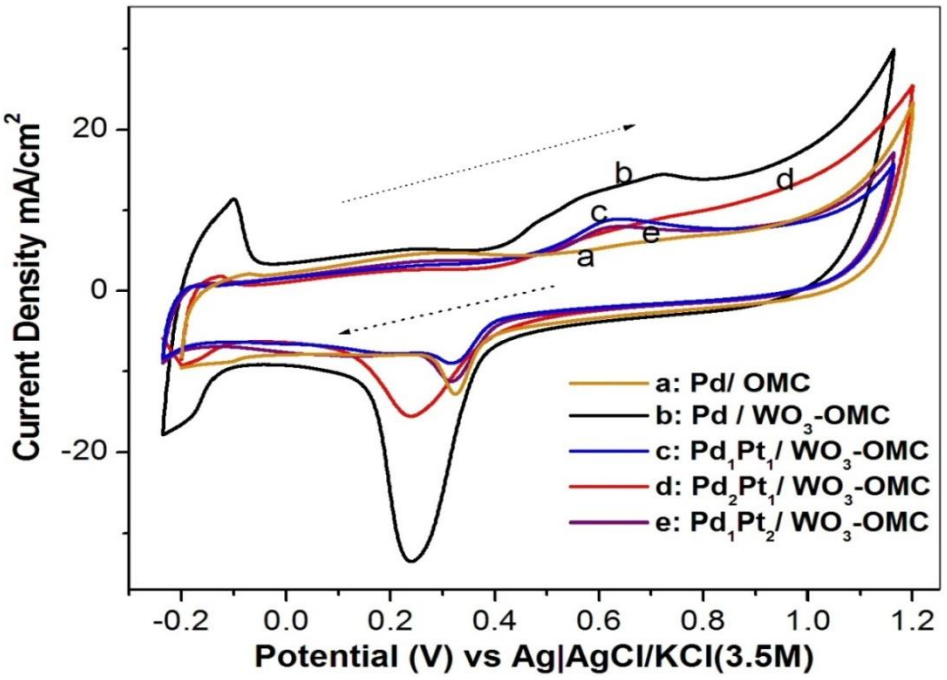


Figure 5.21:Cyclic voltammograms for PtPd/$WO_3$-OMC electrocatalystsin 0.5M $H_2SO_4$ at a scan rate of 20mV/s

### *5.2.2 CO stripping Analysis*

CO stripping voltammetry is performed to demonstrate the CO poisoning resistance of PtPd based electrocatalysts. Fig. 5.22(A) and 5.22(B) shows the kinetics and onset potential of CO oxidation on the surface of electrocatalysts. In Fig.5.22 (A), the first voltammogram represents Pd/OMC catalyst, which shows only one peak at 580mV with the onset potential about 505mV. The scan potential peak of $Pd/CeO_2$-OMC catalyst is around at 550mV. However, the addition of $CeO_2$ the onset potential is negatively shifted by 65mV and is seen at 440mV. By increasing Pt-contents, peak potential shows a positive shift and moves towards higher potential. For $Pd_3Pt_1/CeO_2$-OMC catalyst the onset potential first decreases to 400mV and then positively increases for higher Pt-content catalysts. The relatively higher values of peak and onset potentials of $Pt/CeO_2$-OMC catalyst is possibly due to the poisoning of Pt surface in which no reactive sites are available for hydrogen oxidation. Table 5-4 summarizes the CO stripping intensity, peak and onset potentials for all the studied catalysts. One can see form this table that the intensity of CO oxidation peaks is varied with the variation of Pt contents. For $Pd_3Pt_1/CeO_2$-OMC catalyst, intensity of CO peak is about 13.6mA/cm$^2$ which is remarkably higher than that of $Pd/CeO_2$-OMC (7.8 mA/cm$^2$) but is smaller than $Pd_1Pt_3/CeO_2$-OMC catalyst (15.5 mA/cm$^2$). Catalysts with lower onset potential are found to be better in catalytic activity for CO oxidation. Accordingly, one can consider that $Pd_3Pt_1/CeO_2$-OMC electrocatalyst is more CO tolerant than the other catalysts with higher Pt contents. Table 5-4 also lists electrochemical active surface area (ECAS) of Pt and Pd calculated by using 0.42mC/cm$^2$ [96-97] as charge associated to the monolayer on Pt and Pd nano particles. The $Pd_3Pt_1/CeO_2$-OMC catalyst shows highest ECAS values

(48.7 $m^2$/g metal) as compared to the all other catalyst studied. The high ECAS value further indicates that the bimetallic $Pd_3Pt_1/CeO_2$-OMC catalyst is a potential CO tolerance catalyst.

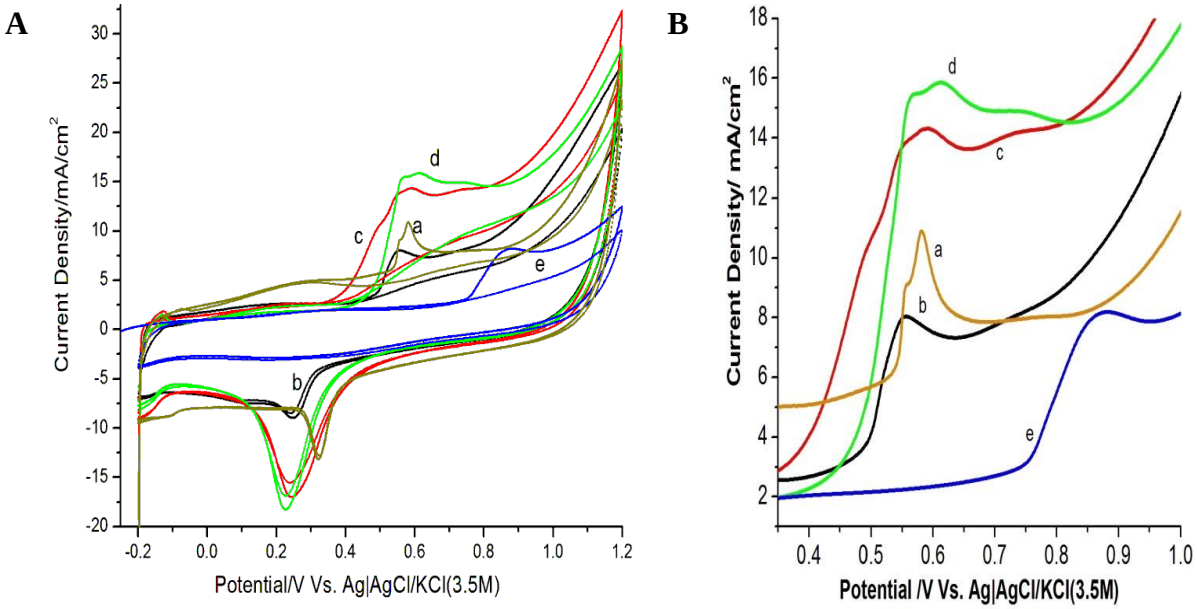


Figure 5.22: (A) 1st& 2nd Cycles of CO stripping measurements for PtPd/$CeO_2$-supported electrocatalysts in 0.5 M $H_2SO_4$ at a scan rate of 20 mV/s, and (B): enlargement of the CO oxidation peaks: (a) Pd/OMC, (b) Pd/$CeO_2$-OMC, (c) $Pd_3Pt_1/CeO_2$-OMC, (d) $Pd_1Pt_3/CeO_2$-OMC and (e) Pt/$CeO_2$-OMC

Table 5.4: Electrochemical properties of CeO2-OMC supported catalysts

| Catalyst | Area of desorbed CO peak($mC/cm^2$) | CO Stripping $E_{onset}$ (mV) | $E_{peak}$ (mV) | ECAS[a] ($m^2/g_{metal}$) | Peak Intensity ($mA/cm^2$) |
|---|---|---|---|---|---|
| Pd/OMC | 8.7 | 505 | 580 | 16.3 | 11 |
| $Pd/CeO_2$-OMC | 8.6 | 440 | 550 | 16.1 | 7.8 |
| $Pd_3Pt_1/CeO_2$-OMC | 25.93 | 400 | 585 | 48.7 | 13.6 |
| $Pd_1Pt_3/CeO_2$-OMC | 21.7 | 430 | 620 | 40.6 | 15.5 |
| $Pt/CeO_2$-OMC | 16.24 | 750 | 860 | 30.4 | 8.2 |

[a] $ECAS_{co}=\frac{\theta c}{w*0.42}$ , $\theta_c=mC/cm^2$ , w = 0.127 $mg/cm^2$, $0.42mC/cm^2$

CO poisoning tolerance of PtPd based electrocatalysts is demonstrated in Fig. 5.23(A) & 5.23(B) by using carbon monoxide (CO) stripping voltammetry. Fig. 5.23(A) shows that the 2nd CV cycle (dotted lines) in CO oxidation is almost overlapped with pre adsorbed CO stable curve (Fig. 5.21), which suggest that CO is completely oxidized in 1st cycle of CO oxidation and electrochemical active surface area of active metal is relieved for hydrogen adsorption/desorption. From figure, it can be seen that onset potential of Pd/ $WO_3$-OMC (432mV) is 108mV negatively shifted to that of Pd/OMC (540mV) while peak potential is shifted 68mV positively. Catalysts with lower onset potential are found to be better in catalytic activity for CO oxidation. So, this demonstrated that $WO_3$addition

has enhanced (onset potential) CO oxidation ability of modified support catalysts. For $Pd_2Pt_1/WO_3$-OMC catalyst the onset potential and CO peak intensity laid at 358mV and 16.3mA/cm$^2$ respectively which showed 1.2 times –ve shift in potential and 2.1 times rise in current intensity as compared to Pd/ $WO_3$-OMC electrocatalyst. Table 5-5 summarized both electrochemical active surface areas (ECAS) of metals. One can see form this table that the intensity of CO oxidation peaks and onset potential are varied with the change (Increase) of Pt contents. Lowest onset potential and maximum ECSA (62.4m$^2$/g) of $Pd_2Pt_1/WO_3$-OMC catalyst declared it as a potential CO tolerance catalyst.

Table 5.5: Electrochemical properties of catalysts on CO oxidation

| Catalyst | Area of desorbed CO peak(mC/cm$^2$) | CO Stripping | | $ECAS_{CO}$[a] | Peak Intensity |
|---|---|---|---|---|---|
| | | $E_{onset}$ (mV) | $E_{peak}$ (mV) | (m$^2$/g metal) | (mA/cm$^2$) |
| Pd/OMC | 9.5 | 540 | 580 | 17.8 | 10.8 |
| Pd/$WO_3$-OMC | 67.6 | 432 | 648 | 126.7 | 20.7 |
| $Pd_1Pt_1$/ $WO_3$-OMC | 15.7 | 636 | 682 | 29.4 | 14.6 |
| $Pd_2Pt_1$/ $WO_3$-OMC | 33.3 | 358 | 551 | 62.4 | 14.2 |
| $Pd_1Pt_2$/ $WO_3$-OMC | 23.4 | 454 | 689 | 43.9 | 6.4 |

[a] $ECAS_{CO}=\frac{\theta c}{w*0.42}$ , $\theta_C$=mC/cm$^2$ , w = 0.127 mg/cm$^2$, 0.42mC/cm$^2$

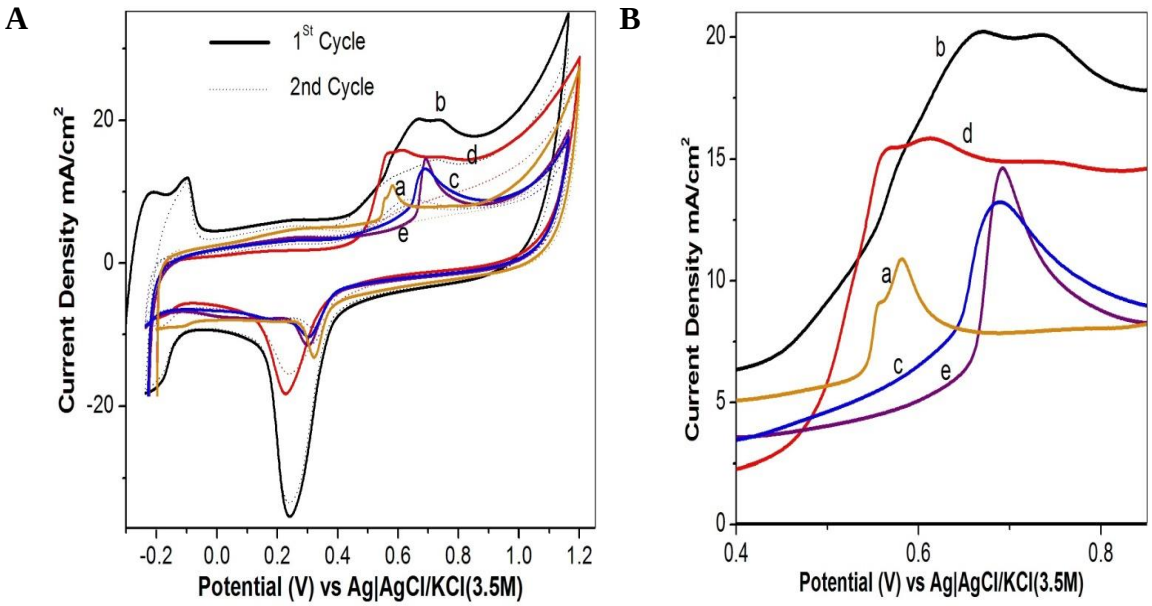


Figure 5.23: (A) 1st& 2nd Cycles of CO stripping measurements for PtPd/$WO_3$-supported electrocatalysts in 0.5 M $H_2SO_4$ at a scan rate of 20 mV/s, and (B): enlargement of the CO oxidation peaks: (a) Pd/OMC, (b) Pd/$WO_3$-OMC, (c) $Pd_1Pt_1$/WO3-OMC, (d) $Pd_2Pt_1$/$WO_3$-OMC and (e) $Pd_1Pt_2$/$WO_3$-OMC

### *5.2.3 Cyclic voltammetry Analysis*

The formic acid oxidation activity of the $CeO_2$ modified electrocatalysts is established by cyclicvoltametry (CV; scan rate of 20 mV/s) in 0.5 M HCOOH and 0.5 M $H_2SO_4$ solution. Prior to the measurements, the electrolyte solution and electrodes were purged with $N_2$ for 20 min to deaerate the system and to attain the steady state. The CV analysis of all the catalysts is presented in Fig. 5.24 while Fig. 5.25 plots the maximum current for each catalyst. It is clear from these figures that both intensities and peak potential of PtPd/$CeO_2$-OMC catalysts are changing with Pd to Pt ratios. At peak potential of 70 mV, oxidation current density of Pd/$CeO_2$-OMC catalyst is around 46.32 mA/cm$^2$ (3.24 A/mg) which is about 5 mA/cm$^2$ higher than that of Pd/OMC (41.1 mA/cm$^2$) catalyst. This improved catalytic performance of Pd/$CeO_2$-OMC is due to superior dispersion of noble metals on the $CeO_2$ modified OMC as observed in SEM and TEM analysis. Furthermore, the current density of Pd/$CeO_2$-OMC is much greater than that of previously reported commercially available carbon supports with Pd [17-18, 21-22, 98-99]. As shown in Fig. 5.25, the current density of $Pd_3Pt_1$/$CeO_2$-OMC catalyst for anodic scan is 74.6mA/cm$^2$. This current density is 1.8, 1.61, 1.67 and 28.3 times higher than that of Pd/OMC, Pd/$CeO_2$-OMC, $Pd_1Pt_3$/$CeO_2$-OMC (44.6 mA/cm$^2$) and Pt/$CeO_2$-OMC (2.6 mA/cm$^2$) catalysts, respectively. The peak potential of $Pd_3Pt_1$/$CeO_2$-OMC catalyst is also shifted positively as compared to the Pd/OMC, Pd/$CeO_2$-OMC and $Pd_1Pt_3$/$CeO_2$-OMCcatalysts. One can thus generally interpret that the formic acid electro oxidation on the two Pd/OMC and Pd/$CeO_2$-OMC catalysts are much easier. However, due to large ECAS (reported in Table 5-4) and smaller crystal size of Pt, electrochemical oxidation of formic acid was enhanced for $Pd_3Pt_1$/$CeO_2$-OMC catalyst [17]. Especially, with the decrease of

particle size and Pd content ratio, the peak potential for formic acid electro oxidation shifted positively.

Moreover, the oxidation peak of $Pt/CeO_2$-OMC catalyst at 790mV is ascribed to go through a multiple steps or indirect oxidation pathway; CO species are intermediates which strongly adsorbed on the surface of the catalysts. Due to the poisoning effects on Pt surface oxidation current intensity reduced to $2.6mA/cm^2$ [20], while in Pd/OMC, formic acid oxidation goes through a direct oxidation pathway [100].

Form the above observation it can be concluded that the modification of OMC with $CeO_2$ helps improving the peak current density (1.6 times higher than OMC), which positively affects the current activity of PtPd electrocatalysts. Also the peak potential of $Pd_3Pt_1/CeO_2$-OMC catalyst was shifted positively ca. 467 mV but it did not largely affect on catalytic activity of catalyst towards formic acid oxidation.

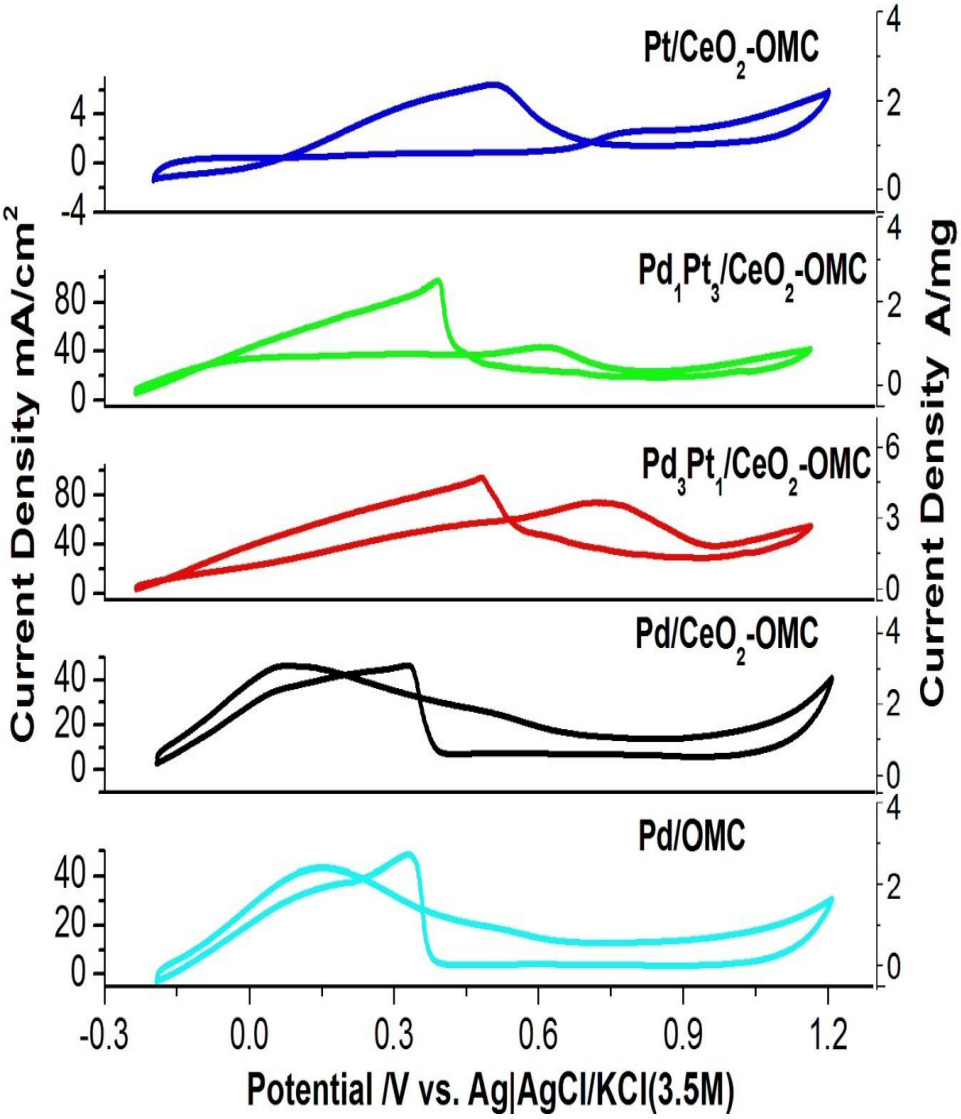


Figure 5.24: CV patterns of Pd/OMC, Pd/$CeO_2$-OMC and Pt Pd/$CeO_2$-OMC catalysts with various Pt:Pd ratios in 0.5M ($H_2SO_4$ + HCOOH) solution.

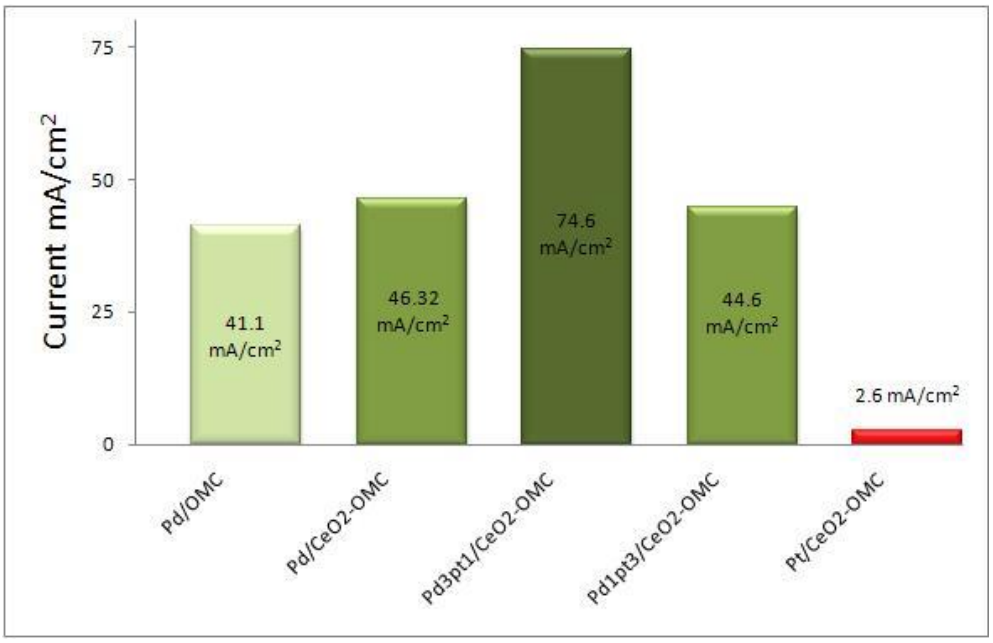


Figure 5.25: Maximum currents during CV patterns

Fig. 5.26 presented the cyclicvoltametry measurements for $WO_3$-OMC supported PtPd bimetallic electrocatalysts under same operating conditions as described in above CV analysis. Increasing Pt to Pd ratios result a significant change in current density with positive shift in peak potential. High anodic current density, 48.8mA/cm$^2$ (3.41A/mg) of Pd/$WO_3$-OMCelectrocatalyst with negative shift in peak potential (-8.6 mV), in comparison of Pd/OMC (41.1 mA/cm$^2$) catalystrepresents a well-built integration of OMC and $WO_3$as observed in SEM and TEM analysis. Similarly,comprehensive review of literature showed that the current density of$WO_3$-OMC supported Pd electrocatalystis much greater than that of Pd/C, Pd/OMC, Pd/CNT and Pd/MWCNT catalysts. Fig. 5.27 plotted the current density of all catalyst sample,showed that the current density of $Pd_2Pt_1$/$WO_3$-OMC catalyst for anodic scan is 56.8mA/cm$^2$which is 1.4, 1.2, 1.65 and 5.2 times higher than that of Pd/OMC, Pd/$WO_3$-OMC, $Pd_1Pt_1$/$WO_3$-OMC(34.5mA/cm$^2$) and $Pd_1Pt_2$/$WO_3$-OMC (10.9mA/cm$^2$) catalysts, respectively. The peak potential of $Pd_2Pt_1$/$WO_3$-OMC catalyst is also shifted positively as compared to the Pd/OMC, Pd/$WO_3$-OMC and $Pd_1Pt_1$/$WO_3$-OMC catalysts. One can thus generally interpret that the formic acid electro oxidation on the two Pd/OMC and Pd/$WO_3$-OMC catalysts are much easier. However, due to largeECAS(reported in Table 5-5) and smaller crystal size of Pt,electrochemical oxidation of formic acid was enhanced for $Pd_2Pt_1$/$WO_3$-OMCcatalyst. Positive shift in onset potential with increasing Pt contents confirmed the dominant indirect oxidation mechanism, in which poisoned active sites are reinstated by ad metal Pd at relative high anodic potential. Similarly, relative lower current density of$Pd_1Pt_2$/$WO_3$-OMC (10.9mA/cm$^2$) electrocatalyst at 677mV potential ascribed the oxidation via multiple steps pathway.

Form the above discussion, it can be concluded that $WO_3$ modification of OMC helps in improving the peak current density (1.2 times higher than Pd/OMC). Also the peak potential of $Pd_2Pt_1/WO_3$-OMC catalyst was shifted positively ca. 387 mV but it did not largely affect on catalytic activity of catalyst towards formic acid oxidation.

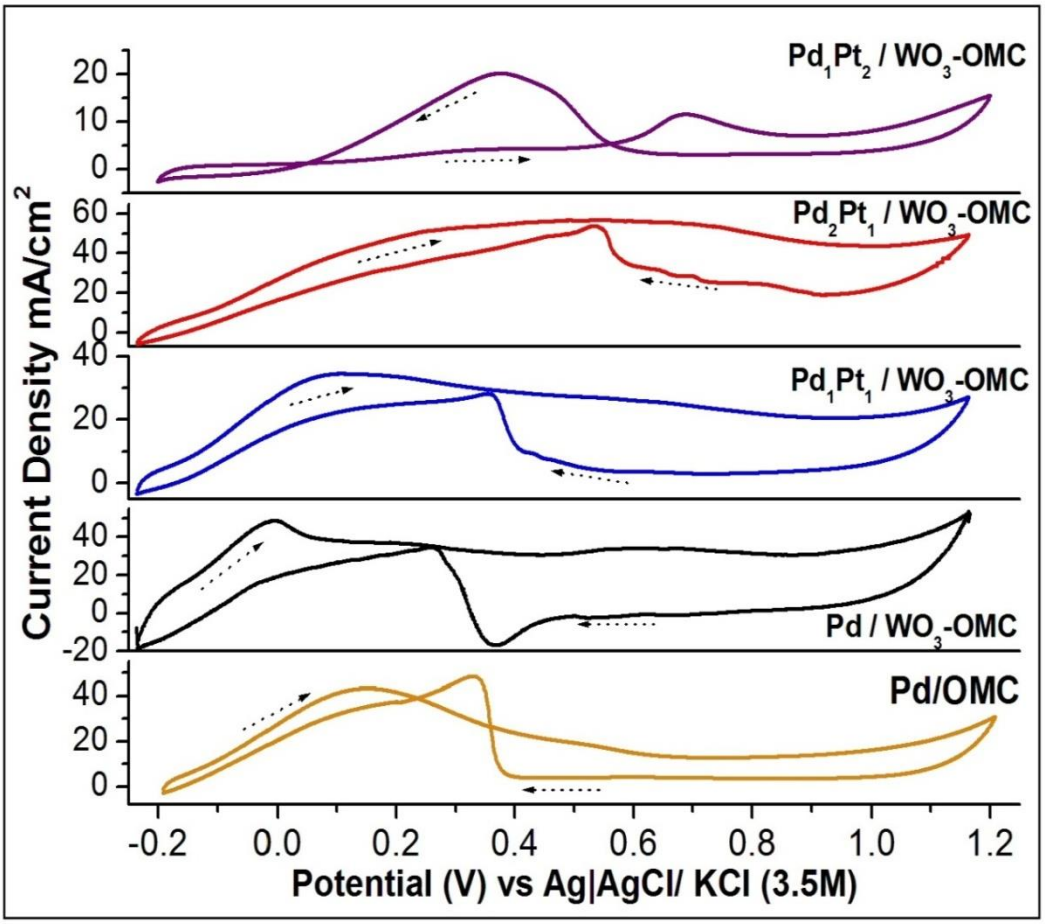


Figure 5.26: CV patterns of Pd/OMC, $Pd/WO_3$-OMC and $PtPd/WO_3$-OMC catalysts with various Pt:Pd ratios in 0.5 M ($H_2SO_4$ + HCOOH)solution.

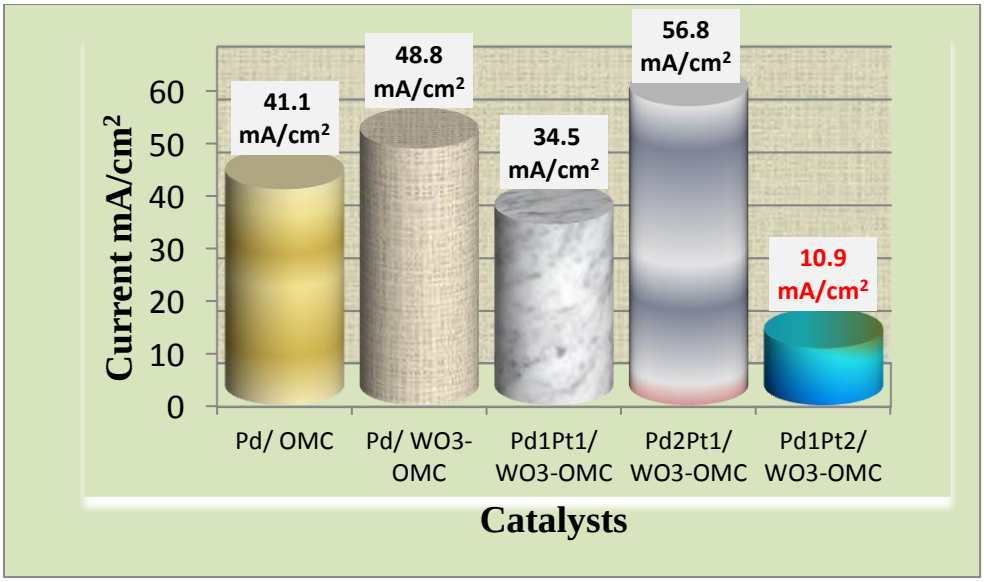


Figure 5.27: Maximum currents during CV

### *5.2.4 Chronoamperometry Analysis*

Fig. 5.28 displays the current density-time response curves during the formic acid oxidation (in presence of various electrocatalysts) at 0.3 V fixed potential in a solution of 0.5 M HCOOH and 0.5 M $H_2SO_4$ at 25n$^{\circ}$C. In all the catalysts, initially a rapid fall in current density was observed. After that the current decreased smoothly and finally reached a steady state at 1800s. The activityof $Pd_3Pt_1/CeO_2$-OMC electrocatalyst for formic acid oxidation was higher than the activities using Pd/OMC and $PtPd/CeO_2$-OMCelectrocatalysts. The steady state current density recorded on $Pd_3Pt_1/CeO_2$-OMC catalyst was about 32.8 mA/cm$^2$ which was 5.2 times higher than the steady state current density with Pd/OMC (6.2 mA/cm$^2$) catalyst. Current densities for $Pd/CeO_2$-OMC, $Pd_1Pt_3/CeO_2$-OMC and $Pt/CeO_2$-OMC catalysts were 11mA/cm$^2$, 20.3mA/cm$^2$ and 0.46mA/cm$^2$, respectively. From these results it is confirmed that $CeO_2$ based electrocatalyst showed somewhat high performance and particularly $Pd_3Pt_1/CeO_2$-OMC catalyst exhibit high catalytic activity and stability towards HCOOH electro oxidation.

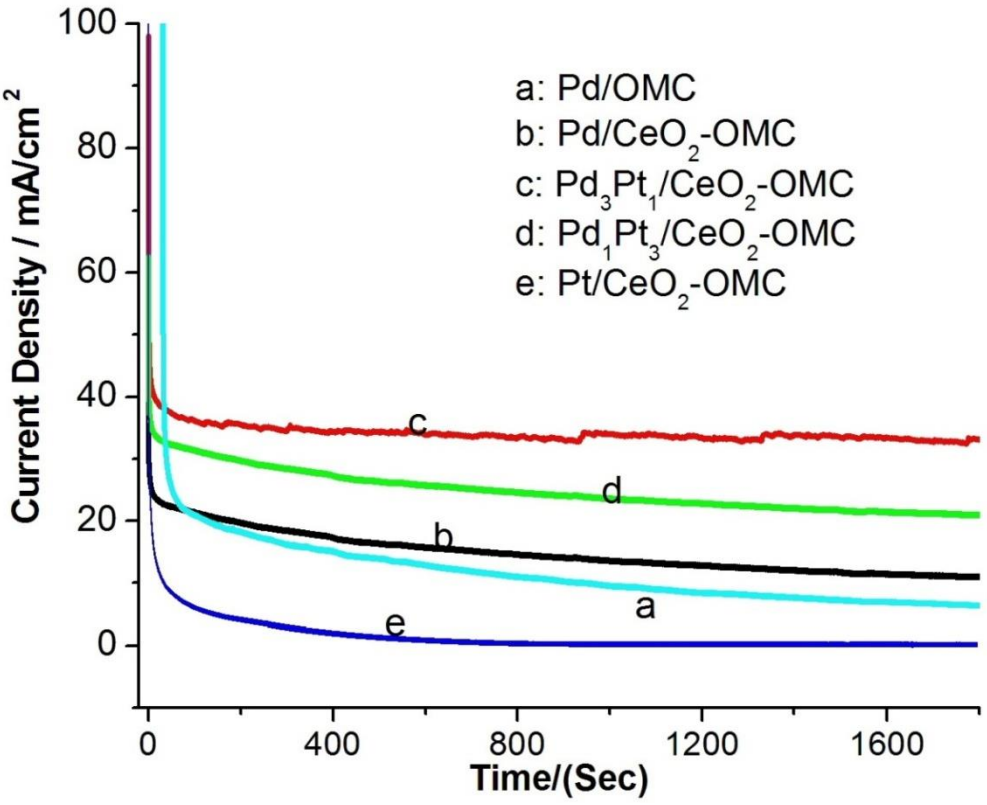


Figure 5.28: CA at 0.3 V (vs. Ag/AgCl) for Pd/OMC and PtPd/$CeO_2$-OMC electrocatalysts in 0.5M $H_2SO_4$ and HCOOH solution.

Fig. 5.29 displays the response curves of chronoamperometry measurements which performed to determine the performance durability and poisoning rate of tested catalysts in a solution of 0.5 M HCOOH and 0.5 M $H_2SO_4$ at 0.3V constant potential. In all the catalysts, current density initially fall rapidly following a parabolic path and finally

reached a pseudo steady state at 1400s. Bimetallic $Pd_2Pt_1/WO_3$-OMCelectrocatalyst showed higher activity for formic acid oxidation than the activities using Pd/OMC and other $PtPd/WO_3$-OMCelectrocatalysts. The steady state current density recorded on $Pd_2Pt_1/WO_3$-OMC catalyst was about 10.9 $mA/cm^2$ which was1.6 times higher than the steady state current density with Pd/OMC (6.6 $mA/cm^2$) catalyst. Current densities for $Pd/WO_3$-OMC, $Pd_1Pt_1/WO_3$-OMCand $Pd_1Pt_2/WO_3$-OMCcatalysts were 3.3$mA/cm^2$, 1.4$mA/cm^2$ and 6.1$mA/cm^2$, respectively. From these results it is confirmed that $WO_3$ based electrocatalyst showed somewhat high performance stability and particularly $Pd_2Pt_1/WO_3$-OMC catalyst exhibit high catalytic activity and stability towards HCOOH electro oxidation.

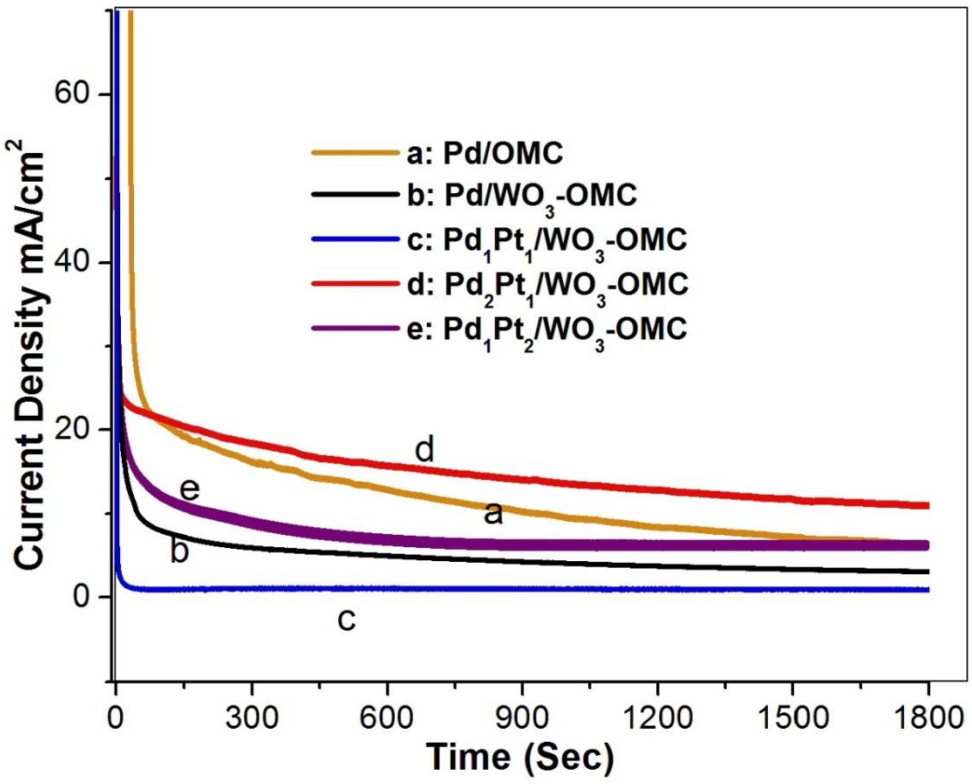


Figure 5.29: CA at 0.3 V (vs. Ag/AgCl) for Pd/OMC and PtPd/$WO_3$-OMC electrocatalysts 0.5 M $H_2SO_4$ and HCOOH solution.

# Chapter 6

# CONCLUSION AND RECOMMENDATIONS

## 6.1 Conclusion

In this investigation two separate series of $CeO_2$and $WO_3$modified ordered mesoporous carbon (OMC) supported Pd/Pt based electrocatalysts were prepared, characterized and evaluated using different electrochemical analysis techniques. Following are the conclusions of this study:

i. The $CeO_2$modification helped increasing the specific surface area of OMC (from 1005 to 1119 $m^2/g$). While, $WO_3$-OMC modification decreased the pore size of OMC (from 3.8nm to 3.4nm). After metal loading in both set of catalysts, the surface area was significantly decreased due to the blockage of the pores.

ii. SEM, XRD and TEM techniques revealed that the presence of metal oxidesenhanced the uniform metal dispersion on the support surface. The average crystal size decreased with the increase of Pt mass fraction in the bimetallic PdPt/$CeO_2$-OMCandPdPt/$WO_3$-OMCsamples.

iii. Cyclic voltammetry and chronoamperometry measurements showed that both Pd based electrocatalysts supported on $CeO_2$-OMC and $WO_3$-OMC have higherelectrocatalytic activity and long term stability for formic acid oxidation as compared to Pd/OMC catalyst.

iv. CO stripping results indicated that the addition of Pd metal has enhanced the CO poisoning tolerance effects of Pt based electrocatalysts as compared to Pt/$WO_3$-OMC catalyst. Support modification also played vital role which could be seen by

comparative analysis of Pd/OMC, Pd/$WO_3$-OMC and Pd/$CeO_2$-OMCelectrocatalysts.

v. $Pd_3Pt_1$/$CeO_2$-OMC electrocatalyst exhibited superior activity and stability among all $CeO_2$-OMC supported catalysts for oxidation reactions and also possessed large electrochemical active surface area (48.7$m^2$/g). For $WO_3$-OMC supported catalysts $Pd_2Pt_1$/$WO_3$-OMC showed optimal activity among all.

## 6.2 Recommendations

Based on the study performed, following suggestions will be useful to continue this work

i. For better dispersion and metal loading of noble metals on modified support material, other impregnation methods such as Prepetation deposition method, Wetness impregnation method and Sol gel method should be employed to get the maximum activity using same operating conditions and system.

ii. In all samples Pt metal has used which also proved good catalytic activity for methanol system, so, these samples can be tested for direct methanol fuel cell (DMFC).

iii. Nickel oxide can also be used and tested as support modifier instead of ceria and tungsten using same active matels for both methanol and formic acid oxidation system

iv. These samples can also be used for electrochemical reduction of $CO_2$ to hydrocarbon using solid electrolyte membrane as reduction reaction is very favourable in alkaline media.

v. Catalytic performance of these synthesized samples can be checked by using higher concentrated solution of formic acid and sulphuric acid. Kinetic modeling of optimized catalysts should be carried out to get more inside the the activity of samples.

**References**


[1] Ball, M. and M. Wietschel, The future of hydrogen-Opportunities and challenges. International Journal of Hydrogen Energy, 2009. 34: p. 615-627.

[2] G.A.Olah, A. Goeppert, and G.K.S. Prakash, Beyond Oil and Gas:Methanol Economy. 2006, Wiley-VCH: Weinheim.

[3] Conte, M. and G. Editor-in-Chief, ENERGY | Hydrogen Economy, in Encyclopedia of Electrochemical Power Sources. 2009, Elsevier: Amsterdam. p. 232-254.

[4] Rice, C., et al., Direct formic acid fuel cells. Power Sources, 2002. 111(1): p. 83-89.

[5] Aricò, A.S., V. Baglio, and V. Antonucci, Direct Methanol Fuel Cells: History, Status and Perspectives, in Electrocatalysis of Direct Methanol Fuel Cells. 2009, Wiley-VCH Verlag GmbH & Co. KGaA. p. 1-78.

[6] Centi, G. and S. Perathoner, Opportunities and prospects in the chemical recycling of carbon dioxide to fuels. Catalysis Today, 2009. 148(3-4): p. 191-205.

[7] Oloman C. and H. Li, Electrochemical Processing of Carbon Dioxide. ChemSusChem, 2008. 1(5): p. 385-391.

[8] Aresta, M. and A. Dibenedetto, Utilisation of CO2 as a chemical feedstock: opportunities and challenges. Dalton Transactions, 2007(28): p. 2975-2992.

[9] Cynthia A R, Akshay B, PeterG P. Recent Advances in Electrocatalysis of Formic Acid Oxidation. J. Springer London , Lecture Notes in Energy 2013; 9: 69-87. http://dx.doi.org/10.1007/978-1-4471-4911-8_4

[10]Olumide W, Zhiyong Z, Changhai L, Wenzhen L. Carbon nanotube supported platinum palladium nanoparticles for formic acid oxidation. Electrochim Acta 2011; 55(13): 4217-4221.

[11]W L Qu, Z B Wang, X L Sui, D M Gu, G P Yin. ZrC–C and ZrO2–C as Novel Supports of Pd Catalysts for Formic Acid Electro oxidation. Fuel Cells 2013; 13 (2): 149-157.

[12]Zhiming C, Cheng G, Chun X G and Chang M L. $Mo_2C$/CNTs supported Pd nano particles for highly efficient catalyst towards formic acid electro oxidation. Mater.Chem.A, 2013; 1: 1179–1184.

[13]Charles D, Paul L. R, John B. K and John N.Design of an Electrochemical Cell Making Syngas (CO + $H_2$) from $CO_2$ and $H_2O$ Reduction at Room Temperature. Electrochemical Society 2008; 155 (1): 42-49.

[14] Hui Li and Oloman, C. Continuous co-current electrochemical reduction of carbon dioxide. WO2007041872 B1, 2007.

[15]Satoshi Y, Hiroshi H, Masahiro D, Yuji Z, Reiko H, Yuka Y, Momoko D, and Kazuhiro O. Highly efficient photochemical HCOOH production from CO2 and water using an inorganic system. AIP Advances 2012; 2: 042160; doi: 10.1063/1.4769356

[16]Richard R, Christian B and Bernhard R. Conversion of CO2 via Visible Light Promoted Homogeneous Redox Catalysis. Catalysts 2012; 2: 544-571; doi:10.3390/catal2040544

[17] Yang L Jun, SU Neng, Ting and Shi Jun, Enhanced electro-oxidation of formic acid by a PdPt bimetallic catalyst on a CeO2-modified carbon support, Sci China Chem 2012; 55: 391- 397.

[18]Feng, LG; Yang, J; Hu, Y; Zhu, JB; Liu, CP Xing, W. Electrocatalytic properties of PdCeOx/C anodic catalyst for formic acid electro oxidation. International Journal of Hydrogen Energy 2012; 37: 4812–4818.

[19]Yuan H Qin, Yue-J, Hou-H Y, Xin S Z, Xing G Z, Li N, Wei K Y. Synthesis of highly dispersed and active palladium/carbon nanofiber catalyst for formic acid electrooxidation. Power Sources 2011; 196 (10): 4609-4612.

[20] Haan JL, Masel RI, The influence of solution pH on rates of an electrocatalytic reaction: Formic acid electro oxidation on platinum and palladium. Electrochim Acta 2009; 54: 4073–4078.

[21]Yu Zhu, Yongyin K, Zhiqing Z, Qun Z, Junwei Z, Baojia X and Hui Y. A facile preparation of carbon-supported Pd nanoparticles for electrocatalytic oxidation of formic acid.Electrochem. Commun 2008;10: 802-805.

[22]Xiao M Wang, Yong Y X.Synthesis, characterization and catalytic activity of an ultrafine Pd/C catalyst for formic acid electrooxidation. Electrochim. Acta 2009; 54: 7525-7530.

[23]Lu Zhang, Ling W, Yanrong Ma, Yu C, Yiming Z, Yawen T, Tianhong L. Crystalline palladium–cobalt alloy nano assemblies with enhanced activity and

stability for the formic acid oxidation reaction, Applied Catalysis B, Environmental (2013), http://dx.doi.org/10.1016/j.apcatb.2013.02.051.

[24]Rongfang Wang, HuiW, XingliW, Shijun L, VladimirL and Shan j. Effect of the structure of Ni nanoparticles on the electro catalytic activity of Ni@Pd/C for formic acid oxidation. International Journal of Hydrogen Energy 2013; 38 : 13125 – 13131.

[25] Maja D., Obradovic, Sne, Gojkovi, HCOOH oxidation on thin Pd layers on Au: Self-poisoning by the subsequent reaction of the reaction product, Electrochim Acta 2013; 88: 384– 389.

[26] Zhao, Zhua, Liuc and Wei Xing,Surface reconstruction enhancing activity of Pt/C for formic acid electro oxidation by ultrasonic mixing with Pb/C and electrochemical activation process.Applied Catalysis B: Environmental 2013; 129: 146– 152.

[27] Zhang, Chun He, Jiang, Rao and Shi-Gang Sun, High activity of PtBi intermetallics supported on mesoporous carbon towards HCOOH electro-oxidation, Electrochemistry Communications 2012; 25: 105–108.

[28] DandanTu, Bing, Wang, Deng and Ying Gao, A highly active carbon-supported PdSn catalyst for formic acid electro oxidation, Applied Catalysis B: Environmental 2011; 103: 163–168.

[29] Yanxian Jin, Chun'an M, Meiqin S, Youqun C, Yinghua X, Tao H, Qian H and Yiwai M. Highly Active Carbon Nanotube-Supported Bimetallic Palladium-Iron

Electrocatalysts for Formic Acid Electro oxidation. Electrochem.Sci. 2012; 7: 3399 – 3408.

[30] Ermete Antolini. Carbon supports for low-temperature fuel cell catalysts. Applied Catalysis B: Environmental 2009; 88: 1–24.

[31]Yuyan Shao, Geping Y, Jiajun W, Yunzhi G and Pengfei S. Multi-walled carbon nanotubes based Pt electrodes prepared with in situ ion exchange method for oxygen reduction. Power Sources 2006; 161 (1): 47–53.

[32]Sudong Yang, Xiaogang Z, Hongyu M, Xiangguo Y. Pd nanoparticles supported on functionalized multi-walled carbon nanotubes (MWCNTs) and electro oxidation for formic acid. Power Sources 2008; 175: 26–32.

[33]Bruce R. R J, Frank R. M and Elton J. C. Direct anodic oxidation of methanol on supported platinum/ruthenium catalyst in aqueous cesium carbonate. Electrochem Soc. 1995; 142: 1073–1084.

[34] Seger B and Kamat PV. Electrocatalytically active graphene– Platinum nano composites.Role of 2-D carbon support in PEM fuel cells.Phy. Chem. C 2009;113: 7990–95.

[35]Dong J H and Jae S L. Transition Metal Carbides and Nitrides as Electrode Materials for Low Temperature Fuel Cells. Energies 2009; 2: 873-899; doi:10.3390/en20400873

[36]J. Zeng, C. Francia, C. Gerbaldi, V. Baglio, S. Specchia, A.S. Aricò, P. Spinelli. Hybrid ordered mesoporous carbons doped with tungsten trioxide as supports for Pt

electrocatalysts for methanol oxidation reaction, Electrochim Acta 2013; 94: 80–91.

[37]Sang H Joo, Seong J C, Ilwhan O, Juhyoun K, Zheng L, Osamu T & Ryong R. Ordered nanoporous arrays of carbon supporting high dispersions of platinum nanoparticles. Nature 2001; 412: 169-172.

[38]Sang Hoon Joo, Chanho P, Dae J Y, Seol-Ah L, Hyung I L, Ji M K, Hyuk C, Doyoung S. Ordered mesoporous carbons (OMC) as supports of electrocatalysts for direct methanol fuel cells (DMFC): effect of carbon precursors of OMC on DMFC performances, Electrochim Acta 2006; 52: 1618-1626.

[39]Zhi-Peng Sun, Xiao G Z, Hao Tong, Yan Y L, Hu L L. Sulfonation of ordered mesoporous carbon supported Pd catalysts for formic acid electrooxidation. Colloid and Interface Science 2009; 337: 614–618.

[40] Juqin Zeng, Carlotta F, Mihaela A. D, Alessandro H. A. M V, Vijaykumar S. I, Stefania S, and Paolo S. Electrochemical Performance of Pt-Based Catalysts Supported on Different Ordered Mesoporous Carbons (Pt/OMCs) for Oxygen Reduction Reaction. Ind. Engg.Chem. Res. 2012; 51: 7500–7509.

[41] Chuntao L, Meng C, Chunyu D, Jing Z, Geping Y, Pengfei S and Yongrong Sun. Durability of Ordered Mesoporous Carbon Supported Pt Particles as Catalysts for Direct Formic Acid Fuel Cells. Electrochem.Sci. 2012; 7: 10592 – 10606.

[42] Grove E.R, “On voltaic series and combination of gases by platinum” Philosophical Magazine and Journal of Science, series 3, 14, 127-130, 1839.

[43] http://americanhistory.si.edu/fuelcells/origins/origins2.htm, last date 3/11/2013.

[44] Eric, C, “Fuel cell technology history in fuel cell technology handbook” Gregor H., CRC press LLC, New York, USA (2003) pp 2-1 to 2-40.

[45]http://orgs.kettering.edu/altfuel/fcback.htm, November, 2013.

[46]http://www.nfcrc.uci.edu/2/FUEL_CELL_INFORMATION/FCexplained/ fueltypes .aspx

[47] Lui, h. and j. zhang, eds. Electrocatalysis of Direct Methanol Fuel Cells. 2009, Wiley-VCH.

[48] Viestich, W., A. Lamm, and A.G. Hubert, eds. Fuel Cell Handbook. 2003, Wiley.

[49] Moore, A.D., S.M. Holmes, and E.P.L. Roberts, Evaluation of porous carbon substrates as catalyst supports for the cathode of direct methanol fuel cells. RSC Advances, 2012.2(4).

[50] Qian, W., et al., Architecture for portable direct liquid fuel cells. Power Sources, 2006. 154(1): p. 202-213.

[51] Bai, Y., et al., Electrochemical oxidation of ethanol on Ptâ€“ZrO2/C catalyst. Electrochemistry Communications, 2005. 7(11): p. 1087-1090.

[52] Du, C., et al., Nanoporous PdNi Alloy Nanowires As Highly Active Catalysts for the Electro-Oxidation of Formic Acid. ACS Applied Materials & Interfaces, 2011. 3(2): p. 105-109.

[53] Hong, P., et al., A 4-cell miniature direct formic acid fuel cell stack with independent fuel reservoir: Design and performance investigation. Power Sources, 2011. 196(14): p. 5913-5917.

[54] Hwang, K.-r., S.-k. Ihm, and J.-s. Park, Enhanced CeO2-supported Pt catalyst for water & gas shift reaction.Fuel Processing Technology, 2010. 91(7): p. 729-736.

[55] Jin-nyeong, J., L. Hong-Gi, and Y. Yeon-Tae, Size Effect of Au Nanoparticle on Electrocatalytic Activity of Pt-Au/C Composite Catalysts for Methanol Oxidation. Electrochemical and Solid-State Letters, 2011. 14(9): p. B89-B91.

[56] Jung, W.S., et al., Performance degradation of direct formic acid fuel cell incorporating a Pd anode catalyst. Power Sources, 2011. 196(10): p. 4573-4578.

[57] Justin, P. and G.R. Rao, Enhanced activity of methanol electro-oxidation on Pt & $V_2O_5$/C catalysts. Catalysis Today, 2009. 141(1 & 2): p. 138-143.

[58] Kim, D.B., et al., Preparation of Pt/NiO-C electrocatalyst and heat-treatment effect on its electrocatalytic performance for methanol oxidation. Hydrogen Energy, 2010. 35(1): p. 313-320.

[59] Larsen, R., et al., Unusually active palladium-based catalysts for the electrooxidation of formic acid. Power Sources, 2006. 157(1): p. 78-84.

[60] Lee, E., A. Murthy, and A. Manthiram, Carbon-supported Pt nanoparticles prepared by a modified borohydride reduction method: Effect on the particle morphology and catalytic activity for COad and methanol electro-oxidation. Electrochemistry Communications, 2011. 13(5): p. 480-483.

[61] Chen, Y.X., et al., Kinetics and Mechanism of the Electrooxidation of Formic Acid—Spectroelectrochemical Studies in a Flow Cell. Angewandte Chemie International Edition, 2006. 45(6): p. 981-985.

[62] Zhou, W. and J.Y. Lee, Particle Size Effects in Pd-Catalyzed Electrooxidation of Formic Acid. Physical Chemistry C, 2008. 112(10): p. 3789-3793.

[63] Li, R., et al., Ultrasonic-assisted synthesis of Pd & Ni alloy catalysts supported on multi-walled carbon nanotubes for formic acid electrooxidation. Electrochim Acta, 2011. 56(19): p. 6860-6865.

[64] Sathe, B.R., B.K. Balan, and V.K. Pillai, Enhanced electrocatalytic performance of interconnected Rh nano-chains towards formic acid oxidation. Energy & Environmental Science, 2011. 4(3): p. 1029-1036.

[65] Bard, A.J. and L.R. Faulkner, Electrochemical Methods: Fundamentals and Applications 2000: Wiley.

[66] Winjobi, O., et al., Carbon nanotube supported platinum & palladium nanoparticles for formic acid oxidation. Electrochimica Acta, 2011. 55(13): p. 4217-4221.

[67] Jianyu C, Zhuanxia C, Juan X, Wenchang W and Zhidong C. Mesoporous carbon synthesized from dual colloidal silica/block copolymer template approach as the support of platinum nanoparticles for direct methanol fuel cells. ElectrochimActa 88 (2013) 184– 192.

[68] Bernard C, Muaffak N and Julien A. Oxidation of formic acid in aqueous solution by Palladium catalysts. Applied Catalysis, 11 (1984) 217-225.

[69] H Li, Gongquan S, Qian J, Mingyuan Z,S Sun and Qin Xin. Synthesis of highly dispersed Pd/C electro-catalyst with high activity for formic acid oxidation. Electrochemistry Communications 9 (2007) 1410–1415.

[70] Hong Zhao, T.S. Zhao. Highly active carbon nanotube-supported Pd electrocatalyst for oxidation of formic acid prepared by etching copper template method. International journal of hydrogen energy 38 ( 2013 ) 1391 -1396.

[71] Marjan M, Martin S, B Jancar. A study towards superior carbon nanotubes-supported Pd-based catalysts for formic acid electro-oxidation: Preparation, properties and characterization. Power Sources 235 (2013) 111-116.

[72] E A. Baranova, Neil M, Patrick H.J. M, Yvon L P and B Patarachao. Formic acid electro-oxidation on carbon supported $Pd_xPt_{1-x}$ ($0 \geq x \geq 1$)nanoparticles synthesized via modified polyol method. Electrochim Acta 55 (2010) 8182–8188.

[73] R Wang, Hui W, Xingli W, Shijun L, Vladimir L and Shan Ji. Effect of the structure of Ni nanoparticles on the electrocatalytic activity of Ni@Pd/C for formic acid oxidation. International journal of hydrogen energy xxx ( 2 0 1 3 ) 1 -7.

[74] Akshay S. Bauskar, Cynthia A. Rice. Spontaneously Bi decorated carbon supported Pt nanoparticles for formic acid electro-oxidation. Electrochim Acta 93 (2013) 152–157.

[75] D Basu, S Basu. Synthesis and characterization of PteAu/C catalyst for glucose electro-oxidation for the application in direct glucose fuel cell. International journal of hydrogen energy 36 ( 2011 ) 14923 -14929.

[76]Bin Peng, J Y Wang, H. X Zhang, Y H Lin and Wen-Bin Cai. A versatile electroless approach to controlled modification of Sb on Pt surfaces towards efficient electrocatalysis of formic acid. Electrochemistry Communications 11 (2009) 831–833.

[77]Gumaa A. El-Nagara, A M. Mohammad, M S. Deab, B E. El-Anadouli. Electrocatalysis by design: Enhanced electrooxidation of formic acid at platinum nanoparticles–nickel oxide nanoparticles binary catalysts. Electrochim Acta 94 (2013) 62– 71.

[78] I. A. Rutkowska, Diana M, Christian P, Mohamed J, Pawel J. K. Admixing palladium nanoparticles with tungsten oxide nanorods toward more efficient electrocatalytic oxidation of formic acid. Colloids and Surfaces A: Physicochem. Eng. Aspects 439 (2013) 200–206.

[79] A Ciftci, D.A.J. M Ligthart, Pietro P, Emiel J.M. H. Nanostructured ceria supported Pt and Au catalysts for the reactions of ethanol and formic acid. Applied Catalysis B: Environmental 130–131 (2013) 325–335.

[80] M S. El-Deab. Platinum nanoparticles–manganese oxide nanorods as novel binary catalysts for formic acid oxidation. Advanced Research (2012) 3, 65–71.

[81]T. Maiyalagan, B. Viswanathan, U.V. Varadaraju. Nitrogen containing carbon nanotubes as supports for Pt – Alternate anodes for fuel cell applications. Electrochem.Commun. 7 (2005) 905-912.

[82]C. Arbizzani S. Beninati, E. Manferrari, F. Soavi, M. Mastragostino. PtRu supported on mesoporous carbons for DMFC application. Power Sources 161 (2006) 826-830.

[83] J. Prabhuram, T.S. Zhao, Z.K. Tang, R. Chen, Z.X. Liang. Multiwalled Carbon Nanotube Supported PtRu for the Anode of Direct Methanol Fuel Cells. Phys. Chem. B 110 (2006) 5245.

[84] C. Park, R.T.K. Baker. Effect of carbon nanofiber-induced microstrain on the catalytic activity of Ni crystals.Phys. Chem. B 102 (1998) 5168.

[85] D.A. Bulushev, I. Yuranov, E.I. Suvorova, P.A. Buffat, L. Kiwi-Minsker. Highly dispersed gold on activated carbon fibers for low-temperature CO oxidation.Catal. 224 (2004) 8-17.

[86] S. Jun, S.H. Joo, R. Ryoo, M. Kruk, M. Jaroniec, Z. Liu, T. Ohsuna, O. Terasaki. Synthesis of New, Nanoporous Carbon with Hexagonally Ordered Mesostructure.Am.Chem. Soc. 122 (2000) 10712-13.

[87] R. Ryoo, S.H. Joo, M. Kruk, M. Jaroniec. Ordered Mesoporous Carbons. Adv. Mater. 13 (2001) 677-681.

[88] L. Calvillo, M.J. Lazaro, E. Garcy´ a-Bordeje, R. Moliner, P.L. Cabot, I. Esparbe, E. Pastor, J.J. Quintana.Platinum supported on functionalized ordered mesoporous carbon as electrocatalyst for direct methanol fuel cells. Power Sources 169 (2007) 59-64.

[89] S.H. Joo, C. Pak, D.J. You, S.A. Lee, H.I. Lee, J.M. Kim, H. Chang, D. Seung.Ordered mesoporous carbons (OMC) as supports of electrocatalysts for direct methanol fuel cells (DMFC): Effect of carbon precursors of OMC on DMFC performances. Electrochim. Acta 52 (2006) 1618-26.

[90]Dongyuan Z, Jianglin F, Qisheng H, Nicholas M, Glenn H F, Bradley F C,Galen D S.Triblock copolymer syntheses of mesoporous silica with periodic 50 to 300 angstrom pores. Science 1998; 279: 548-552.

[91]Lifeng Wang, Sen L, Kaifeng L, Chengyang Y, Desheng L, Yan Di, Peiwei F, Dazhen J and Feng S X. A facile synthesis of highly ordered mesoporous carbon

monolith with mechanically stable mesostructure and superior conductivity from SBA-15 powder.Microporous and Mesoporous Materials 2005; 85: 136–142.

[92] Bio-Logic Technical Note #8 (http://www.bio-logic.info)

[93]Sun CW , Xie Z , Xia CR, Li H, Chen LQ. Investigations of mesoporous CeO2-Ru as a reforming catalyst layer for solid oxide fuel cells. Electrochemistry Communications 2006; 8: 833-838.

[94]Zhao HT, Gang W, Bing W and Ying G. High activity Pt/C catalyst for methanol and adsorbed CO electro-oxidation. Power Sources 2007; 164: 105- 110.

[95] Zhang HX, Wang C, Wang JY, Zhai JJ, Cai WB. Carbon supported Pd–Pt nanoalloy with low Pt content and superior catalysis for formic acid electro oxidation, Phys Chem C 2010; 114: 6446–6451.

[96]Hyun J K, Won l K, Tae J P, Hyung S P and Dong J S. Highly dispersed platinum–carbon aerogel catalyst for polymer electrolyte membrane fuel cells. J. Carbon 2008; 46; 1393-1400.

[97] Ing. habil. Kai Sundmacher, Mihai Christov, habil. Helmut Weiß, Kinetics of Methanol Electrooxidation on PtRu Catalysts in a Membrane Electrode Assembly, 2005, page 27, http://diglib.uni-magdeburg.de/Dissertationen/2005/tanvidakovic.pdf.

[98]Jun Y,Chungui T,Lei andHonggang F. An effective strategy for small-sized and highly-dispersed palladium nanoparticles supported on graphene with excellent performance forformic acid oxidation, Mater. Chem. 2011; 21: 3384-3390.

[99]Yizhong Lu and Wei C. Nanoneedle-Covered Pd-Ag Nanotubes: High Electrocatalytic Activity for Formic Acid Oxidation. Phys. Chem. C 2010; 114: 21190–21200.

[100] Wang J, Yin G, Chen Y, Li R, Sun X. Pd nanoparticles deposited on vertically aligned carbon nanotubes grown on carbon paper for formic acid oxidation. International Journal of Hydrogen Energy 2009; 34: 8270–8275.

## Vitae

| | |
|---|---|
| Name | : Ateeq Ur Rehman |
| Nationality | : Pakistani |
| Date of Birth | :11/7/1984 |
| Email | : fahad_118c@yahoo.com |
| Address | : Pak Bhatti Manzil,Rail Bazar, New Mondi Pattoki, Pak. |
| Academic Background | : Chemical Engineering |
| List of publications | : ARehman, SS Hossain, S Rahman, S Ahmed, M.Hossain. Electrocatalytic activity of $CeO_2$-modified ordered mesoporous (OMC) carbon supported Pt-Pd bimetallic catalysts for formic acid oxidation. International Journal of Hydrogen energy. |
| | : ARehman, SS Hossain, S Rahman, S Ahmed, M.Hossain.Investigate the hybrid $WO_3$-ordered mesoporous carbon (OMC) support effect on electrocatalytic oxidation of formic acid using Pt-Pd bimetallic catalysts. Journal of Carbon. |